Calhoun: The NPS Institutional Archive

DSpace Repository

Theses and Dissertations | 1. Thesis and Dissertation Collection, all items

2001-09

Measurements and modeling enhancements for the NPS minimum resolvable temperature difference model, VISMODII

Celik, Mustafa.

Monterey, California. Naval Postgraduate School

http://hdl.handle.net/10945/1772

Downloaded from NPS Archive: Calhoun

http://www.nps.edu/library

Calhoun is a project of the Dudley Knox Library at NPS, furthering the precepts and goals of open government and government transparency. All information contained herein has been approved for release by the NPS Public Affairs Officer.

Dudley Knox Library / Naval Postgraduate School
411 Dyer Road / 1 University Circle
Monterey, California USA 93943

NAVAL POSTGRADUATE SCHOOL
Monterey, California

THESIS

MEASUREMENTS AND MODELING ENHANCEMENTS FOR THE NPS MINIMUM RESOLVABLE TEMPERATURE DIFFERENCE MODEL, VISMODII

by

Mustafa Celik

September 2001

Thesis Advisor:	Ronald J. Pieper
Thesis Co-Advisor:	Alfred W. Cooper

Approved for public release; distribution is unlimited

REPORT DOCUMENTATION PAGE

Form Approved OMB No. 0704-0188

Public reporting burden for this collection of information is estimated to average 1 hour per response, including the time for reviewing instruction, searching existing data sources, gathering and maintaining the data needed, and completing and reviewing the collection of information. Send comments regarding this burden estimate or any other aspect of this collection of information, including suggestions for reducing this burden, to Washington headquarters Services, Directorate for Information Operations and Reports, 1215 Jefferson Davis Highway, Suite 1204, Arlington, VA 22202-4302, and to the Office of Management and Budget, Paperwork Reduction Project (0704-0188) Washington DC 20503.

1. AGENCY USE ONLY *(Leave blank)*	2. REPORT DATE	3. REPORT TYPE AND DATES COVERED
	September 2001	Master's Thesis

4. TITLE AND SUBTITLE: Measurements and Modeling Enhancements for the NPS Minimum Resolvable Temperature Difference Model, VISMODII

5. FUNDING NUMBERS

6. AUTHOR(S)
Celik, Mustafa

7. PERFORMING ORGANIZATION NAME(S) AND ADDRESS(ES)
Naval Postgraduate School
Monterey, CA 93943-5000

8. PERFORMING ORGANIZATION REPORT NUMBER

9. SPONSORING / MONITORING AGENCY NAME(S) AND ADDRESS(ES)
N/A

10. SPONSORING / MONITORING AGENCY REPORT NUMBER

11. SUPPLEMENTARY NOTES The views expressed in this thesis are those of the author and do not reflect the official policy or position of the Department of Defense or the U.S. Government.

12a. DISTRIBUTION / AVAILABILITY STATEMENT
Approved for public release; distribution is unlimited.

12b. DISTRIBUTION CODE

13. ABSTRACT ***(maximum 200 words)***

Minimum Resolvable Temperature Difference (MRTD) measurement has long been used to describe the performance of thermal imaging systems. Computer models such as U.S. Army's FLIR92, that were developed to predict the MRTD, were reported to have deficiencies in dealing with sampling and aliasing effects. The models also include assumptions regarding the observer recognition process and therefore cannot predict the MRTD of an imager that incorporates an "objective" automatic target recognition device instead of a "subjective" human observer. The Visibility Model II developed for second generation thermal imaging systems at the Naval Postgraduate School (NPS) in the mid 90's takes sampling and aliasing issues into account and makes no assumptions about the observer. Modeling enhancements in VISMODII and its extension to predict objective MRTD are proposed and tested in this thesis. A parallel thesis at the NPS has shown that aliasing effects on image appearance are fundamentally different from noise. The improved VISMODII model accounts for the fact that unlike noise, aliasing may have a visual enhancing effect and therefore may lower MRTD. Experiments were conducted to measure subjective and objective MRTD. Experimental results demonstrated that the VISMODII model successfully predicts the MRTD both for the subjective and the objective schemes.

14. SUBJECT TERMS VISMODII Model, MRTD Prediction, Objective MRTD, Thermal Imaging Systems, FLIR92, NVTherm.

15. NUMBER OF PAGES
194

16. PRICE CODE

17. SECURITY CLASSIFICATION OF REPORT	18. SECURITY CLASSIFICATION OF THIS PAGE	19. SECURITY CLASSIFICATION OF ABSTRACT	20. LIMITATION OF ABSTRACT
Unclassified	Unclassified	Unclassified	UL

NSN 7540-01-280-5500

Standard Form 298 (Rev. 2-89)
Prescribed by ANSI Std. 239-18

THIS PAGE INTENTIONALLY LEFT BLANK

Approved for public release; distribution is unlimited

MEASUREMENTS AND MODELING ENHANCEMENTS FOR THE NPS MINIMUM RESOLVABLE TEMPERATURE DIFFERENCE MODEL, VISMODII

Mustafa Celik
1st Lieutenant, Turkish Army
B.S., Turkish War College, 1996

Submitted in partial fulfillment of the
requirements for the degree of

MASTER OF SCIENCE IN SYSTEMS ENGINEERING

from the

NAVAL POSTGRADUATE SCHOOL
September 2001

Author: _____
Mustafa Celik

Approved by: _____
Ronald J. Pieper, Thesis Advisor

_____
Alfred W. Cooper, Thesis Co-Advisor

_____
Dan C. Boger, Chairman
Information Warfare Academic Group

THIS PAGE INTENTIONALLY LEFT BLANK

ABSTRACT

Minimum Resolvable Temperature Difference (MRTD) measurement has long been used to describe the performance of thermal imaging systems. Computer models such as U.S. Army's FLIR92, that were developed to predict the MRTD, were reported to have deficiencies in dealing with sampling and aliasing effects. The models also include assumptions regarding the observer recognition process and therefore cannot predict the MRTD of an imager that incorporates an "objective" automatic target recognition device instead of a "subjective" human observer. The Visibility Model II developed for second generation thermal imaging systems at the Naval Postgraduate School (NPS) in the mid 90's takes sampling and aliasing issues into account and makes no assumptions about the observer. Modeling enhancements in VISMODII and its extension to predict objective MRTD are proposed and tested in this thesis. A parallel thesis at the NPS has shown that aliasing effects on image appearance are fundamentally different from noise. The improved VISMODII model accounts for the fact that unlike noise, aliasing may have a visual enhancing effect and therefore may lower MRTD. Experiments were conducted to measure subjective and objective MRTD. Experimental results demonstrated that the VISMODII model successfully predicts the MRTD both for the subjective and the objective schemes.

THIS PAGE INTENTIONALLY LEFT BLANK

TABLE OF CONTENTS

I. INTRODUCTION....1

II. OVERVIEW OF TERMINOLOGY....5
- A. FUNDAMENTALS OF THERMAL IMAGING SYSTEMS....5
  - 1. Target and Background....5
  - 2. Atmosphere....6
  - 3. Optics....6
  - 4. Detector and Scanner....7
  - 5. Electronics....7
  - 6. Display....7
  - 7. Human Vision and ATR Devices....8
- B. GENERATIONS OF FLIR....8
- C. SENSITIVITY AND RESOLUTION....9
- D. PERFORMANCE MEASURES....10
  - 1. Parameters of Interest....10
  - 2. Modulation Transfer Function (MTF)....12
  - 3. Noise Equivalent Temperature Difference (NETD)....15
  - 4. Minimum Detectable Temperature Difference (MDTD)....16
  - 5. Minimum Resolvable Temperature Difference (MRTD)....18
- E. PERFORMANCE PREDICTION MODELS....22
  - 1. Ratches Model....22
  - 2. Lloyd's Model....23
  - 3. FLIR92 Model....23
  - 4. Visibility Model....24
  - 5. NVTherm Model....24

III. VISMODII, OVERVIEW OF TERMINOLOGY AND PRINCIPLES OF OPERATION....25
- A. ORIGINS OF THE VISIBILITY MODEL....25
  - 1. Modeling Principles....25
  - 2. Advantages over Non-visibility Models....26
- B. SECOND GENERATION MODELING REQUIREMENTS....27
  - 1. Noise in Second Generation Staring Systems....27
  - 2. Sampling and Aliasing Effects....33
  - 3. Sample-scene Phasing Effects....37
- C. VISMODII MODELING CONCEPTS....38
  - 1. MRTD Formulation....38
  - 2. Threshold Input Contrast....40
  - 3. Contrast Transference Parameter....41
  - 4. Sampling and Aliasing Effects....41
  - 5. MTF Analysis in VISMODII....44
- D. AREAS OF IMPROVEMENT....46

IV. AMENDMENTS AND REFINEMENTS IN VISMODII 47
A. CALCULATION OF THRESHOLD INPUT CONTRAST 47
1. SNR Improvement Factor (Et) 47
2. Total Noise Bandwidth 48
B. CALCULATION OF CONTRAST TRANSFERENCE PARAMETER 49
1. Changes in MTF/PTF Analysis 49
2. Changes in Simulating Aliasing Effects 52
3. Changes in Calculation of Contrast 52
V. SUBJECTIVE MRTD 61
A. EXPERIMENTAL SETUP 61
B. PROCEDURE 63
C. MEASUREMENT RESULTS 64
D. COMPARISON WITH VISMODII AND FLIR92 MODEL RESULTS 66
E. ASSESSMENT OF SAMPLING, ALIASING AND SCENE PHASING EFFECTS ON THE MRTD PREDICTIONS 71
VI. OBJECTIVE MRTD 75
A. EXPERIMENTAL SETUP 75
B. PROCEDURE 76
C. MEASUREMENT RESULTS 78
D. OBJECTIVE MRTD MODELING CONCEPTS 81
E. COMPARISON OF MODEL RESULTS WITH MEASURED DATA 83
VII. CONCLUSIONS AND RECOMMENDATIONS 91
A. CONCLUSIONS 91
B. DIRECTIONS FOR FURTHER RESEARCH 92
APPENDIX A. TIS PARAMETERS 95
APPENDIX B. DETAILED SPATIAL FREQUENCY ANALYSIS IN VISMODII 97
APPENDIX C. ASSESSMENT OF MTF SQUEEZE MODEL FOR ACCOUNTING FOR ALIASING EFFECTS 101
A. SPURIOUS RESPONSE TERM USED IN THE MTF SQUEEZE MODEL 101
B. MTF SQUEEZE FACTORS 104
C. COMPARISON WITH VISMODII APPROACH 107
APPENDIX D. MEASUREMENT RESULTS 109
A. SUBJECTIVE MRTD MEASUREMENTS 109
B. SUBJECTIVE MRTD MEASUREMENTS 111
APPENDIX E. VISMODII SOURCE CODE 113
A. SUBJECTIVE MRTD SOURCE CODE 113
1. Mitsv2.m 113

2. Meffcnt.m 117
3. Alias.m 127
B. OBJECTIVE MRTD SOURCE CODE 130
1. Mitsv2obj.m 130
2. Meffcntobj.m 133
APPENDIX F. FLIR92 MODEL OUTPUT FILE 141
APPENDIX G. FLIR92 MRTD PREDICTION AT ZERO SPATIAL FREQUENCY 149
APPENDIX H. NOISE SAMPLE DATA 151
APPENDIX I. PRE-PRINT OF THE PAPER ACCEPTED FOR PRESENTATION AT THE THIRTY-FIFTH ASILOMAR CONFERENCE 153
LIST OF REFERENCES 163
INITIAL DISTRIBUTION LIST 167

THIS PAGE INTENTIONALLY LEFT BLANK

LIST OF FIGURES

Figure 2.1. Thermal Imaging Scenario "From [Ref. 2]". 5
Figure 2.2. Atmospheric Transmittance Over 1 Km. Path Length. Note the 3-5 and 8-12 micrometer bands where atmospheric transmission is possible "From [Ref. 4]". 6
Figure 2.3. Field-of-View "After [Ref. 2]". 11
Figure 2.4. System MTF (MTF Cascade). The system MTF is the product of the sub-system MTFs "From [Ref. 2]". 13
Figure 2.5. Definition of MTF for Three Spatial Frequencies: (a) Input Modulation, (b) Output Modulation, (c) MTF "From [Ref. 3]". 14
Figure 2.6. Definition of Modulation "From [Ref. 3]". 15
Figure 2.7. MRTD Curve as a Function of Four-Bar Target Spatial Frequency. Note the asymptotic rise at the spatial frequency where MTF goes to zero. "From [Ref. 2]". 18
Figure 2.8. Definition of Spatial Frequency "From [Ref. 3]". 19
Figure 2.9. MRTD and MDTD Illustrating that the Asymptotic Rise Exists only for the MRTD. MDTD shows a relatively linear increase with the spatial frequency. "From [Ref. 8]". 20
Figure 3.1. VISMODI Modeling Concept Illustrating the Reduction in Contrast due to the Sub-System MTF/PTFs "From [Ref. 12]". 26
Figure 3.2. 3-D Noise Coordinate System "From [Ref. 4]". 28
Figure 3.3. Spatial Sampling by Detector Element. The detector elements sample the scene at intervals of the pitch in each direction by integration over the active area. "From [Ref. 9]". 33
Figure 3.4. Staring FPA as a Two-Dimensional Sampling Lattice. Note the delta functions illustrating the sampling by each individual detector element "From [Ref. 9]". 34
Figure 3.5. Representation of Sampling by a FPA in Spatial Frequency Domain. Sampling process creates the replicas of the original spectrum centered at the sampling frequency on positive and negative sides of the spectrum. "From [Ref. 9]". 35
Figure 3.6. Detector Elements Sampling a Four-Bar Target: (a) Maximum Modulation Corresponding to the Perfect Alignment between the Detector Elements and the Bars, (b) Minimum Modulation Corresponding to the Highest Degree of Misalignment. "From [Ref. 21]". 37
Figure 3.7. VISMOD II Modeling Concept "From [Ref. 9]". 39
Figure 3.8. Schematic of Imaging process in Spatial Domain "After [Ref. 22]". 41
Figure 3.9. Schematic of Imaging Process in Spatial Frequency Domain "After [Ref. 22]". 42

Figure 3.10. Calculation of Contrast in the VISMODII Code: Note that T_p is the average over the first bar and T_t is the average over the first pace of the four-bar pattern. 43
Figure 4.1. Two-Dimensional Eye MTF Used in the VISMODII Model. 48
Figure 4.2. Two-Dimensional Image Formation MTF for the Thermal Imaging System Used in VISMODII. 50
Figure 4.3. Two-Dimensional Image Reconstruction MTF for the Thermal Imaging System Used in VISMODII. 51
Figure 4.4. Two-Dimensional Overall System MTF as a Product of the Image Formation and the Image Reconstruction MTFs for the Thermal Imaging System Used in VISMODII. 51
Figure 4.5. Profiles Along the Four-Bar Pattern and its Images with and without Aliasing. Note the contrast enhancement due to aliasing. 53
Figure 4.6. Image with Noise and Aliasing: Note the lack of symmetry, due to aliasing together with blurring due to noise. 54
Figure 4.7. Image with Noise Only (No Aliasing): Note that the four bars are observable and the asymmetric distortion that was clearly observed in Figure 4.6 is not present. 54
Figure 4.8. Spatial Shift in the Image due to Electronics PTF. 55
Figure 4.9. Calculation of Contrast in the Image. 56
Figure 4.10. VISMOD II Block Diagram. 57
Figure 5.1. Subjective MRTD Experimental Setup. 62
Figure 5.2. Mitsubishi IR-M500 Thermal Imaging System. 63
Figure 5.3. Measured Subjective MRTD. 65
Figure 5.4. VISMOD II Subjective MRTD Predictions. 66
Figure 5.5. FLIR92 MRTD Predictions. 67
Figure 5.6. Horizontal Subjective MRTD Comparison. 68
Figure 5.7. Vertical Subjective MRTD Comparison. 68
Figure 5.8. Two-Dimensional Subjective MRTD Comparison. 69
Figure 5.9. Horizontal Subjective MRTD Comparison at Low Spatial Frequencies. 70
Figure 5.10. Vertical Subjective MRTD Comparison at Low Spatial Frequencies. 70
Figure 5.11. Two-Dimensional Subjective MRTD Comparison at Low Spatial Frequencies. 71
Figure 5.12. Sampling and Aliasing Effects on MRTD Prediction. 72
Figure 5.13. Sample Scene-phasing (ssp) Effects on MRTD Prediction. 74
Figure 6.1. Objective MRTD Experimental Setup. 76
Figure 6.2. Noise Measurement Procedure. 77
Figure 6.3. Snapshot of Noise Taken from the Oscilloscope Display (Vertical axis is 10 milliVolts per division). 77
Figure 6.4. Four-Bar Target Representation on the Oscilloscope Display (Vertical Axis is 20 milliVolts per Division). 78
Figure 6.5. Measured Objective MRTD (SNR=6.0). 79
Figure 6.6. Measured Objective MRTD vs. Required SNR for Various Four-Bar Spatial Frequencies. 80

Figure 6.7. Measured Objective MRTD for Various Required SNR Values.....81
Figure 6.8. VISMODII Objective MRTD Predictions (SNR=6.0). 83
Figure 6.9. Objective MRTD Comparison (SNR=6.0). 84
Figure 6.10. VISMOD II Predicted MRTD vs. Required SNR for Various Four-Bar Spatial Frequencies. 84
Figure 6.11. Objective MRTD vs. Required SNR Comparison (f_s=0.12 cy/mrad). 85
Figure 6.12. Objective MRTD vs. Required SNR Comparison (f_s=0.24 cy/mrad). 85
Figure 6.13. Objective MRTD vs. Required SNR Comparison (f_s=0.46 cy/mrad). 86
Figure 6.14. Objective MRTD vs. Required SNR Comparison (f_s=0.56 cy/mrad). 86
Figure 6.15. VISMOD II Objective MRTD vs. Spatial Frequency Predictions for Various Required SNR Values. 87
Figure 6.16. Objective MRTD vs. Spatial Frequency Comparison (SNR=2).....88
Figure 6.17. Objective MRTD vs. Spatial Frequency Comparison (SNR=3).....89
Figure 6.18. Objective MRTD vs. Spatial Frequency Comparison (SNR=4).....89
Figure 6.19. Objective MRTD vs. Spatial Frequency Comparison (SNR=5).....90
Figure 6.20. Objective MRTD vs. Spatial Frequency Comparison (SNR=6).....90
Figure B.1. Horizontal MRTD Bar-Pattern along the x-Axis (f_y = 0) (Four-Bar Target Frequency: 0.65 cy/mrad). 98
Figure B.2. Spatial Frequency Matrix Demonstrating the DC Term. 99
Figure C.1. Definition of In-Band and Out-of Band Spurious Response "From [Ref. 4]". 104
Figure C.2. MTF Squeeze. For recognition f_2=(1-0.32SR) f_1 "From [Ref. 4]". 106
Figure D.1. Horizontal MRTD Measurements.....110
Figure D.2. Vertical MRTD Measurements. 111
Figure I.1. A Typical MRTD Plot "After [Ref. 1]". 157
Figure I.2. Staring FPA as a Two-Dimensional Sampling Lattice "From [Ref. 3]". 157
Figure I.3. Block Diagram of the Virtual Thermal Image-Processing Model. 158
Figure I.4. Single Lines Passing through the Target and Image Centers (Four-Bar Frequency: 0.65 cy/mrad). 159
Figure I.5. Horizontal MRTD Bar-Pattern along the x-Axis (f_y = 0) (Four-Bar Target Frequency: 0.65 cy/mrad). 160
Figure I.6. Image with Noise and Aliasing at 0.05 cycles/mrad.....160
Figure I.7. Image with Noise and Aliasing at 1.10 cycles/mrad.....161
Figure I.8. Image with only Noise (no Aliasing) at 1.10 cycles/mrad.....162

THIS PAGE INTENTIONALLY LEFT BLANK

LIST OF TABLES

Table 3.1. Three-Dimensional Noise Components "From [Ref. 19]". 29
Table 4.1. Steps in the VISMODII Program and Corresponding Chapters/Sections/Subsections and/or Appendices. 58
Table C.1. Performance Dependence on Spurious Response “From [Ref. 28]". 106
Table D.1. Horizontal MRTD Measurements.....109
Table D.2. Vertical MRTD Measurements.....110
Table D.3. Objective MRTD (Constant SNR=6.0). 111
Table D.4. Objective MRTD (Constant Spatial Frequency).....112
Table H.1. Sample Data Set for Noise Analysis.....151

THIS PAGE INTENTIONALLY LEFT BLANK

LIST OF SYMBOLS, ACRONYMS AND/OR ABBREVIATIONS

3-D	: Three-dimensional
α	: Horizontal detector angular subtense
$\alpha(f_z)$	: Contrast transference parameter
α_t	: Temporal sample correlation factor
β	: Vertical detector angular subtense
$\delta(x,y)$	: Delta function with magnitude 1.0 at x=y=0
$\delta W/\delta T$	: Thermal derivative of Planck's equation
Δf_n	: Noise equivalent bandwidth
Δf_p	: Total system noise bandwidth
Δ_m	: Detector active dimension
Δ_s	: Spacing between the detector elements
Δw	: Incremental spacing between the elements in the spatial domain matrix
Δx	: Detector center-to-center spacing (detector pitch)
ΔT	: Target-to-background temperature difference
ΔT_s	: Target-to-background temperature difference at imaging system output
ΔT_{sc}	: Threshold input contrast
ΔT_{sco}	: Objective threshold input contrast
ΔV	: Difference in Volts between the target and background due to ΔT
η_{sc}	: Scan efficiency
λ	: Average (diffraction) wavelength

Λ : Spatial sampling period

ν : Spatial frequency

ρ_x : Noise filter factor

σ : Monitor gaussian spot diameter

σ_{alias} : Alias noise

σ_g : Optics blur spot diameter

σ_h : Fixed column noise standard deviation

σ_t : Frame to frame noise standard deviation

σ_{th} : Temporal column noise standard deviation

σ_{total} : Total system noise standard deviation

σ_{tv} : Temporal row noise standard deviation

σ_{tvh} : Random spatio-temporal noise standard deviation

σ_v : Fixed row noise standard deviation

σ_{vh} : Fixed pattern noise standard deviation

τ_o : Transmittance of optics

Ω_T : Target solid angular subtense

ξ : Spatial frequency

a : Detector horizontal dimension

A : Image horizontal dimension

A : Image horizontal dimension

A_d : Area of a single detector element

$A(f_x,f_y)$: Aliased spectrum

ATR : Automatic target recognition

b : Detector vertical dimension

b_x : Horizontal spatial shift of the image center from the sampling element

b_y : Vertical spatial shift of the image center from the sampling element

B : Image vertical dimension

B_{max} : Maximum intensity level

B_{min} : Minimum intensity level

d : Width of a single bar

D_o : Optics aperture diameter

D* : Specific detectivity

DAS : Detector angular subtense

E_t : Eye-brain temporal integral

E_h : Eye-brain horizontal spatial integral

E_v : Eye-brain vertical spatial integral

f : Two-dimensional spatial frequency

f_{3dB} : Electronics cutoff frequency

f_{max} : Highest spatial frequency component in the spectrum

f_{NX} : Nyquist frequency limit in the horizontal direction

f_{sx} : Spatial sampling frequency in horizontal direction

f_{sy} : Spatial sampling frequency in vertical direction

f_x : Horizontal spatial frequency

f_y : Vertical spatial frequency

f_z : Four-bar target spatial frequency in the "z" direction

f_s : Four-bar target spatial frequency

$\Im$: Fourier transform

F : Optics effective focal length

F/# : F number

F_{dot} : Frame rate

FFT : Fast Fourier transform

FLIR : Forward-looking infrared

FLIR90 : NVESD 1990 thermal imaging system performance model

FLIR92 : NVESD 1992 thermal imaging system performance model

FOV : Field-of-view

FOV_h : Horizontal FOV

FOV_v : Vertical FOV

FPA : Focal plane array

$h_i(x,y)$: Image formation point spread function

$h_r(x,y)$: Image reconstruction point spread function

H : Horizontal axis in the 3-D noise coordinate system

H_d : Display MTF

H_{det} : Detector spatial MTF

H_{elect} : Electronics MTF

H_{eye} : Eye MTF

$H_i(f_x,f_y)$: Image formation MTF

H_{ogb} : Optics geometric blur MTF

H_{opt} : Diffraction limited optics MTF

H_{NF} : Noise filter MTF

$H_r(f_x,f_y)$: Image reconstruction MTF

H_{sys} : System MTF

i(x,y) : Image spatial distribution

$I(f_x,f_y)$: Image spatial frequency spectrum

$I_{correct}(f_x,f_y)$: Properly filtered spectrum

IFOV : Instantaneous filed-of-view

k : Noise correction function

L : Length-to-width ratio (aspect ratio) of a single bar

LOWTRAN : Low resolution transmission code

MODTRAN : Moderate resolution transmission code

m : Integer corresponding to the m^{th} sampling replica in vertical direction

MDT(D) : Minimum detectable temperature (difference)

MRT(D) : Minimum resolvable temperature (difference)

MRTD(fs$\rightarrow$0) : MRTD at the low spatial frequency limit

MTF : Modulation transfer function

$MTF_{squeeze}$: MTF squeeze factor

MTF_{sys} : System MTF

n : Integer corresponding to the n^{th} sampling replica in horizontal direction

N_D : Number of detector elements

N_{os} : Overscan ratio

N_{ss} : Serial scan ratio

NETD : Noise equivalent temperature difference

NVESD : Night Vision and Electronic Sensors Directorate

NVTherm : NVESD 1999 thermal imaging system performance model

OTF : Optical transfer function

OTF_{elect} : Electronics OTF

$p(x,y)$: Sampling function

PSF : Point spread function

PTF : Phase transfer function

PTF_{elect} : Electronics phase transfer function

$P(f_x,f_y)$: Sampling function in the spatial frequency domain

r_B : Back-end resolution

r_S : System resolution

R : Distance between the thermal imager and the target

R_{sp} : Response function of an imager

$s(x,y)$: Object (target scene) spatial distribution

s_h : Samples per horizontal detector angular subtense

s_v : Samples per vertical detector angular subtense

S : Mean of all noise components in the three-dimensional noise model

$S(f_x,f_y)$: Object (target scene) spatial frequency spectrum

$S_{sampled}$: Sampled image spectrum

S_{SP} : Sampled image spectrum with scene phase

SEARAD : A modification of MODTRAN developed by the U.S. Navy

SNR : Signal-to-noise ratio

SNR_{thr} : Threshold SNR for resolution

SR : Total spurious response to transfer response ratio

SR_h : Spurious response to transfer response ratio in horizontal direction

SR_v : Total Spurious response to transfer response ratio in vertical direction

$SR_{in\text{-}band}$: In-band spurious response to transfer response ratio

$SR_{out\text{-}of\text{-}band}$: Out-of-band spurious response to transfer response ratio

t_e : Eye integration time

T : Temporal axis in the 3-D noise coordinate system

T_p : Average value over the peaks of the bar pattern

T_t : Average value over the troughs of the bar pattern

TDI : Time delay integration

TIS : Thermal imaging system

V : Vertical axis in the 3-D noise coordinate system

Vn : Measured rms noise voltage

VISMOD I : First generation visibility model

VISMODII : Second generation visibility model

x : Space variable in horizontal direction

y : Space variable in vertical direction

z : Direction subscript being either horizontal (h) or vertical (v)

THIS PAGE INTENTIONALLY LEFT BLANK

ACKNOWLEDGMENT

First, my appreciation goes to Mr. Robert Sanders for his help in the experimental setup and equipment. I also thank 1st LT Yucel Kenter, Turkish Army, for his cooperation in the laboratory measurements.

I would like to acknowledge my thesis advisors, Professor Ronald J. Pieper and Professor Alfred W. Cooper for their active participation during the development of this work. Their knowledge, experience and continuous guidance have led me to successfully and timely complete this thesis.

I would like to thank my parents for their support during my stay at the Naval Postgraduate School. Finally, I want to express my gratitude to the Turkish Nation for providing this opportunity.

THIS PAGE INTENTIONALLY LEFT BLANK

I. INTRODUCTION

Thermal imaging systems produce a visible image of the thermal variation in the target scene. Although the applications have evolved and various generations of thermal imagers have been developed over the past four decades, the underlying principles and fundamentals of thermal imaging have basically remained unchanged [Refs. 1 through 8]. Minimum resolvable temperature difference (MRTD) has been developed and used as the primary figure of merit, as it is the most complete measure that describes the overall system performance including the operator. Modeling efforts to predict MRTD have resulted in Night Vision and Electronic Sensors Directorate's (NVESD) 1975 Ratches Model. Although the 1975 Ratches Model has been used successfully for many years, second generation staring thermal imaging systems required the development of a new model that could account for directional noise and aliasing effects [Refs. 9 through 18]. FLIR92 included directional noise effects successfully into the predictions through a "three dimensional noise" model [Ref. 19]. However, the model did not address aliasing issues that are unavoidable consequences of the two dimensional staring focal plane arrays (FPAs) incorporated in these state-of-the-art imagers [Refs. 20 through 23]. In 1996, a second-generation visibility based model was introduced [Ref. 24] that incorporates the sampling and aliasing issues into performance modeling. Efforts at NVESD also led to the development of a new model in 1999, NVTherm, which includes aliasing effects into MRTD predictions through a semi-empirical analysis of sampling and aliasing artifacts [Refs. 26 through 28]. Laboratory experiments with the objective of measuring MRTD have been performed and reported in the literature [Refs. 29 through 35].

The experiment results serve as useful measures to compare different systems as well as benchmarks to evaluate simulation results from performance prediction models. However, these manual and subjective MRTD experiments are time-consuming. The involvement of a human observer makes the measurements subjective and the results are not reproducible. These reasons motivated the efforts to measure and predict MRTD

objectively with the use of an automated procedure [Refs. 36 through 39]. The Visibility model, VISMODII in its current form, had the advantage of making no assumptions about the observation process and therefore was extendable to predict "objective" MRTD, where no human observer is needed to make the decision as to whether a resolution condition is achieved.

There are three main objectives of this thesis. The first objective is to refine the VISMODII model to get better predictive results and improve the model especially in the sampling and aliasing areas. The second objective is to develop an experimental procedure for objective MRTD and to extend the VISMODII model to predict the objective MRTD. The final objective is to perform laboratory experiments to measure MRTD both subjectively and objectively and compare the experimental results with simulated MRTD results from VISMODII with the purpose of validating VISMODII as a complete predictive model. A comparative analysis of the VISMODII and FLIR92 subjective MRTD predictions will also be performed. We will start Chapter II by presenting the fundamentals of thermal imaging and performance modeling for thermal imaging systems. An overview of the visibility based modeling concept will follow in Chapter III. In Chapter IV, we will present the amendments and refinements on the VISMODII model. Subjective MRTD measurement procedure and results along with comparisons with simulated results will be given in Chapter V. This will be followed by the description of the experimental design and modeling concepts for objective MRTD. Chapter VI will also include a comparison between simulated and measured objective MRTD results. Finally, Chapter VII will summarize and conclude this thesis.

Several topics will be discussed in appendices for purposes of completeness and to avoid overcrowding the main text with detailed information such as source codes and tabular experimental results. Appendix A lists the parameters of the thermal imaging system used in the VISMODII and FLIR92 models as well as in the MRTD experiments. Details of the spatial frequency analysis of VISMODII will be discussed in Appendix B. Appendix C will provide an assessment of the MTF Squeeze approach which is used in the NVTherm model to account for sampling and aliasing effects. The MRTD

measurement results will be given in Appendix D in graphical and tabular form. VISMODII MATLAB code will be given in Appendix E and Appendix F will provide the short-listing output from the FLIR92 model. In Appendix G, a mathematical argument will be presented showing that the FLIR92 model predicts the MRTD to be zero at the limit where spatial frequency is equal to zero. The noise sample data set, which was taken to calculate the rms noise value for objective MRTD, will be given in Appendix H. The community outside the NPS has also recognized the Visibility model concepts. Appendix I will provide a pre-print of the paper that was accepted for presentation at the Thirty-Fifth Asilomar Conference on Signals, Systems, and Computers on November 4 – November 7, 2001.

THIS PAGE INTENTIONALLY LEFT BLANK

II. OVERVIEW OF TERMINOLOGY

This chapter summarizes the fundamental elements of a thermal imaging scenario and thermal imaging systems (TIS) performance modeling.

A. FUNDAMENTALS OF THERMAL IMAGING SYSTEMS

Thermal imaging system(s) (TIS) extend human vision beyond the visible region of the electromagnetic spectrum. In principle, TISs detect the variation in thermal radiation in the scene and form a visible real image of this variation [Ref. 1]. Figure 2.1 depicts the elements of a typical thermal imaging scenario.

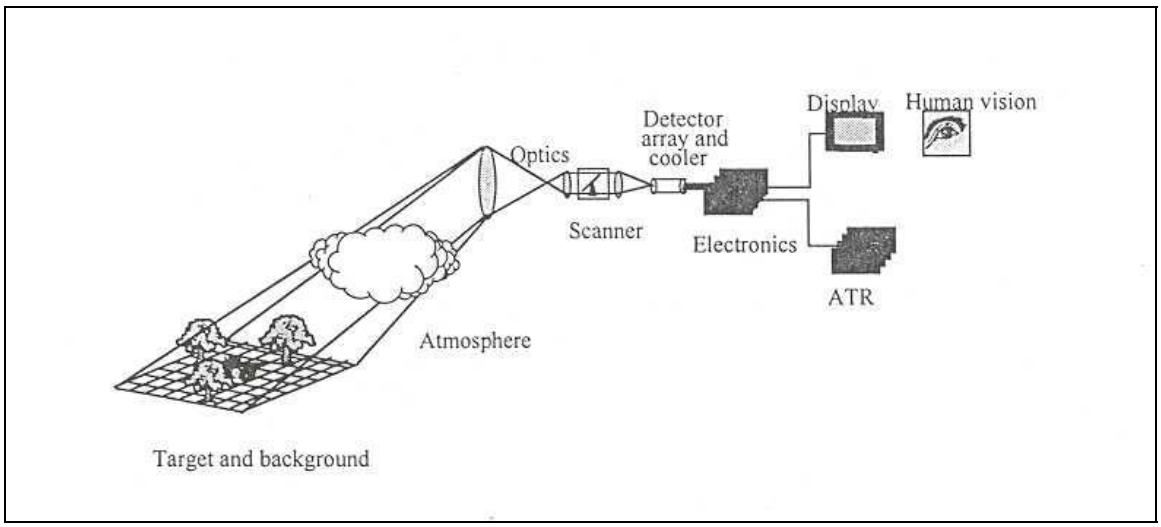

Figure 2.1. Thermal Imaging Scenario "From [Ref. 2]".

1. Target and Background

All objects with a temperature above absolute zero emit thermal radiation. The rate of radiation depends on the temperature and the surface characteristics of the object. Scene includes objects of interests (targets) and the background that interferes with the TIS's function by concealing the targets [Ref. 2]. Although the radiance variation can be due to many parameters, for modeling purposes target to background temperature difference (Delta T or ΔT) is the important characteristic [Ref. 3].

2. Atmosphere

Between the target scene and the TIS is the atmosphere. Atmosphere attenuates the radiation from the scene with its absorptive and scattering properties. Atmospheric extinction, which is the combination of absorption and scattering, limits thermal imaging to specific wavelength regions called "windows" through which atmospheric transmission is possible. Figure 2.2 illustrates atmospheric transmission as a function of wavelength of radiation. The radiation reaching the TIS is a combination of the attenuated scene radiation, radiation from the objects other than the scene that is scattered into the TIS field of view (FOV) and the path radiance [Refs. 3 and 4]. Atmospheric propagation models such as the Low Resolution Transmission Code (LOWTRAN), Moderate Resolution Transmission Code (MODTRAN) or SEARAD (A modification of MODTRAN developed by the United States Navy, NCCOSC) are used to predict the effects of the atmosphere on TIS performance.

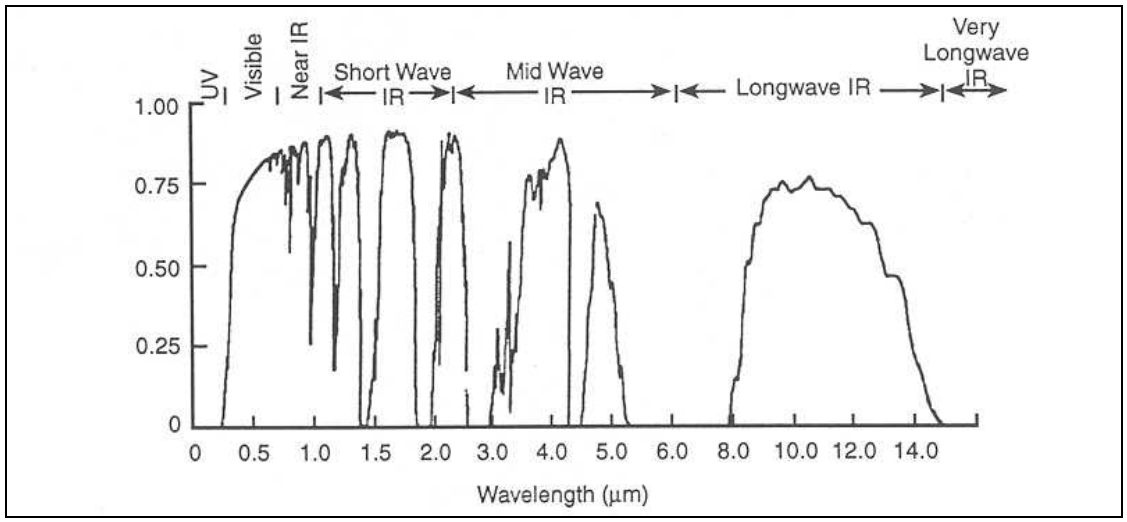

Figure 2.2. Atmospheric Transmittance Over 1 Km. Path Length. Note the 3-5 and 8-12 micrometer bands where atmospheric transmission is possible "From [Ref. 4]".

3. Optics

Optics of the TIS collect the scene radiation, form an image and project this image onto the detector element(s). Size and material properties of optics determine the

amount of the scene radiation collected and transmitted to the detector. Optical materials that provide high transmission in the wavelength band of interest are preferred.

Although the optics consist of a number of refractive and reflective elements, for modeling purposes a single lens of diameter D_o and an effective focal length of F is considered.

4. Detector and Scanner

A scanner is used to move the image produced by the optics across the detector elements. The particular method of scanning depends on the TIS type and the detector array geometry. No scanner is required in a staring TIS where the entire image area is covered by discrete detector elements.

Detector elements serve as transducers that convert the optical radiation into electrical signals. The electrical signal is proportional to the radiation received from a particular section of the image. The detector electrical output is a temporal representation of the scene spatial information [Ref. 4]. The detector also generates noise that interferes with perception, as increased noise decreases the signal-to-noise ratio (SNR). SNR is given as peak signal voltage divided by rms noise voltage. Higher SNR implies better detection processes [Ref. 3]. A cooling device is usually present associated with the cooling requirements of the detector array.

5. Electronics

The electronics can be a simple filter and amplifier combination, or it can incorporate highly sophisticated digital signal processing techniques. Whatever the level of sophistication, the function of the electronics is to refine the signal output from the detector element(s) and present an improved signal-to-noise ratio (SNR) to the display for human vision or to an automatic target recognition (ATR) device for machine evaluation.

6. Display

The display converts the electrical signal output of the electronics into a visible image and presents it to the human observer.

7. Human Vision and ATR Devices

The human visual system consists of eye-brain combination. The eye-brain combination's ability to integrate (sum) signals over space and time improves the performance.

The use of ATR devices has been the interest of research for a variety of military and commercial applications. An ATR device processes the information and no visible display is required in this case.

B. GENERATIONS OF FLIR

The term FLIR, meaning forward-looking infrared is a term that has been used to refer to thermal imaging systems [Ref. 2].

U.S. Department of Defense initiated a modular approach to thermal imaging system design to minimize cost and to increase flexibility. This initiative resulted in Generation I Common Module FLIRs [Ref. 4]. First generation TIS has a vertical linear array of detectors. A scanning mechanism is used to sweep the image across the detector array. It incorporates analog filters and amplifiers [Ref. 2].

Second generation TIS can either be scanning or staring. In the 1980s, proposed staring array devices were called second generation FLIRs. However, the difficulty of producing large long wave (8-12 micrometer) detector arrays led to use of a smaller two-dimensional array scanning type system [Ref. 4]. Scanning second generation TIS consists of a two dimensional array of detector elements (usually 480x4 or 480x2) and has the capability of time delay integration (TDI), a technique in which several detector outputs corresponding to the same point in the image are integrated to increase sensitivity of the TIS. This technique gives an additional SNR improvement due to signal adding directly and noise adding in quadrature [Ref. 2]. Staring arrays are produced in the 3-5 micrometer band due to manufacturing ease. Staring second-generation systems have two-dimensional detector arrays that cover the entire image area without any scanning mechanisms involved. In this thesis these systems are referred to as staring TIS. Staring TIS has much higher sensitivity compared to scanning systems due to having longer integration times. Integration time is defined as the amount of time a detector element

actively integrates signal from a particular area of the image. Absence of a scanner minimizes mechanical problems and complexity. However, spatial sampling characteristics of the detector array result in sampling and aliasing problems. These effects are examined thoroughly in Chapter III.

Third generation TIS is still in the development stage. It will include a large (over 1000x1000 elements) staring array. It is expected to be able to operate on both 3-5 and 8-12 micrometer bands or a different combination of multiple spectral bands [Ref. 2].

C. SENSITIVITY AND RESOLUTION

Sensitivity is related to the ability of TIS to detect small signals. Optical system properties, detector responsivity and system noise are all factors that determine sensitivity [Ref. 4]. Sensitivity can also be defined quantitatively as the change in signal that equals the rms noise value at some point in the TIS. When defined in this manner, sensitivity is described as a noise equivalent parameter. In thermal imaging, a commonly used sensitivity parameter is the Noise Equivalent Temperature Difference (NETD) [Ref. 3]. NETD is defined in the following section.

Resolution is an important factor that determines image quality [Ref. 5]. Imaging is fundamentally limited by the smallest angular detail that can be discerned. This limit is described by the term resolution. Higher resolution indicates a system's ability to correctly image higher spatial frequencies. Higher spatial frequencies represent finer details. Therefore, a system with high resolution will produce sharper and clearer images. Lloyd points out that there are three main reasons for this limitation. First, optical diffraction and aberrations cause a point source to be imaged as a spread point, the size of which is determined by the point spread function (PSF) of the optics. Second, the atmosphere affects the transmission of optical radiance, causing the blur spot to increase in size, change its amplitude and shift in space. Third, the detector is not a point, but has a finite-size aperture that integrates and averages signal over an area of the target scene [Ref. 3].

The Modulation Transfer Function (MTF) is commonly used to characterize resolution. MTF is explained in sufficient detail in the following section. Degradation of

system resolution by each component in the imaging chain can be represented by an MTF. Component MTFs are cascaded to obtain the overall system MTF.

System performance depends on both sensitivity and resolution. Generally, an increase in sensitivity comes at the price of a decrease in resolution. Because it is not possible to design a TIS with infinite resolution and infinite sensitivity, optimum TIS design involves trade-off analyses between sensitivity and resolution [Ref. 2]. MRTD is an appropriate performance measure that relates thermal sensitivity to spatial resolution. We will look at MRTD in detail in the next section.

D. PERFORMANCE MEASURES

1. Parameters of Interest

Before starting the discussion on summary performance measures, we will look at some of the critical parameters that will help understand the more complex and complete performance measures.

a. Field-of-View (FOV)

FOV of a TIS describes the angular space through which the TIS receives optical radiation. Area coverage of a TIS at a given range is determined by its FOV. From the geometry depicted in Figure 2.3 we can see that:

$$FOV_h = 2\tan^{-1}\left(\frac{A}{2F}\right) \tag{2.1}$$

$$FOV_v = 2\tan^{-1}\left(\frac{B}{2F}\right) \tag{2.2}$$

where:

FOV_h is the horizontal FOV in radians,

FOV_v is the vertical FOV in radians,

A and B are the image dimensions in millimeters, and

F is the optics effective focal length in millimeters,

For small angles where $\tan\theta = \theta$, the equations become

$$FOV_h = \frac{A}{F} \tag{2.3}$$

$$FOV_v = \frac{B}{F} \tag{2.4}$$

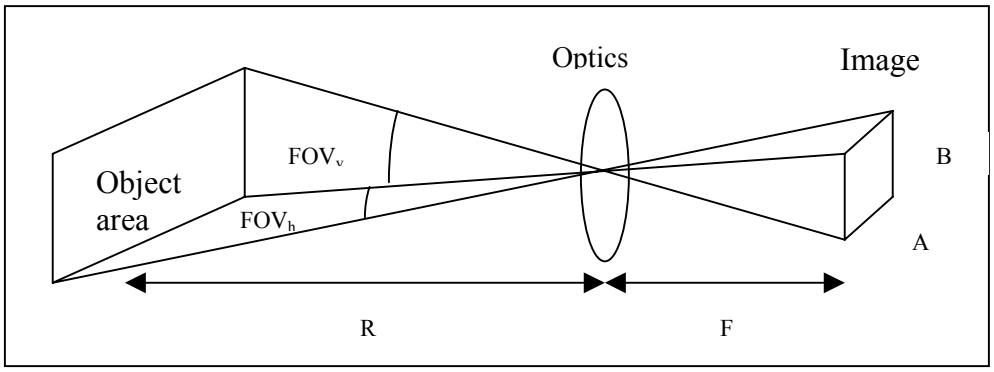

Figure 2.3. Field-of-View "After [Ref. 2]".

b. F Number (F/#)

F/# determines the light collecting ability of the lens and is given as

$$F/\# = \frac{F}{D_o} \tag{2.5}$$

where:

F is the optics effective focal length in mm,

D_o is the optics diameter in mm.

The F/# refers to the "speed" of the optics, and smaller F/# is faster. An F/# of one is an applicable limit, as smaller F/#s tend to give heavier optics [Ref. 2].

c. Instantaneous Field-of-View (IFOV) and Detector Angular Subtense (DAS)

IFOV describes the solid angular coverage of an individual detector element. It is given as

$$IFOV = \frac{A_d}{F^2} \tag{2.6}$$

where:

A_d is the detector element area in mm^2,

F is the optics effective focal length in mm

DAS defines the maximum resolution that can be achieved due to detector limitations. For a rectangular detector:

$$\alpha = \frac{a}{F} \tag{2.7}$$

$$\beta = \frac{b}{F} \tag{2.8}$$

where:

α and β are the horizontal and vertical detector angular subtenses in milliradians,

a and b are the detector horizontal and vertical dimensions in micrometers,

F is the optics effective focal length in mm.

2. Modulation Transfer Function (MTF)

Imaging is a convolutionary process. The image distribution is the object distribution convolved with the point spread function (PSF). Thermal imaging systems include a series of components, and the object space includes complicated objects. The convolutionary process in this case becomes too difficult to deal with analytically. Using the convolution theorem makes the analysis easier to handle [Ref. 6].

The convolution theorem says that the Fourier transform of the convolution of two functions is equal to the product of the Fourier transforms of the individual functions. This translates into the fact that the image spectrum is the Optical Transfer Function (OTF) multiplied by the object spectrum. Taking the inverse Fourier transform gives the image distribution [Ref. 7].

The Fourier transform of the PSF is the OTF. OTF is the spatial frequency response of the TIS. It is given as a complex quantity.

$$OTF = MTFe^{-jPTF} \tag{2.9}$$

The magnitude of OTF is the MTF, and the phase is defined by the Phase Transfer Function (PTF). MTF is the primary measure of the overall system resolution. System MTF is obtained by point-by-point multiplication of component MTFs. [Ref. 2]. Figure 2.4 demonstrates this process.

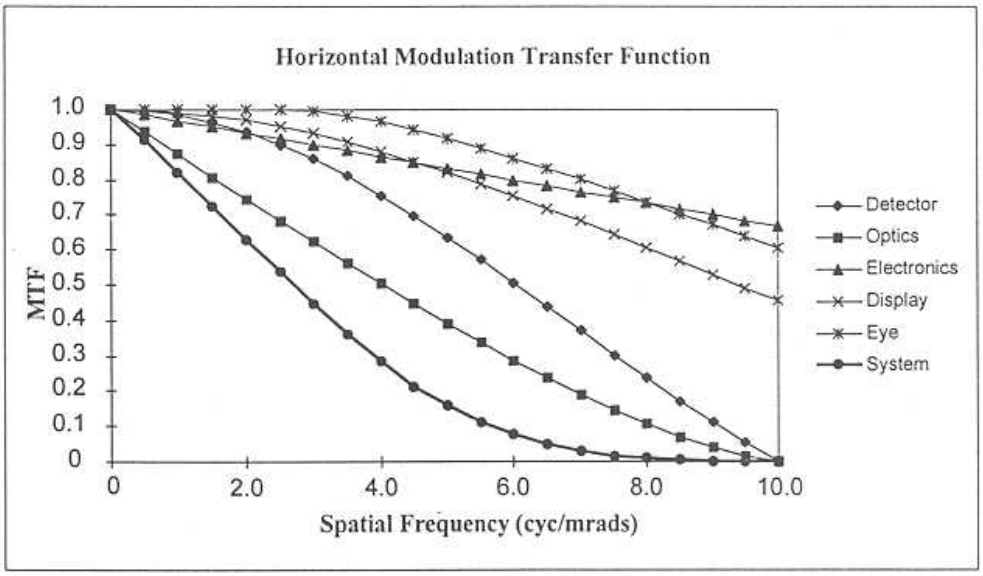

Figure 2.4. System MTF (MTF Cascade). The system MTF is the product of the sub-system MTFs "From [Ref. 2]".

Higher MTF values mean that the system can faithfully reproduce the scene at those spatial frequencies. Lower values of MTF indicate that the scene details corresponding to those spatial frequencies will be reproduced with low contrast.

System cutoff is that spatial frequency where MTF goes to zero. Beyond the cutoff, the system can still detect the target, but resolution is not possible. A four-bar target, for example may appear as a single square target [Ref. 3].

Modulation transfer is given as

$$MTF = \frac{Output\ Modulation}{Input\ Modulation} \tag{2.10}$$

Figure 2.5 depicts how MTF is obtained.

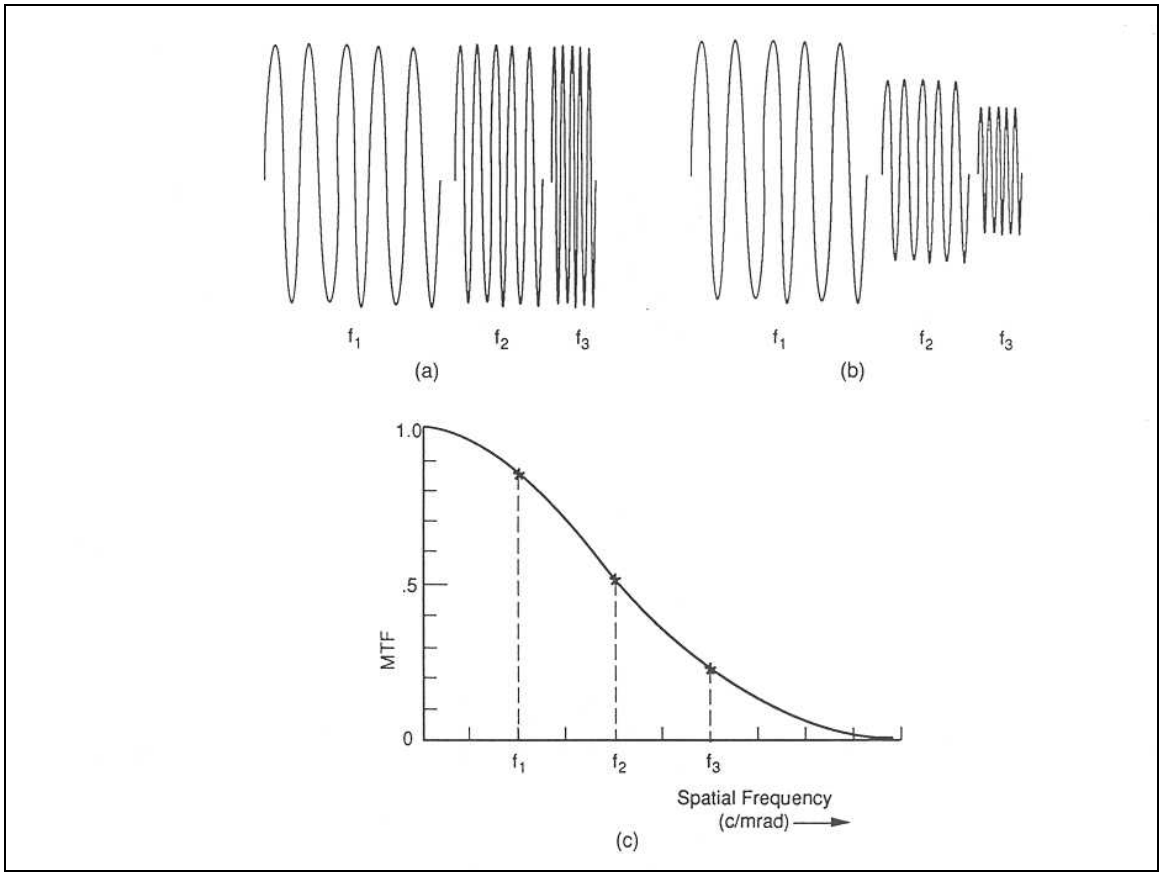

Figure 2.5. Definition of MTF for Three Spatial Frequencies: (a) Input Modulation, (b) Output Modulation, (c) MTF "From [Ref. 3]".

Modulation is shown in Figure 2.6 and its formulation is given as

$$Modulation = \frac{B_{\max} - B_{\min}}{B_{\max} + B_{\min}} \tag{2.11}$$

where:

B_{max} and B_{min} are the maximum and minimum intensity levels as defined in Figure 2.6.

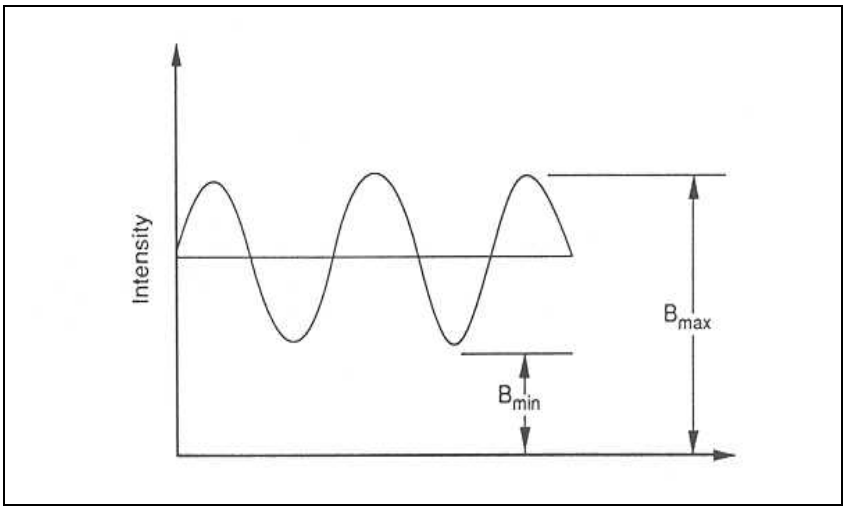

Figure 2.6. Definition of Modulation "From [Ref. 3]".

3. Noise Equivalent Temperature Difference (NETD)

NETD is a convenient measure of the sensitivity of a TIS. It is defined as the temperature difference between a large square target and its uniform background, which is required to produce a peak signal to rms noise ratio of unity at a particular point in the signal processing chain [Ref. 3]. Holst [Ref. 3] points out that it is often easier to measure performance parameters than to calculate them. Measurement schemes for the performance parameters defined in this chapter are treated in Reference 3. It is beyond the scope of this thesis to rigorously treat the measurement procedures and the derivations of these performance parameters. Complete derivation of NETD can be found in References 2 and 6. Here we will look at the final formulation to appreciate the significance of the system parameters and to have a "feel" for the factors that have to be considered in the design and performance modeling of TIS.

The following formulation of NETD is taken from Shumaker etal. [Ref. 8].

$$NETD = \frac{20F\left(FOV_h FOV_v F_{dot} N_{os} N_{ss}\right)^{1/2}}{\tau_o \left(\pi N_D \eta_{sc}\right)^{1/2} D_o{}^2 \alpha\beta D^* \partial W / \partial T} \tag{2.12}$$

where:

F is the optics effective focal length in meters

FOV_h is the horizontal FOV in mrad

FOV_v is the vertical FOV in mrad

F_{dot} is the frame rate in Hz.

N_{os} is the overscan ratio

N_{ss} is the serial scan ratio

τ_o is the transmittance of the optics

N_D is the number of detectors

η_{sc} is the scan efficiency

D_o is the optics aperture diameter in meters

α is the horizontal DAS in mrad

β is the vertical DAS in mrad

D* is the band average detectivity in cm $Hz^{1/2}$ /Watts

$\partial W / \partial T$ is the thermal derivative of Planck's equation in Watts/(cm^2KSr)

Inherent in the definition and the formulation of NETD is the assumption that the sources are blackbody radiators and atmospheric transmittance is equal to one. NETD is a simplistic performance measure in the sense that it does not include the observer and display performance. It also does not include any spatial frequency effects. It is not a convenient measure to compare overall TIS performance. However it does provide a general idea on system performance and it is a fundamental step in the derivation of more complex and complete performance measures [Ref. 3].

4. Minimum Detectable Temperature Difference (MDTD)

MDTD is a laboratory measure of TIS sensitivity including the observer and display effects. It relates to the noise-limited detection performance of TIS and it is used in some detection range prediction schemes [Ref. 8]. MDTD is defined as the temperature difference between a square target and its uniform background, which is

required for a trained observer to just detect the target when viewing the target through the TIS. The observer is given unlimited time for detection and knows where on the display to look for the target [Ref. 3].

MDTD is given in Reference 8 as

$$MDTD(f_s) = \frac{(SNR_{thr})(NETD)(\Omega_T + r_s{}^2)(\alpha\beta)^{1/2}}{\Omega_T \left[\frac{\pi}{4} \left(r_s{}^2 + r_B{}^2 + \Omega_T \right) t_e F_{dot} N_{os} N_{ss} \right]^{1/2}} \tag{2.13}$$

where:

f_s is the spatial frequency of the MDTD target in cy/mrad and given as $1/\left(2\sqrt{\Omega_T}\right)$

SNR_{thr} is the threshold signal-to-noise ratio for detection

NETD is the noise equivalent temperature difference

Ω_T is the target solid angular subtense in $(\text{mrad})^2$

α is the horizontal DAS in mrad

β is the vertical DAS in mrad

r_s is the resolution of the system in mrad

r_B is the resolution of the back-end in mrad

t_e is eye integration time in seconds

F_{dot} is the frame rate in Hz.

N_{os} is the overscan ratio

N_{ss} is the serial scan ratio

System resolution includes front-end and back-end resolution. The back-end resolution includes detector electronics, preamplifiers, multiplexer, display and eye resolution effects.

5. Minimum Resolvable Temperature Difference (MRTD)

MRTD is a noise-limited threshold measure of TIS spatial resolution and thermal sensitivity including the characteristics of the human observer. It is defined as the temperature difference between a four-bar target and its uniform background, which is required by a trained observer to just resolve all four bars when viewing the target through the TIS [Ref. 3].

The MRTD measurement scheme is presented in Chapter V. The MRTD measurement procedure allows the observer to adjust display gain and controls as well as his or her position to optimize the resolvability of the bar pattern. MRTD is plotted as a function of bar-pattern spatial frequency in Figure 2.7.

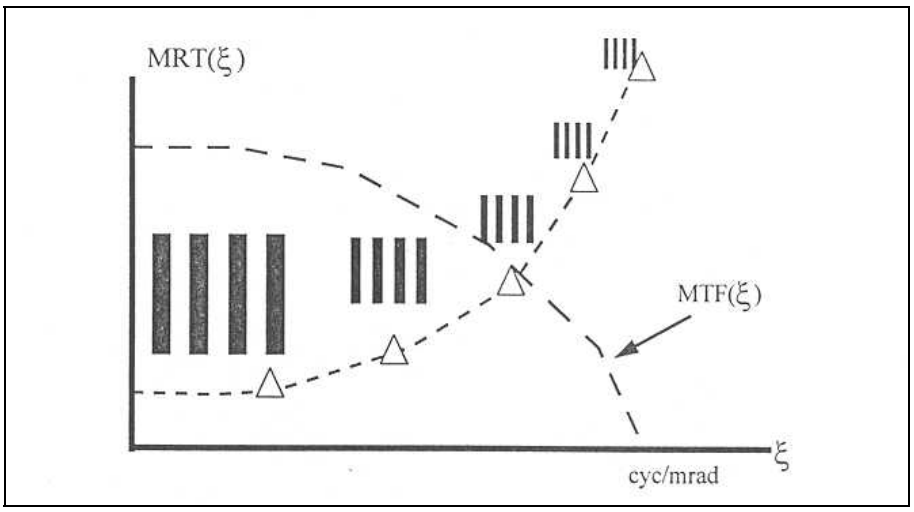

Figure 2.7. MRTD Curve as a Function of Four-Bar Target Spatial Frequency. Note the asymptotic rise at the spatial frequency where MTF goes to zero. "From [Ref. 2]".

The reason to use a four-bar target is that there is a correlation between the ability to resolve a bar pattern and the probabilities of detecting, recognizing and identifying targets in the field. Figure 2.8 shows an example four-bar target.

At range R the angle subtended by one cycle of the bar pattern (one bar and a space) in mrad is given as

$$\theta = \frac{2d}{R} \tag{2.14}$$

where:

d is the bar width in millimeters

R is the distance from the TIS to the bar pattern in meters

The reciprocal of this quantity gives us the four-bar pattern spatial frequency (f_s) in cycles/mrad.

$$f_s = \frac{R}{2d} \tag{2.15}$$

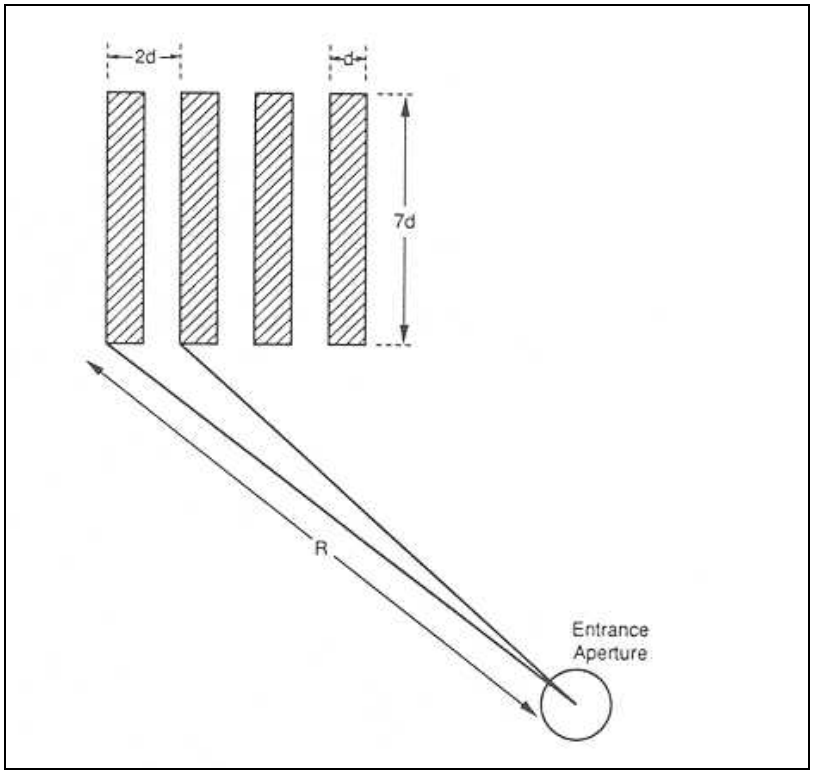

Figure 2.8. Definition of Spatial Frequency "From [Ref. 3]".

Unlike NETD, both MDTD and MRTD are not single parameters. They are functions of target spatial frequency. Also, they are overall TIS performance measures,

which include observer and display effects. Including the human in the loop makes them subjective measures. MRTD and MDTD measurement results depend on the training and motivation of the observer. Therefore, several observers are required to decrease the subjectivity and variability in the measurements [Ref. 3].

As depicted in Figure 2.7, MRTD shows an asymptotic behavior at the spatial frequency where MTF goes to zero. MDTD, on the other hand does not exhibit such an asymptotic rise, as MDTD is not linearly dependent on MTF. Figure 2.9 demonstrates this difference. The lack of this asymptotic behavior in MDTD suggests that if target-to-background temperature difference is high enough, target detection is possible out to very long ranges regardless of the size of the target.

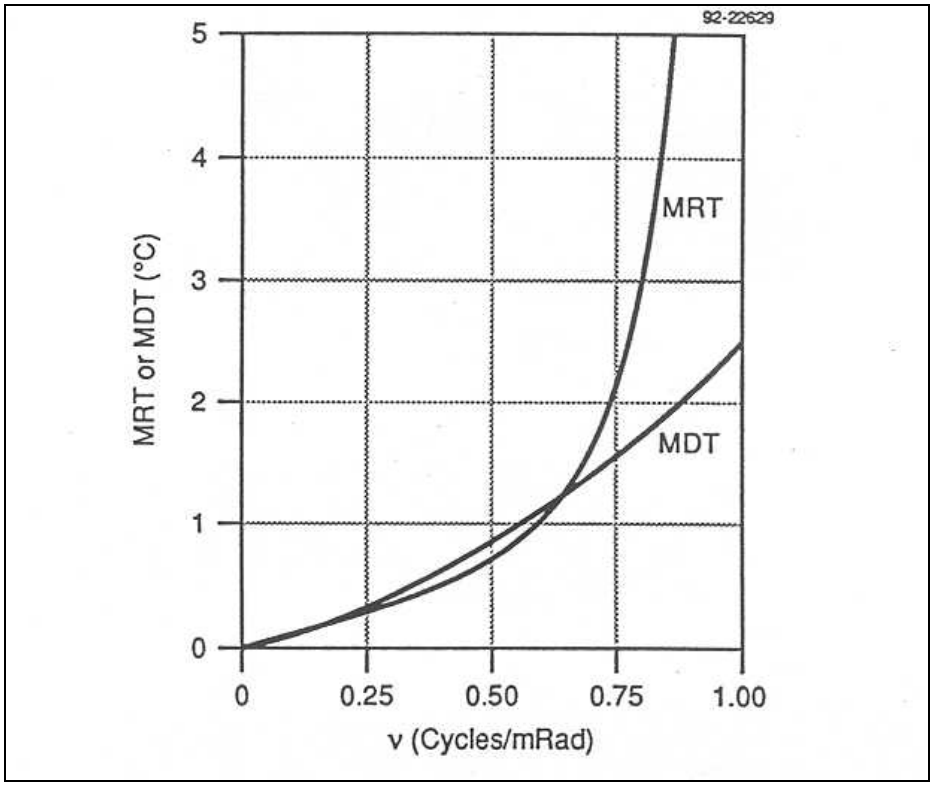

Figure 2.9. MRTD and MDTD Illustrating that the Asymptotic Rise Exists only for the MRTD. MDTD shows a relatively linear increase with the spatial frequency. "From [Ref. 8]".

MRTD is given by Shumaker etal. in the following form

$$MRTD(f_s) = \frac{2SNR_{thr}NETD\rho_x^{1/2}}{MTF_{sys}(f_s)}\left(\frac{f_s^{\,2}\alpha\beta}{L}\right)^{1/2}\left(t_e F_r N_{os} N_{ss}\right)^{-1/2} \tag{2.16}$$

where:

f_s is the spatial frequency of the MRTD target in cy/mrad and given in Equation 2.15

SNR_{thr} is the threshold signal-to-noise ratio

NETD is the noise equivalent temperature difference

ρ_x is the noise filter factor given in Equation 2.17

$MTF_{sys}(f_s)$ is the system MTF at spatial frequency f_s

α is the horizontal DAS in mrad

β is the vertical DAS in mrad

L is length-to-width ratio of the bar target, which is always equal to seven

t_e is eye integration time in seconds

F_{dot} is the frame rate in Hz.

N_{os} is the overscan ratio

N_{ss} is the serial scan ratio

The noise filter factor is given as

$$\rho_x = \left[1 + \left(2 f_s r_B\right)^2\right]^{-1/2} \tag{2.17}$$

However, this MRTD form does not account for noise sources other than detector noise and it does not incorporate sampling and aliasing effects. In the next chapter we will examine modeling for sampled staring TIS and we will look at different MRTD formulations that do include additional noise sources and sampling artifacts.

E. PERFORMANCE PREDICTION MODELS

Predicting the performance of TIS serves a number of uses. Modeling results provide a system designer with necessary tools to find out if a particular design will meet the requirements. Predictions also serve as a means of comparing different systems during the development process [Ref. 3].

As staring arrays become the prevalent type of detector arrays in thermal imaging systems, there has been extensive study in the infrared community in modeling their performance. Earlier models such as Ratches and Lloyd's, which were used efficiently in modeling the performance of scanning systems, do not cover sampling and noise concepts brought about by the staring systems. FLIR92, developed by U.S. Army Night Vision and Electronics Sensors Directorate (NVESD), do not include eye contrast limitations and aliasing effects due to under-sampling. New models have been proposed to include these effects in MRTD modeling. This section outlines the basic features and deficiencies of each model.

Modulation Transfer Function (MTF), Noise Equivalent Temperature Difference (NETD), Minimum Detectable Temperature Difference (MDTD) and Minimum Resolvable Temperature Difference (MRTD) are of particular importance pertaining to TIS performance. Among these, MRTD is the most important parameter that gives insight into the field performance of the system. Therefore most of the modeling efforts focus on MRTD modeling.

Some early models, also known as the first generation performance models, are developed to predict the performance of scanning TIS.

1. Ratches Model

Named after one of its principal authors, J.A. Ratches, the model was developed by U.S Army Night Vision Laboratory in 1975 [Ref. 9]. The model is also known as the "Night Vision Laboratory Static Performance Model", because it does not consider target acquisition and positioning concerns for actual field systems. The computer based Ratches model predicts NETD, MDTD, and MRTD for scanning TIS based on device

parameters. This model has been used as the standard MRTD prediction model for over a decade [Ref. 9].

2. Lloyd's Model

Introduced by J.M. Lloyd, this model for MRTD prediction (not coded for computer use) appeared near the same time with Ratches model. Lloyd's formulation for MRTD, which is much simplified through some assumptions compared to the Ratches Model, still remains popular [Ref. 9]. MRTD values predicted by the Lloyd's model tend to be more optimistic than those of the Ratches Model [Ref. 10].

Although Ratches' and Lloyd's models were quite popular in modeling the performance of scanning TIS, they did not address some important issues in TIS modeling, such as effects of sampling and noise characteristics other than the random detector noise [Refs. 9 and 10].

3. FLIR92 Model

In 1990, the FLIR90 TIS performance model was developed to account for different noise sources and effects of sampling. This model was then upgraded to FLIR92 by NVESD [Ref. 10]. FLIR92 is a desktop computer model that predicts standard summary performance measures for thermal imaging systems. The model uses basic system parameters to calculate MTF, NETD, MRTD and MDTD for scanning and staring systems. The model predicts whether or not a system achieves the required MTF, system noise, MRTD and MDTD determined necessary to perform target acquisition and discrimination tasks [Ref. 11], but does not address field performance (i.e. discrimination range prediction).

FLIR92 uses a sophisticated three-dimensional noise (3-D noise) concept to include the effects of noise sources other than the random detector noise [Ref. 10]. Chapter III covers this concept in greater detail. These effects are not predictable from the basic system parameters.

FLIR92 does have some limitations, too. First of all it does not address "aliasing" that is a common problem with staring sensors. FLIR92's method of dealing with the under-sampling problem is to cut off MRTD predictions at the system Nyquist frequency

[Ref. 9]. FLIR92 also assumes the presence of the human observer in the observation process. Therefore, it is not a suitable model to predict objective MRTD. These deficiencies are explained in greater detail in the next chapter.

4. Visibility Model

The Visibility model, presented in 1994 by Ronald J. Pieper and Alfred W. Cooper of the Naval Postgraduate School, is a MRTD prediction model that is based on a minimum threshold resolvable temperature difference [Refs. 9 and 12]. The basics of the model are explained in the next chapter.

The Visibility Model, VISMODII in its current form, successfully extends the MRTD prediction beyond the Nyquist frequency by incorporating sampling and aliasing effects. No assumptions are made about the observation process, which gives the model the flexibility to be used as an objective MRTD predictor.

5. NVTherm Model

The deficiencies of FLIR92 as a performance prediction model for staring TIS have led to researches to develop a new generation performance model.

Two characteristics of staring arrays can lead to errors in FLIR92 performance predictions. First, staring systems have high sensitivity, which causes the contrast limitations of the eye to become important in establishing performance limitations. Second, the limitations on detector size, spacing and fill factor can result in under-sampled imagery [Ref. 13].

NVTherm has been developed by NVESD to replace FLIR92. This new model predicts the MRTD for scanning and staring thermal imagers. It also offers a new option to calculate threshold contrast [Ref. 13].

The basic changes in MRTD calculation in NVTherm relative to FLIR92 may be grouped into two main areas, eye modeling and sampling effects. Sampling effects are incorporated into the model through "MTF Squeeze", a technique in which performance degradation due to undersampling is modeled as a corresponding decrease in system MTF. The MTF Squeeze approach will be explained in Appendix C.

III. VISMODII, OVERVIEW OF TERMINOLOGY AND PRINCIPLES OF OPERATION

The purpose of this chapter is to present the reader the origins and basic concepts of visibility-based modeling for MRTD prediction.

A. ORIGINS OF THE VISIBILITY MODEL

1. Modeling Principles

Thermal imaging system performance modeling efforts were introduced in Chapter II. Both the Ratches model and the FLIR92 model have been reported to produce MRTD results that are overly optimistic in the low spatial frequency limit and pessimistic at high spatial frequencies [Refs. 12, 14, 15 and 16].

The 1975 Ratches Model used the matched filter approach to model the eye-brain target recognition process [Ref. 17]. The FLIR92 model uses the matched filter concept in MDTD predictions, and a synchronous integrator concept for MRTD predictions [Ref. 11]. No matter how the eye-brain recognition process is modeled, the result remains controversial due to the subtleties involved in the actual recognition process.

The MRTD prediction models discussed in Chapter I, with the exception of the Visibility Model, use signal-to-noise ratio analysis to predict MRTD [Ref. 17]. The main idea in signal-to-noise ratio based MRTD prediction is that the eye requires a threshold signal-to-noise ratio depending on the level of the discrimination task.

Figure 3.1 demonstrates the VISMODI modeling concept. The Visibility model avoids the complex and controversial eye-brain modeling and introduces the threshold input contrast. This is intuitive since we expect that no matter how low the spatial frequency, i.e. how large the target pattern; one would require a threshold contrast for recognition [Ref. 9]. The threshold input contrast is the minimum temperature difference that can be detected by an observer or an ATR [Ref. 17]. The MRTD at the low frequency limit (where MTF is close to 1) is then modified by the system MTF to give the MRTD as a function of spatial frequency. This implies the MRTD formulation as

$$MRTD(f_s) = MRTD(f_s \rightarrow 0) \times MTF_{system}(f_s) \tag{3.1}$$

where:

f_s is the four bar pattern spatial frequency and $MRTD(f_s \rightarrow 0)$ is the MRTD in the low spatial frequency limit.

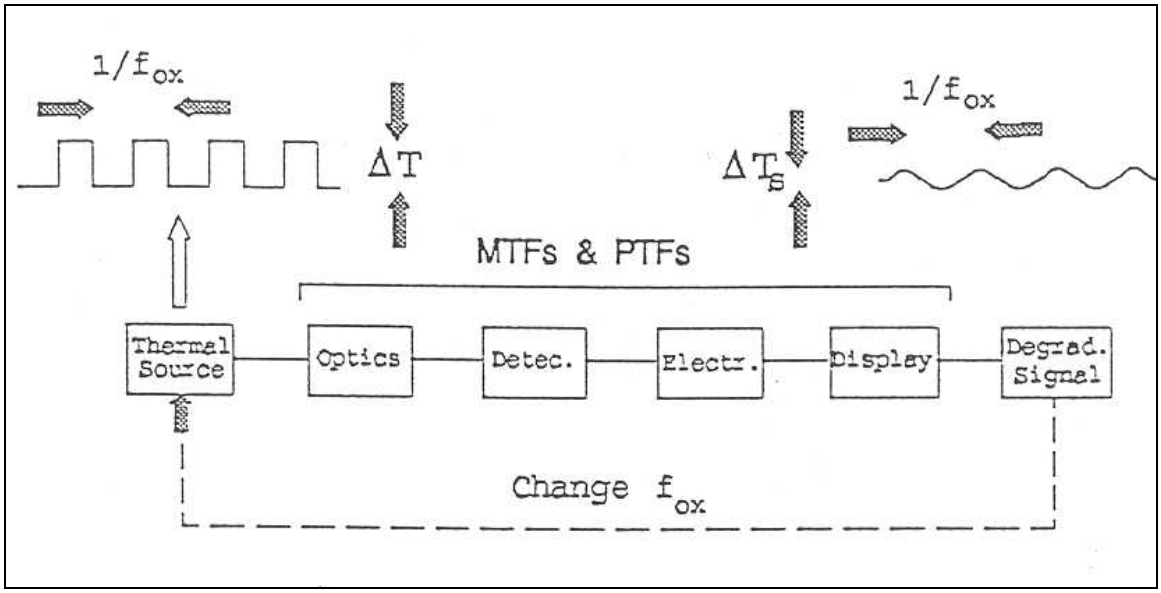

Figure 3.1. VISMODI Modeling Concept Illustrating the Reduction in Contrast due to the Sub-System MTF/PTFs "From [Ref. 12]".

In all of the MRTD prediction models discussed throughout this thesis, contrast is modeled by a target-to-background temperature difference. The Visibility model inherently suggests that a four-bar pattern is not recognizable below a minimum value, which is defined as "the critical delta T" [Ref. 17].

2. Advantages over Non-visibility Models

Although the 1975 NVL Model has served as a useful tool for MRTD prediction and was widely used by the infrared community, a number of shortcomings in the model and inconsistencies in MRTD predictions as compared with laboratory measurements have been reported [Ref. 17].

The Visibility model is not complicated and is based on a fairly understandable and physically intuitive observation that there should be a threshold contrast in the low

frequency limit, which enables the model to bypass the complexity of eye-brain modeling. Instead, the analysis in the model places the main emphasis on the reduction of contrast due to spatial frequency limiting factors, i.e., the MTFs of the subsystem components and sampling [Ref. 17].

MRTD predictions from the Visibility model have been shown to be in better agreement with the laboratory measurements. For example, the model does not predict an MRTD that goes to zero at the low spatial frequency limit.

The typical MRTD measurement process involves the decision of a human observer, which makes it subjective, and limits repeatability. Automatic target recognition technology is an area that is rapidly developing and being incorporated in a number of applications. Therefore, a predictive model for objective MRTD is required [Ref. 12]. The Visibility model makes no assumptions about the recognition process, and has the potential to be used as an objective MRTD predictor [Ref. 17].

B. SECOND GENERATION MODELING REQUIREMENTS

The developments in staring focal plane arrays brought about the need for revision of the performance models. Among the modeling concerns that need to be addressed are the effects of different noise sources other than detector noise, aliasing effects due to undersampling in the focal plane arrays and the sample scene phasing effects that occur when there is misalignment between the image to be sampled and the sampling lattice, i.e., the detector elements [Ref. 9]. This section covers how these effects manifest themselves in the imagery and how they are handled by FLIR92. In the next two sections of this chapter we will cover how these modeling concerns are addressed in the VISMODII code and in what areas the previous version of the VISMODII model [Ref. 9] needed improvement.

1. Noise in Second Generation Staring Systems

Staring focal plane arrays introduced some noise components that were not included in the models originally developed for serial and parallel scanning TIS. Noise has been introduced in the models through NETD for the first and second-generation scanning systems. However, this approach is not accurate for staring systems. The

directional noise components present in the staring FPA imagers may sometimes become more significant than the detector noise that was treated as the dominant noise source in the first generation systems [Ref. 9].

Directional noise is incorporated the in FLIR92 code as a three-dimensional noise model [Refs. 2-4, 9-11 and 18]. The advantage of the 3-D noise model is its ability to divide a fairly complex phenomenon into understandable components [Ref. 4]. Figure 3-2 illustrates the three-dimensional noise coordinate system. The T axis is the temporal dimension representing subsequent frames. H and V represent the horizontal and the vertical spatial coordinate axes respectively. The detector elements in the staring array are represented by m and n.

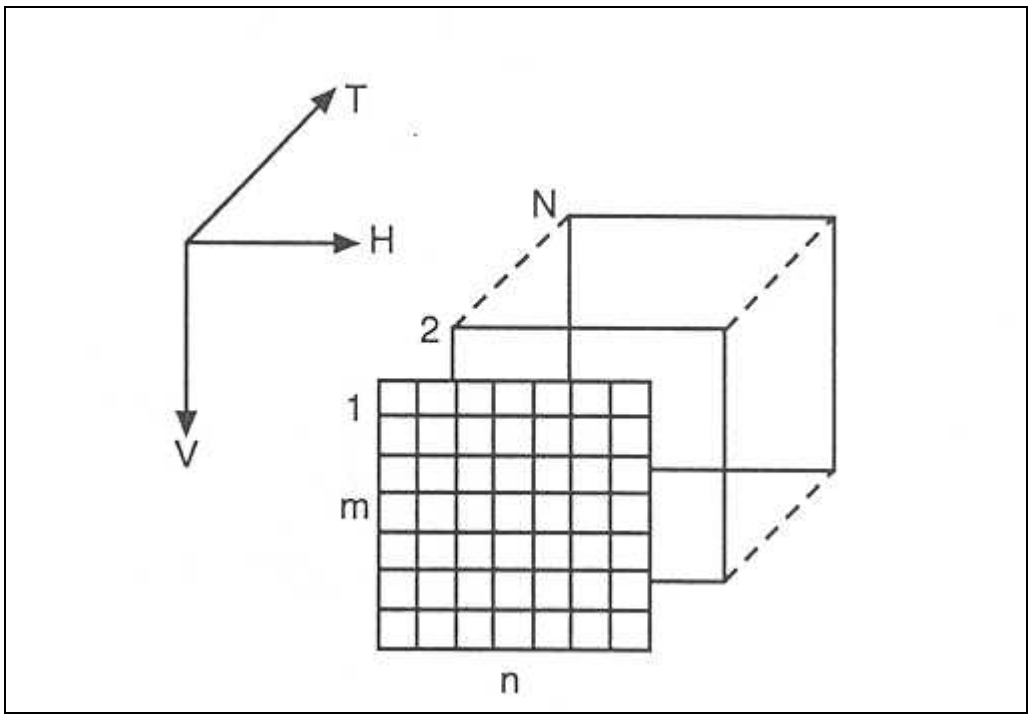

Figure 3.2. 3-D Noise Coordinate System "From [Ref. 4]".

Directional noise component descriptions along with the main sources are given in Table 3-1.

Noise	Description	Source
σ_{tvh}	Random spatio-temporal noise	Basic detector temporal noise
σ_{tv}	Temporal row noise, e.g. line bounce	Line processing, 1/f, read-out
σ_{th}	Temporal column noise, e.g. column bounce	Scan effects
σ_{vh}	Random spatial noise, e.g. bi-directional fixed pattern noise	Pixel processing, detector-to-detector non uniformity, 1/f
σ_{v}	Fixed row noise, e.g. line-to-line non-uniformity	Detector-to-detector non-uniformity
σ_{h}	Fixed column noise, e.g. column-to-column non-uniformity	Scan effects, detector-to-detector non-uniformity
σ_{t}	Frame-to-frame noise, e.g. frame bounce	Frame processing
S	Mean of all noise components	

Table 3.1. Three-Dimensional Noise Components "From [Ref. 19]".

The noise components described in Table 3.1 are considered to be statistically independent and each noise component has zero mean. The noise components have different origins and their existence is system specific [Ref. 4]. Total system noise is considered to be the summation of individual directional noise components. The total noise variance is then the sum of the variances of the individual components. The system noise standard deviation is:

$$\sigma_{total} = (\sigma_t^{\,2} + \sigma_v^{\,2} + \sigma_h^{\,2} + \sigma_{tv}^{\,2} + \sigma_{th}^{\,2} + \sigma_{vh}^{\,2} + \sigma_{tvh}^{\,2})^{1/2} \tag{3.2}$$

The basic detector noise, $\sigma_{tvh,}$ was the only noise included in the early models through NETD. FLIR92 can predict only the random detector noise from the parameters of the TIS. The other components are either measured or estimated [Ref. 11]. The directional noise components in the 3-D noise model are converted into temperature units in a similar way to that used in NETD [Ref. 2]. Some noise components may not be present for the particular system being modeled [Ref. 9].

σ_{tvh} is similar to NETD with the bandwidth taken as the actual noise bandwidth of the system instead of the equivalent noise bandwidth associated with the reference filter concept used in NETD calculation:

$$\sigma_{tvh} = NETD \times \frac{\sqrt{\Delta f_p}}{\sqrt{\Delta f_n}} \tag{3.3}$$

where:

Δf_p is the actual noise bandwidth of the TIS

Δf_n is the noise equivalent bandwidth used in NETD calculation.

MRTD in the two-dimensional prediction models is defined for two orthogonal directions as horizontal and vertical MRTD corresponding to the orientation of the bar pattern. Therefore, the noise components are combined into horizontal and vertical noise correction functions, which are then used as multiplicative terms in the MRTD equation. Eye-brain integration factors E_t, E_v and E_h corresponding to the eye-brain temporal and spatial integrations in the subscripted direction are applied to each noise component to model the signal-to-noise improvement by the eye-brain recognition process.

The following definitions and equations are adapted from the ones used for staring array imagers in Reference 11.

The MRTD equation is given by:

$$\mathrm{MRTD}_z(f_s) = \left(\frac{\frac{\pi^2}{8}\mathrm{SNR}_{thr}\,\sigma_{tvh}\,k_z(f_s)}{H_{sys_z}(f_s)} \right) [E_t E_{h_z}(f_s) E_{v_z}(f_s)]^{1/2} \qquad (3.4)$$

where:

z is the direction of interest, either horizontal or vertical,

SNR_{thr} is the threshold signal-to-noise ratio,

σ_{tvh} is the random spatio-temporal noise in degrees C,

$H_{sys_z}(f_s)$ is the overall system MTF,

$k_z(f_s)$ is the noise correction function,

E_t is the eye-brain temporal integral,

$E_{h_z}(f_s)$ is the eye-brain horizontal spatial integral, and

$E_{v_z}(f_s)$ is the eye-brain vertical spatial integral,

Random spatio-temporal noise is predicted from system parameters:

$$\sigma_{tvh} = \frac{4\,F/\#^2\,\sqrt{\Delta f_p}}{\pi\tau_o\sqrt{A_d}\left(\int_{\lambda 1}^{\lambda 2} D^*(\lambda,300)\,\frac{\partial W}{\partial T}(\lambda)\,d\lambda\right)} \tag{3.5}$$

and the noise correction factors are defined as:

$$k_h(f_s) = \left(1 + \frac{\sigma^2_{vh}}{\sigma^2_{tvh}E_t} + \frac{\sigma^2_{th}}{\sigma^2_{tvh}E_{vh}(f_s)} + \frac{\sigma^2_{h}}{\sigma^2_{tvh}E_tE_{vh}(f_s)}\right)^{1/2} \tag{3.6}$$

for the horizontal direction, and

$$k_v(f_s) = \left(1 + \frac{\sigma^2_{vh}}{\sigma^2_{tvh}E_t} + \frac{\sigma^2_{tv}}{\sigma^2_{tvh}E_{hv}(f_s)} + \frac{\sigma^2_{v}}{\sigma^2_{tvh}E_tE_{hv}(f_s)}\right)^{1/2} \tag{3.7}$$

for the vertical.

In the equations given above, $\frac{\partial W}{\partial T}$ is the thermal derivative of Planck's equation, and f_x and f_y are the horizontal and vertical spatial frequencies respectively.

The eye-brain temporal integration factor is given by:

$$E_t = \frac{\alpha_t}{F_{dot}\,t_e} \tag{3.8}$$

where α_t is the temporal sample correlation factor that is usually set to 1.

The eye-brain spatial integration factor is given in doubly subscripted notation with the first subscript being the direction of spatial integration and second subscript

being the orientation of the MRTD target bar pattern. The spatial integration terms for horizontal MRTD are:

$$E_{hh}(f_s) = \frac{\alpha}{s_h}\left[\int_{-\infty}^{\infty} H^2{}_{NF\,h}(f)\left(\frac{\sin\left(\frac{\pi f}{2f_s}\right)}{\frac{\pi f}{2f_s}}\right)^2 df\right] \tag{3.9}$$

and

$$E_{vh}(f_s) = \frac{\beta}{s_v}\left[\int_{-\infty}^{\infty} H^2{}_{NF\,v}(f)\left(\frac{\sin\left(\frac{7\pi f}{2f_s}\right)}{\frac{7\pi f}{2f_s}}\right)^2 df\right] \tag{3.10}$$

For vertical MRTD

$$E_{hv}(f_s) = \frac{\alpha}{s_h}\left[\int_{-\infty}^{\infty} H^2{}_{NF\,h}(f)\left(\frac{\sin\left(\frac{7\pi f}{2f_s}\right)}{\frac{7\pi f}{2f_s}}\right)^2 df\right] \tag{3.11}$$

and

$$E_{vv}(f_s) = \frac{\beta}{s_v}\left[\int_{-\infty}^{\infty} H^2{}_{NF\,v}(f)\left(\frac{\sin\left(\frac{\pi f}{2f_s}\right)}{\frac{\pi f}{2f_s}}\right)^2 df\right] \tag{3.12}$$

In Equations 3.9 through 3.12, $H_{NF\,v}$ and $H_{NF\,h}$ are the horizontal and vertical system noise filter MTFs respectively, and s_h and s_v are defined as the number of samples per horizontal and vertical DAS respectively.

2. Sampling and Aliasing Effects

All imaging systems feature some form of sampling process. Staring FPAs usually sample the scene at equal sampling rates in both horizontal and vertical dimensions due to the symmetry of detector locations [Ref. 4].

Figure 3.3 demonstrates the spatial sampling by the detector elements. Samples are obtained at intervals of the detector pitch.

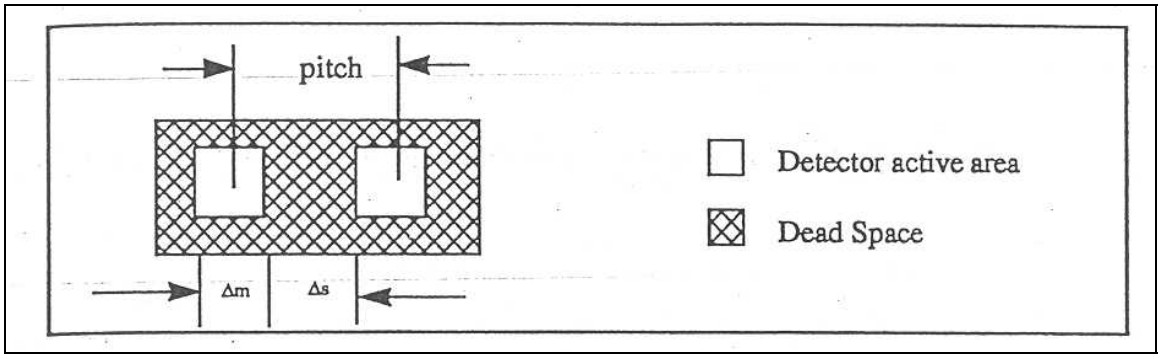

Figure 3.3. Spatial Sampling by Detector Element. The detector elements sample the scene at intervals of the pitch in each direction by integration over the active area. "From [Ref. 9]".

The spatial angular sampling period is given by:

$$\Lambda = \frac{\Delta m + \Delta s}{F} \tag{3.13}$$

where:

Λ is the sampling period in milliradians

F is the optics effective focal length in meters

Δm and Δs are detector active dimension and spacing between the detector elements respectively in mm .

The spatial sampling frequency is the reciprocal of the spatial sampling period. A value one half of the sampling frequency is known as the Nyquist frequency. Aliasing occurs when the scene contains frequency content above the Nyquist limit. Input signals

above the Nyquist frequency cannot be faithfully reproduced by the system and are aliased back into lower frequencies.

Aliasing is always present in undersampled systems. However, effects of aliasing and the degree to which it interferes with the recognition and detection depend on the scene. Aliasing tends to become more apparent as image distortion and degradation when viewing periodic scenes such as a four bar pattern and may increase MRTD [Ref. 4].

The detector array acts as a sampling lattice that spatially samples the scene in two dimensions. This process can be thought of as multiplying the image of the target scene that falls on the detector plane by an array of delta functions centered at the individual detector locations. Figure 3.4 demonstrates the staring FPA as a two dimensional sampling lattice.

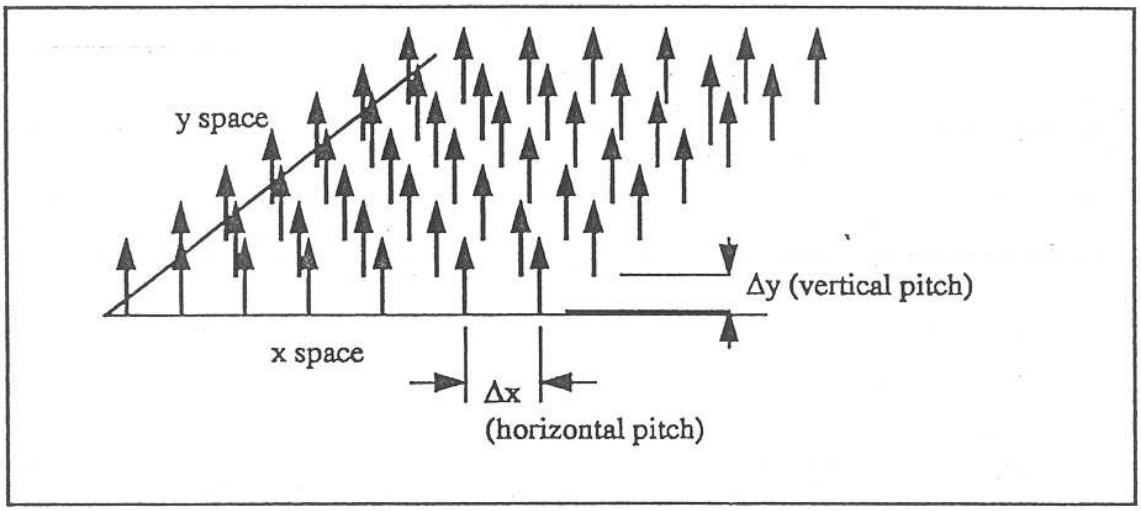

Figure 3.4. Staring FPA as a Two-Dimensional Sampling Lattice. Note the delta functions illustrating the sampling by each individual detector element "From [Ref. 9]".

Sampling and aliasing effects are more easily appreciated when examined in the spatial frequency domain. The convolution theorem states that multiplication in the space domain corresponds to convolution in the frequency domain. Since convolution by a delta function gives the original spectrum centered on the location where delta function is

defined, the sampling effect reduces to replication of the image spectrum at integer multiples of the sampling frequency. This effect is demonstrated in Figure 3.5.

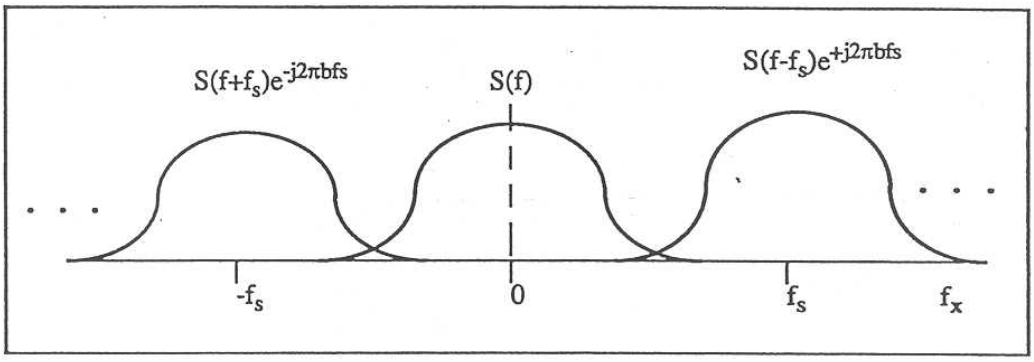

Figure 3.5. Representation of Sampling by a FPA in Spatial Frequency Domain. Sampling process creates the replicas of the original spectrum centered at the sampling frequency on positive and negative sides of the spectrum. "From [Ref. 9]".

If the highest spatial frequency component (f_{max}) is greater than half the sampling frequency, replicas generated by the sampling process interfere with the base band signal.

Aliasing cannot be removed once it has occurred. There are some proposed methods to reduce aliasing. One method is to optically band limit the input scene by matching the optical cutoff frequency to the Nyquist limit. This can be achieved by low pass filtering the signal by pre-sampling MTFs. This method is not desirable since it degrades system MTF in the base band and decreases resolution.

Holst [Ref. 4] points out that using an anti-alias filter that eliminates all frequencies beyond the Nyquist limit is not practical in imaging applications. He also points out that sampling theory has been developed by the audio industry where frequency distortion caused by aliasing is highly undesirable since the human ear is a frequency detector. However in imagery some degree of aliasing can be tolerated since the eye is not as sensitive to changes in the frequency spectrum since, unlike the human ear, the human eye is an intensity detector.

Another approach is known as microscanning in which the sampling frequency is increased by decreasing the detector center-to-center spacing. This is achieved by moving

the detector line of sight in small increments [Ref. 4]. One disadvantage of microscan is, however, the reduction in the integration time, which can result in reduced sensitivity. For detailed treatments of the microscanning technique the reader is referred to References 4 and 20.

There is a trade-off between preventing aliasing and maintaining high resolution. The optics and detector MTFs and the sampling spacing are optimized to reduce aliasing and preserve high overall system MTF [Ref. 2].

H.V. Kennedy [Ref. 18] states that the standard first-generation model does not take into account sampling and aliasing effects. He points out that in modeling staring array type imagers, sampling and aliasing are features that cannot be ignored.

Various concepts have been developed to model aliasing sampling effects. The FLIR92 model does not predict MRTD results beyond the Nyquist limit and avoids this problem by ignoring aliasing effects [Ref. 11]. The approach of FLIR92 is clearly inadequate, since some useful information is still present beyond the Nyquist limit.

E.G.D. Youngs and R.K. McEwen [Ref. 21] present a model in which the definition of MRTD is "relaxed" from the observation of all four bars to simply the observation of bars beyond the Nyquist limit to allow the extension of MRTD into the spatial frequency region where all four bars cannot be observed due to aliasing effects.

VISMODII follows Park and Hazra's [Ref. 22] method of modeling aliasing as noise. This approach is explained thoroughly in the next section.

NVTherm develops a semi-empirical method by extending a "spurious response" concept. Sampling is treated as an additional blurring effect. The MTF Squeeze approach is developed to model this additional blur. The Squeeze model is treated in Appendix C along with a comparison between the concepts used by VISMODII and NVTherm.

3. Sample-scene Phasing Effects

Sampled imagers are not shift invariant. This means that the response of the system, and thus the MTF, is not unique. When viewing a periodic target, misalignment between the target pattern and the detector elements result in a phase difference. The amount of the misalignment affects the output signal level.

Figure 3.6 demonstrates a detector array sampling a four-bar target. Laboratory procedure for MRTD measurement includes the adjustment of target phase so that maximum output can be obtained [Refs. 4 and 11]. If the sensor is not adjusted to optimize the location of target image on the detector array so as to minimize phasing effects, MRTD may degrade. This effect is included in FLIR92 through an additional sample-scene phase MTF [Ref. 11].

C.M. Webb [Ref. 23] points out that the phase relationship between the target and the detector array has a significant impact on MRTD. The scene-phasing effect on MRTD is reported to be greater at spatial frequencies closer to the Nyquist limit [Ref. 21]. An approach can be to represent MRTD as a bundle of curves each corresponding to differing degrees of phase mismatch.

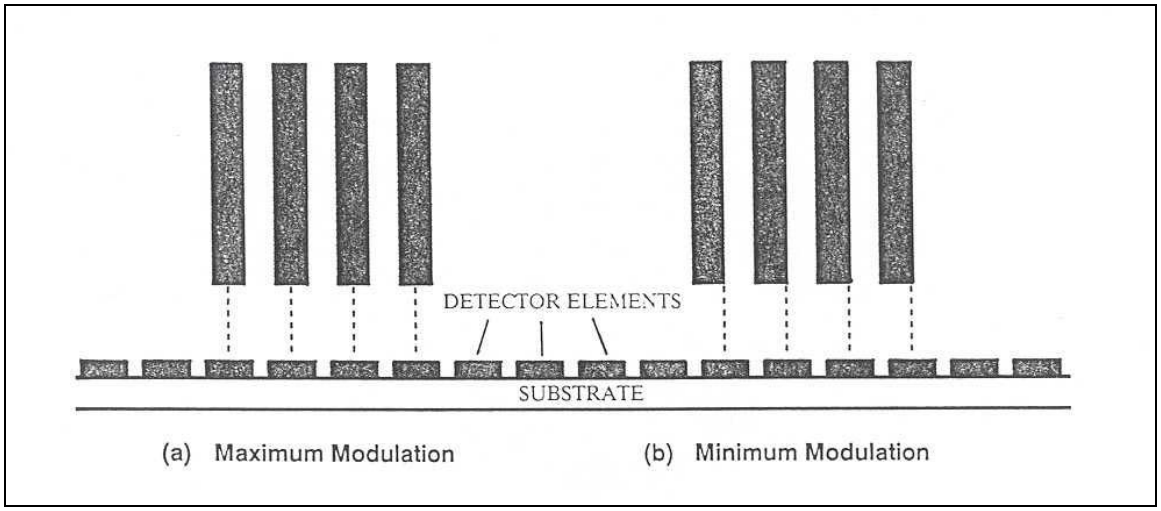

Figure 3.6. Detector Elements Sampling a Four-Bar Target: (a) Maximum Modulation Corresponding to the Perfect Alignment between the Detector Elements and the Bars, (b) Minimum Modulation Corresponding to the Highest Degree of Misalignment. "From [Ref. 21]".

C. VISMODII MODELING CONCEPTS

The VISMODII modeling concept is summarized in Figure 3.7. The basic thrust for VISMODII is to apply the visibility concept introduced by VISMODI to second-generation thermal imaging systems that incorporate staring focal plane arrays. One main advantage of the model is its simplicity, achieved by avoiding complex eye/brain integration factors. The theoretical foundation for this is explained in Reference 12. In the low frequency limit, the four-bar pattern appears as a step function rather than a periodic target. Therefore, application of resolution enhancement factors related to eye/brain perception is not appropriate.

VISMODII was written using MATLAB computational software.

1. MRTD Formulation

The form suggested for MRTD in VISMODII is the form that has been used in VISMODI [Ref. 24].

$$MRTD(f_z) = MRTD(f_z \rightarrow 0) \times \frac{1}{\alpha(f_z)} \tag{3.14}$$

where:

$MRTD(f_z)$ is the MRTD in the direction given by subscript z,

$MRTD(f_z \rightarrow 0)$ is the MRTD in the low frequency limit, and

$\alpha(f_z)$ is the contrast transference parameter.

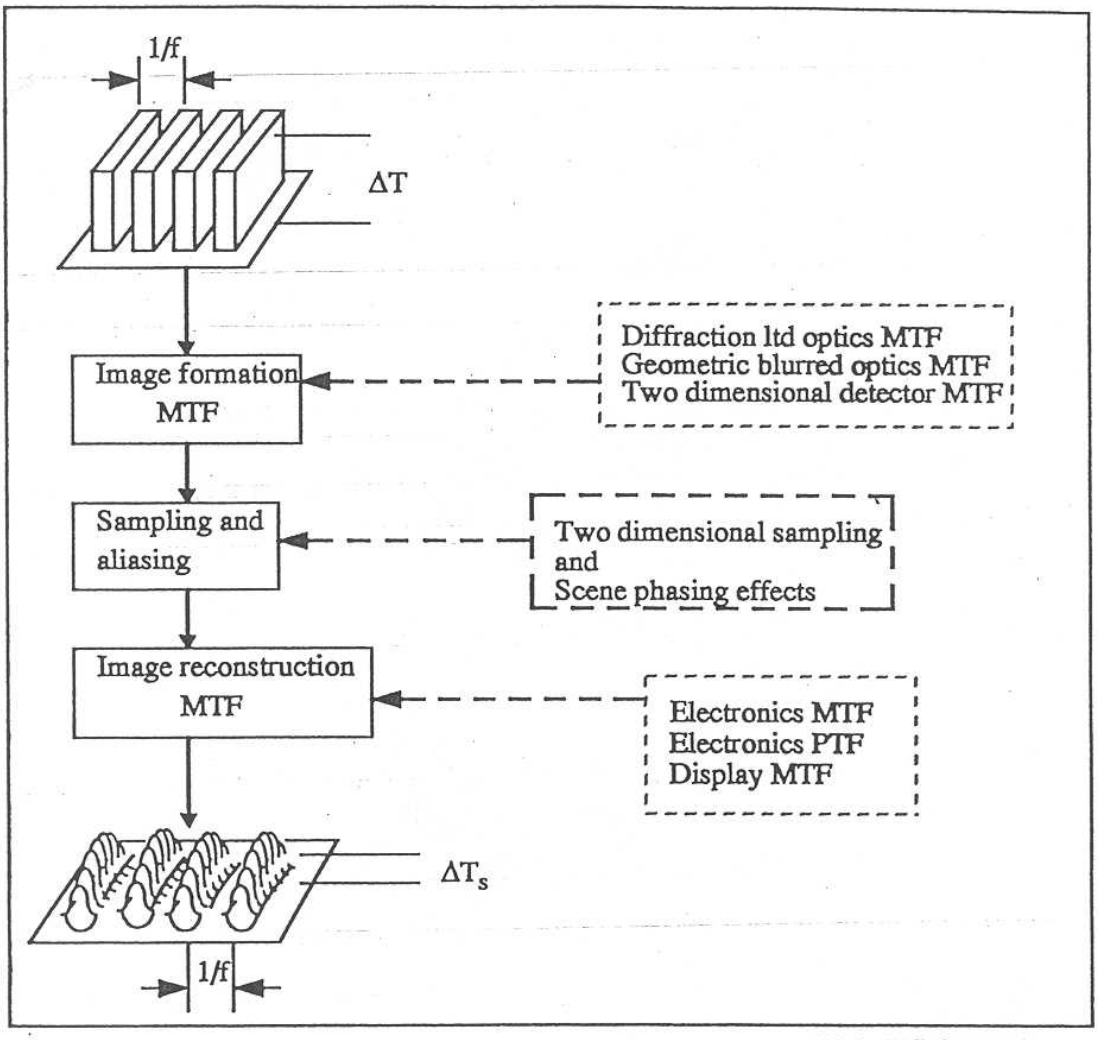

Figure 3.7. VISMOD II Modeling Concept "From [Ref. 9]".

A two dimensional bar pattern of contrast ΔT will have a degraded contrast of ΔT_s at the output of the imager due to aliasing and blurring effects of the TIS. The contrast transference parameter is given as the ratio of output contrast to the input contrast.

$$\alpha(f_z) = \frac{\Delta T_s(f_z)}{\Delta T} \tag{3.15}$$

2. Threshold Input Contrast

All observer and system noise parameters are combined into the threshold input contrast (ΔT_{sc}) parameter with no assumptions being made about the nature of the observation process [Refs. 9 and 24]. This term is system and observer dependent and represents the minimum contrast resolvable by a human observer or an ATR device. It can either be measured as the observer/ATR response to a step function or predicted by the model using device parameters. VISMODII uses a measured value for objective (ATR) threshold input contrast and the following heuristic formulation, which is derived by upgrading the VISMODI formulation with the FLIR92 3-D noise components [Ref. 9], for subjective minimum threshold contrast:

$$\Delta T_{sc} = \frac{\pi^2}{8} SNR_{thr} \sigma_{tvh} \left(1 + \frac{\sigma_{vh}^{\ 2}}{\sigma_{tvh}^{\ 2}} \right)^{1/2} (E_t)^{1/2} \tag{3.16}$$

By definition, the MRTD at the low spatial frequency limit is equal to ΔT_{sc}. E_t is the eye temporal integration term that is used to account for the SNR improvement due to temporal integration by the human eye and is formulated as:

$$E_t = \frac{1}{t_e F_{dot}} \tag{3.17}$$

From the formulation of ΔT_{sc}, it can be readily seen that the VISMODII model incorporates random detector noise and fixed pattern noise in the formulation of the minimum threshold contrast. Eye/brain spatial integration factors do not apply in the low spatial frequency limit, hence they are not included in the formulation. The SNR_{thr} value depends on the desired probability of recognition. Given measured values for σ_{tvh} and σ_{vh}, ΔT_{sc} can be evaluated. If measurement data are not available, σ_{tvh} is calculated using Equation 3.3 and $0.4\,\sigma_{tvh}$ is used as the default value of fixed pattern noise [Refs. 9 and 11].

3. Contrast Transference Parameter

All frequency dependent contrast degradation, aliasing and scene-phasing effects for sampled imaging systems are included in the formulation of this parameter [Ref. 24]. Calculation of contrast transference parameter ($\alpha(f_z)$) is explained in the next section.

4. Sampling and Aliasing Effects

The imaging process in the spatial domain is shown schematically in Figure 3.8. The target scene (s(x,y)) first goes through the image formation process which essentially is the application of a low pass filter with a point spread function of $h_i(x,y)$ to the target scene. The filtered target scene is then sampled by the detector array. Image reconstruction by display and electronics follows the sampling process. Image reconstruction point spread function is defined as $h_r(x,y)$. The output image is formulated as:

$$i(x,y) = \left[\left(s(x,y) \otimes h_i(x,y)\right) \times p(x,y)\right] \otimes h_r(x,y) \tag{3.18}$$

Taking the Fourier transform of this expression and applying the convolution theorem, we have the output image spectrum as:

$$I(f_x,f_y) = \left(\left(S(f_x,f_y) \times H_i(f_x,f_y)\right) \otimes P(f_x,f_y)\right) \times H_r(x,y) \tag{3.19}$$

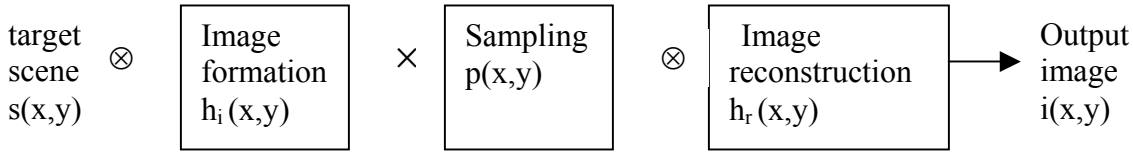

Figure 3.8. Schematic of Imaging process in Spatial Domain "After [Ref. 22]".

Figure 3.9 illustrates the imaging process in the spatial frequency domain. Image formation and reconstruction filters are the cascaded MTFs of the relevant sub-systems and are explained in greater detail in the next subsection.

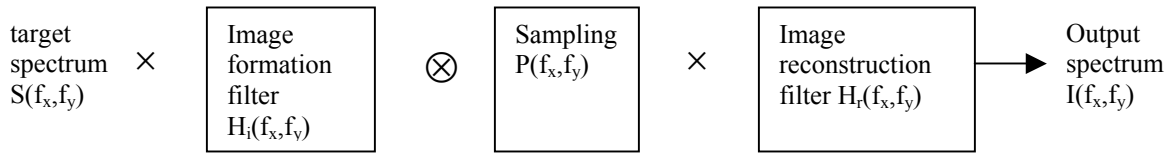

Figure 3.9. Schematic of Imaging Process in Spatial Frequency Domain "After [Ref. 22]".

The spatial sampling process can be mathematically formulated as the convolution with a two-dimensional array of delta functions given by:

$$P(f_x, f_y) = \sum_{n=-\infty}^{+\infty} \sum_{m=-\infty}^{+\infty} \delta(f_x - nf_{sx})\delta(f_y - mf_{sy}) \tag{3.20}$$

where:

n and m are integers,

f_{sx} and f_{sy} are the sampling frequencies in the horizontal and vertical directions.

The net result of this two dimensional sampling is the filtered spectrum repeated at integral multiples of the sampling frequency in the horizontal and vertical directions [Ref. 9]. When aliasing is present, it is not possible to reconstruct the image correctly. Representing the image spectrum as the summation of a "correct", i.e., properly filtered spectrum, and an "aliased" spectrum, we can write:

$$I(f_x, f_y) = Icorrect(f_x, f_y) + A(f_x, f_y) \tag{3.21}$$

where:

$$I_{correct}(f_x, f_y) = S(f_x, f_y)H_i(f_x, f_y)H_r(f_x, f_y) \tag{3.22}$$

and

$$A(f_x, f_y) = \left[\sum_{\substack{n=-\infty \\ n\neq 0}}^{\infty} \sum_{\substack{m=-\infty \\ m\neq 0}}^{\infty} S(f_x - nf_{sx}, f_y - mf_{sy})H_i(f_x - nf_{sx}, f_y - mf_{sy}) \right] \times H_r(f_x, f_y) \tag{3.23}$$

The alias terms are the residual sideband spectrum created by undersampling. The VISMODII model includes only the most significant aliasing artifacts corresponding to the terms where $|m| \le 1$ and $|n| \le 1$.

Image contrast is written in terms of an equivalent apparent temperature difference between the bars (peaks) and the background (troughs) of the degraded bar pattern as described in Figure 3.10. Aliasing is treated as an additive noise term that reduces the contrast. Output contrast is given by:

$$\Delta T_s(f_z) = T_p(f_z) - T_t(f_z) - \sigma_{alias}(f_z) \tag{3.24}$$

where:

T_p is the average over the first peak of the unaliased image,

T_t is the average over the first trough of the unaliased image,

σ_{alias} is the alias noise value,

z is the direction subscript either horizontal (h) or vertical (v),

f_z is the target spatial frequency in the direction denoted by the subscript z.

The alias noise term is determined from the difference between the unaliased and the aliased output images.

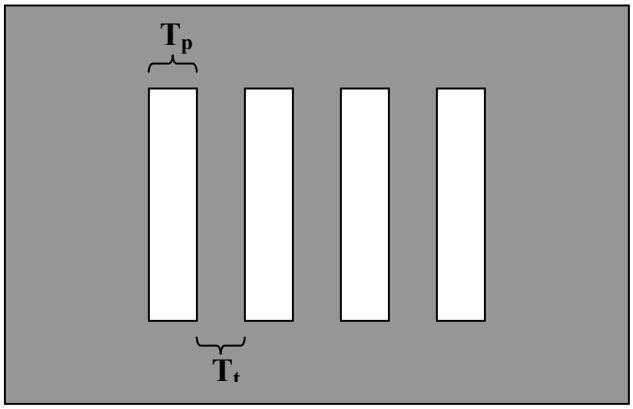

Figure 3.10. Calculation of Contrast in the VISMODII Code: Note that T_p is the average over the first bar and T_t is the average over the first pace of the four-bar pattern.

For all spatial frequencies the input contrast is set to one, which makes the contrast transference parameter equal to the aliased output contrast:

$$\alpha(f_z) = \Delta T_s(f_z) \tag{3.25}$$

5. MTF Analysis in VISMODII

Blurring effects due to the filtering action by the TIS components are incorporated into the system via a cascaded MTF/PTF approach [Ref. 9]. VISMODII is a static performance model in the sense that it does not include any target-imager relative motion MTFs [Ref. 9]. The image formation MTF is made up of optics and detector spatial MTFs [Refs. 9 and 24].

$$H_i = H_{opt}(f)H_{ogb}(f)H_{\det}(f_x)H_{\det}(f_y) \tag{3.26}$$

where:

H_{opt} is the diffraction-limited optics MTF

H_{ogb} is the optics geometric blur MTF related to the aberrations in the optics

$H_{det}(f_x)$ and $H_{det}(f_y)$ are the detector spatial MTFs in the given directions. The equations for these MTFs are:

$$H_{opt}(f) = \frac{2}{\pi}\left[a\cos\left(\frac{\lambda f}{D_o}\right) - \left(\frac{\lambda f}{D_o}\right)\left(1 - \left(\frac{\lambda f}{D_o}\right)^2\right)^{0.5}\right] \tag{3.27}$$

$$Hogb(f) = \exp(-2\pi^2\sigma_g{}^2 f^2) \tag{3.28}$$

$$H_{\det}(f_x) = \frac{\sin(\pi\alpha f_x)}{\pi\alpha f_x} \tag{3.29}$$

$$H_{\det}(f_y) = \frac{\sin(\pi\beta f_y)}{\pi\beta f_y} \tag{3.30}$$

If the detector is square, $H_{det}(f_x)$ and $H_{det}(f_y)$ are symmetrical. In Equations 3.27 through 3.30:

λ is average (diffraction) wavelength in micrometers,

D_o is the optics aperture diameter in mm,

f is the two-dimensional spatial frequency in cycles/mrad,

σ_g is the optics blur spot diameter in mrad, and

α and β are the horizontal and vertical DASs respectively, in mrad.

The image reconstruction MTF includes display MTF, electronics MTF and electronics PTF [Refs. 9 and 24].

$$H_r(f) = H_d(f)H_{elect}(f)\exp\left(jPTF_{elect}(f)\right) \tag{3.31}$$

where:

H_d is the display MTF,

H_{elect} is the electronics MTF and

PTF_{elect} is the electronics PTF.

These MTFs and PTF are given by:

$$H_d(f) = \exp(-2\pi^2\sigma^2 f^2) \tag{3.32}$$

$$H_{elect}(f) = \frac{1}{\sqrt{1+\left(\frac{f}{f_{3dB}}\right)^2}} \tag{3.33}$$

$$PTF_{elect}(f) = -a\tan\left(\frac{f}{f_{3dB}}\right) \tag{3.34}$$

In Equations 3.32 through 3.34:

σ is the monitor gaussian blur spot diameter in mrad,

f is the two-dimensional spatial frequency in cycles/mrad, and

f_{3dB} is the electronics filter cutoff frequency in cycles/mrad.

D. AREAS OF IMPROVEMENT

VISMODII has given MRTD results that are more consistent with the laboratory measured MRTD, especially in the high and low spatial frequency ends than does the community standard FLIR92 [Refs. 9 and 24]. The model successfully incorporates two-dimensional sampling and aliasing effects and provides MRTD results beyond the system Nyquist limit. It also has the advantage of serving as an objective MRTD predictor since it is not tied to the assumption of a human observer in the loop. It is computationally simple, yet theoretically sound. Here we will introduce some areas in the VISMODII code that needed to be further investigated and developed.

We will first introduce a new formulation for threshold input contrast. This improved formulation takes into account the fact that SNR improvement due to eye temporal integration applies only to temporally incoherent noise. It also includes an eye MTF in the reconstruction filter in system total noise bandwidth calculation.

A second issue relates to MTF/PTF analysis. We will introduce a new approach for calculating the electronics OTF directly by a two-dimensional Fourier transform of the filter's impulse response.

It has been suggested that aliasing effects need to be included for target bar frequencies that are below the Nyquist limit. We will investigate the treatment of aliasing as additive noise and suggest a new method of calculating contrast in the four-bar image.

IV. AMENDMENTS AND REFINEMENTS IN VISMODII

In this chapter, we will introduce the refinements made in the VISMODII model. First, the amendments in the calculation of minimum threshold contrast will be covered. Then, the modeling enhancements in the calculation of the contrast transference parameter will be discussed.

A. CALCULATION OF THRESHOLD INPUT CONTRAST

The formulation for ΔT_{sc} was given in Chapter III. It is repeated here for convenience.

$$\Delta T_{sc} = \frac{\pi^2}{8} SNR_{thr} \sigma_{tvh} \left(1 + \frac{\sigma_{vh}^{\ 2}}{\sigma_{tvh}^{\ 2}} \right)^{1/2} (E_t)^{1/2} \tag{4.1}$$

We will introduce the refinements made on this heuristic formulation in two areas.

1. SNR Improvement Factor (Et)

In Equation 4.1, eye temporal integration enhancement applies to both random detector noise (σ_{tvh}) and fixed pattern noise (σ_{vh}). However the fixed pattern noise, by definition, does not include any temporal variation and is correlated from frame to frame.

The new formulation for the $\Delta T_{sc,}$ given in Equation 4.2, accounts for the fact that the SNR improvement factor due to eye temporal integration does not apply to the fixed pattern noise.

$$\Delta T_{sc} = \frac{\pi^2}{8} SNR_{thr} \sigma_{tvh} \left(1 + \frac{\sigma_{vh}^{\ 2}}{\sigma_{tvh}^{\ 2} E_t} \right)^{1/2} (E_t)^{1/2} \tag{4.2}$$

This change in the formulation produces a significant increase in the calculated threshold contrast. The difference is a factor of $\sqrt{12}$ using the 60 Hz frame rate given in Appendix A (TIS parameters) and 0.2 sec eye integration time.

2. Total Noise Bandwidth

In Chapter III we noted that in the formulation of σ_{tvh} the actual system total noise bandwidth is used instead of the reference bandwidth used in the NETD formulation. Total noise bandwidth is calculated in the VISMODII model using Equation 4.3.

$$\Delta f_{sys} = \int_{-\infty}^{\infty}\int_{-\infty}^{\infty}\left(H_{sys}\right)^{2} df_x df_y \tag{4.3}$$

where system MTF is the product of post-detection sub-system MTFs:

$$H_{sys}(f) = H_{elect}(f)H_{d}(f)H_{eye}(f) \tag{4.4}$$

Note that in the revised formulation, the eye MTF (H_{eye}) is added. The eye model used here shows a linear increase up to a normalized peak response at approximately 0.4 cy/mrad, followed by a decaying response predicted by the optical in-focus OTF associated with the finite pupil size of the eye. In the model, the eye diameter is taken to be 3.3 mm and a nominal visible wavelength of 0.55 μm is used [Ref. 12]. Figure 4.1 shows the two-dimensional eye MTF obtained by this model.

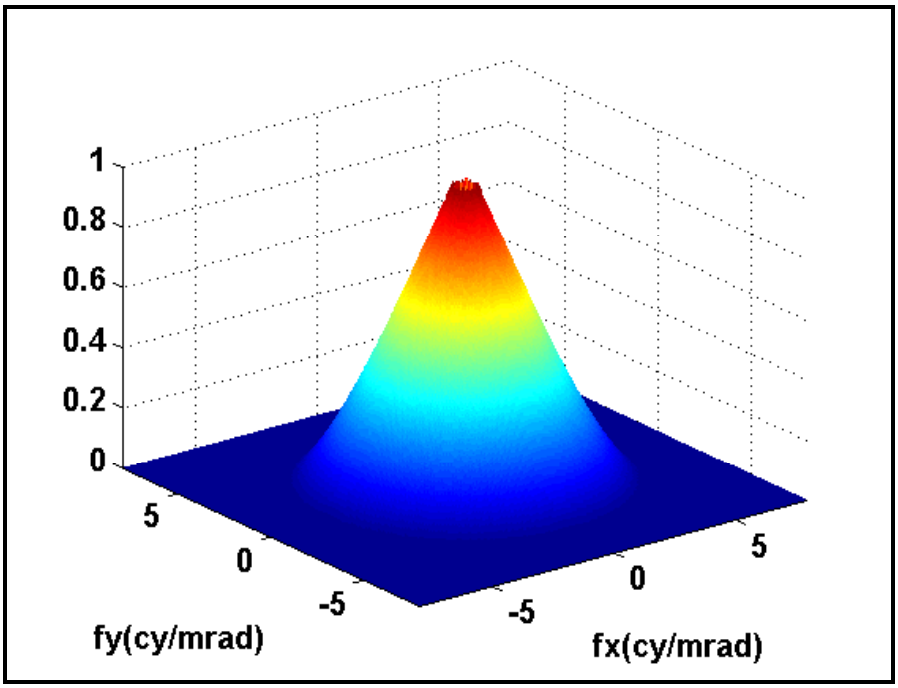

Figure 4.1. Two-Dimensional Eye MTF Used in the VISMODII Model.

B. CALCULATION OF CONTRAST TRANSFERENCE PARAMETER

In VISMODII all spatial frequency dependent effects of the thermal imaging system components are combined in the calculation of the contrast transference parameter. Amendments will be presented in three main categories. Detailed explanations of some specific issues will be referred as necessary to Appendix B.

1. Changes in MTF/PTF Analysis

The way the MTF/PTFs are calculated in the model is changed. The original program calculated MTF/PTFs in one quadrant where horizontal and vertical spatial frequencies are positive and then used the fact that the MTF/PTF values will be the "mirror images" in the other three quadrants. However this method had two main drawbacks. First, although the MTF values corresponding to the same spatial frequencies are equal for all quadrants, PTF has different values for negative and positive spatial frequencies. Second, simply replicating the MTF values in one quadrant causes problems in defining the zero spatial frequency. The final MTF/PTFs turn out to have four values corresponding to the DC term.

A new approach that is based on an actual two-dimensional spatial frequency matrix with frequencies covering all four quadrants is used in the current model. The MTF/PTFs calculated using this approach do not suffer from the drawbacks mentioned. The reader is referred to Appendix B for further details on this issue.

A second fundamental change made in MTF/PTF analysis is the change in the formulation of electronics MTF/PTF. The model originally used Equation 3.33 for electronics MTF and Equation 3.34 for electronics PTF. These equations are basically first order approximations based on modeling the electronics as a simple RC filter.

The current model derives the electronics OTF directly from the exact two-dimensional Fast Fourier Transform (FFT) of the impulse response of an RC filter. The form used for the impulse response is:

$$h_{xy}(x,y) = e^{-2\pi f_{3dB} x} \times e^{-2\pi f_{3dB} y} \tag{4.5}$$

where:

f_{3dB} is the electronics 3dB cutoff frequency in cy/mrad,

x and y are the space variables in the horizontal and vertical directions in mrad. Appendix B explains how the variables x and y are defined depending on the four-bar target spatial frequency.

Finally, VISMODII used Equation 3.31 to calculate the image reconstruction MTF. However, Lloyd's treatment [Ref. 6] of the sampling process for a staring FPA suggests that the detector spatial MTF needs to be included in the reconstruction. The current form of VISMODII uses Equation 4.6, that includes detector MTF along with the display MTF and electronics OTF.

$$H_r(f) = H_d(f)OTF_{elect}(f)H_{\det}(f) \tag{4.6}$$

The resulting image formation and image reconstruction MTFs for the TIS used in experiments are presented in Figure 4.2 and 4.3 respectively. The overall system MTF, which is a combination of the image formation and reconstruction MTFs, is also shown in Figure 4.4.

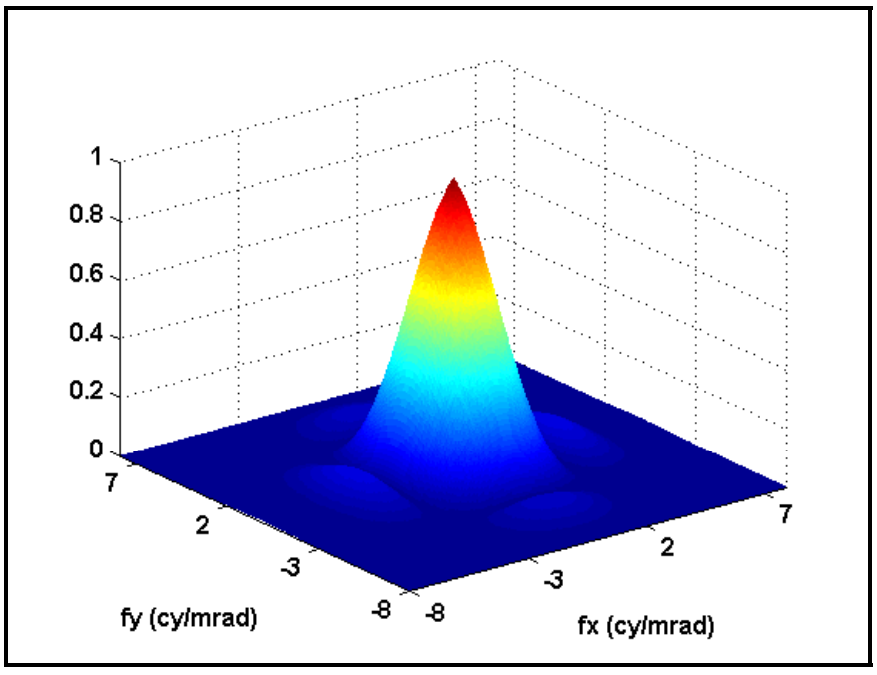

Figure 4.2. Two-Dimensional Image Formation MTF for the Thermal Imaging System Used in VISMODII.

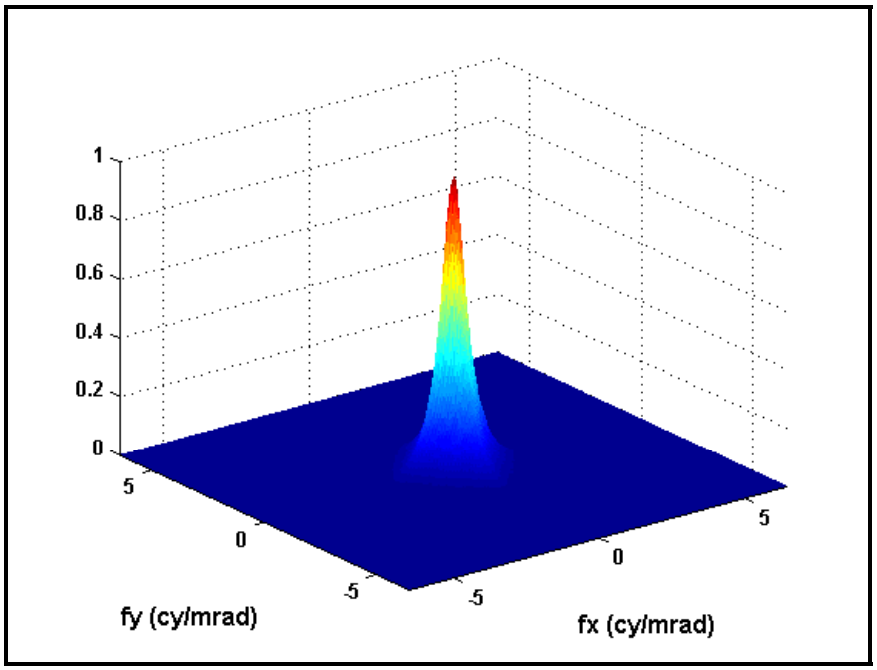

Figure 4.3. Two-Dimensional Image Reconstruction MTF for the Thermal Imaging System Used in VISMODII.

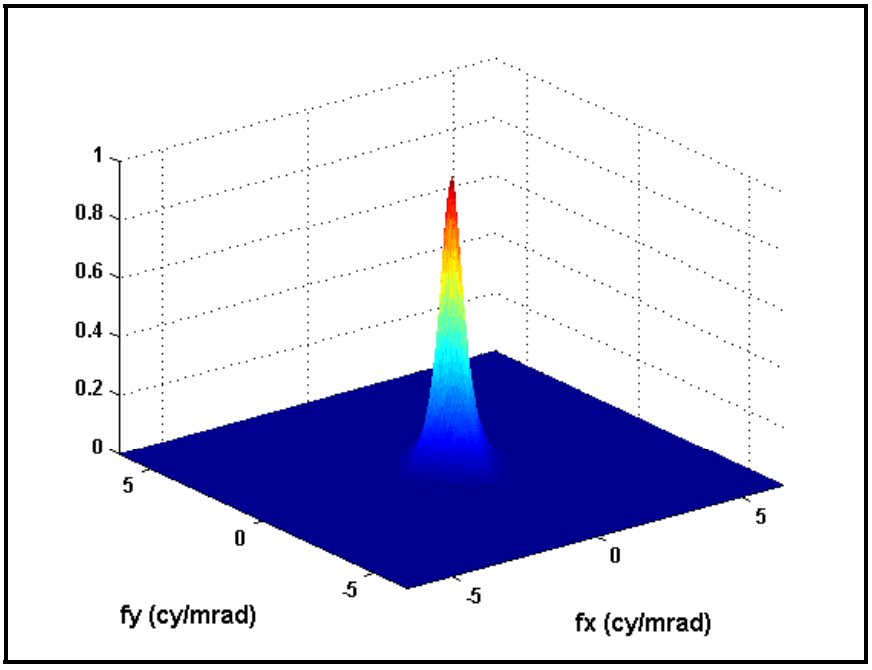

Figure 4.4. Two-Dimensional Overall System MTF as a Product of the Image Formation and the Image Reconstruction MTFs for the Thermal Imaging System Used in VISMODII.

2. Changes in Simulating Aliasing Effects

As stated in the previous chapter, VISMODII treats sampling and aliasing in the spatial frequency domain where it is most convenient. The sampling process creates replicas of the original spectrum. The sampling-generated replicas should by theory be centered at integral multiples of the sampling frequency. Further exploration of the model revealed that the method originally used in the program caused the sampling replica on the negative spatial frequency side to be not exactly centered at the sampling frequency, but shifted a small incremental distance to the left. Although the shift corresponded to just a single element in the two-dimensional FFT spectrum, the consequences on image contrast have been proven to be severe. Negative contrast values and hence negative MRTD values, which are conceptually unacceptable, have been observed. The current version of the program does center all of the replicas exactly at the sampling frequency intervals.

3. Changes in Calculation of Contrast

Two fundamental refinements have been made in this category. The first relates to handling aliasing effects on image contrast. The Visibility model originally assumed aliasing as a signal-dependent additive noise. This assumption led to the treatment of aliasing effects as a contrast reduction in the final image.

A new virtual thermal image-processing model has been developed at the Naval Postgraduate School based on the VISMODII modeling concepts. It takes into account all spatial-frequency-dependent filtering, sampling and aliasing effects. The model uses the basic system parameters of the staring imager and creates a system response; then applies it to the input four-bar pattern. It provides the user with simulations of the visual images that can be obtained with the actual TIS being modeled. The model can be used to "evaluate in a virtual experiment" the effects of filtering, sampling, aliasing and noise on imaging process. For detailed information on the concepts of "The Virtual Thermal Image-Processing Model" the reader is referred to Reference 25.

Virtual experiments with the model provided some useful insights into modeling aliasing effects. Figure 4.5 shows a profile along the four-bar target and its images for a

spatial frequency of 0.65 cy/mrad. The figure demonstrates that aliasing can have a contrast-enhancing effect on the images of four-bar patterns below the Nyquist limit. A theoretical argument proving the existence of aliasing effects at four-bar spatial frequencies below the Nyquist limit is provided in Appendix B.

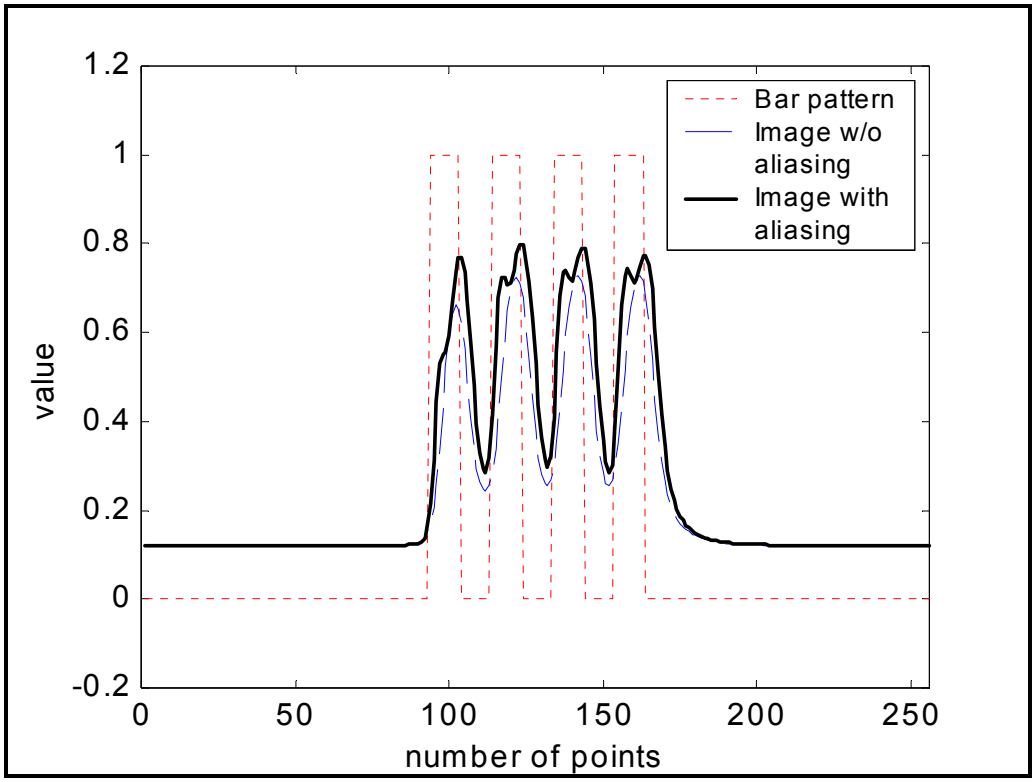

Figure 4.5. Profiles Along the Four-Bar Pattern and its Images with and without Aliasing. Note the contrast enhancement due to aliasing.

Experiments also showed that aliasing effects are fundamentally different from the effects of noise in imagery. Figure 4.6 (including noise and aliasing) shows the image distortion caused by aliasing at a spatial frequency of 1.15 cy/mrad. Noise alone does not have this asymmetric distorting effect and the four-bar target is still resolvable in Figure 4.7 (which includes noise without aliasing).

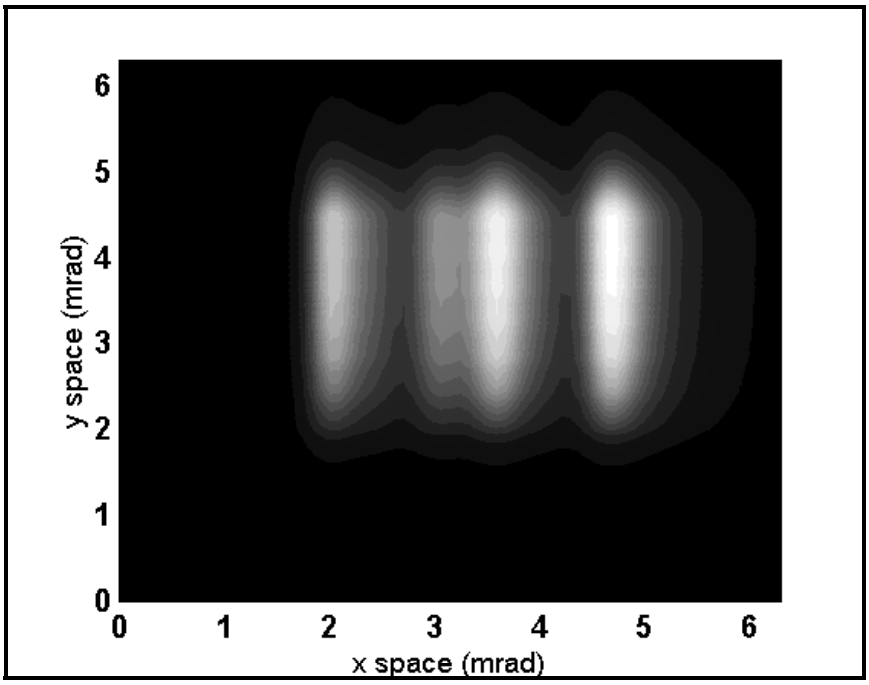

Figure 4.6. Image with Noise and Aliasing: Note the lack of symmetry, due to aliasing together with blurring due to noise.

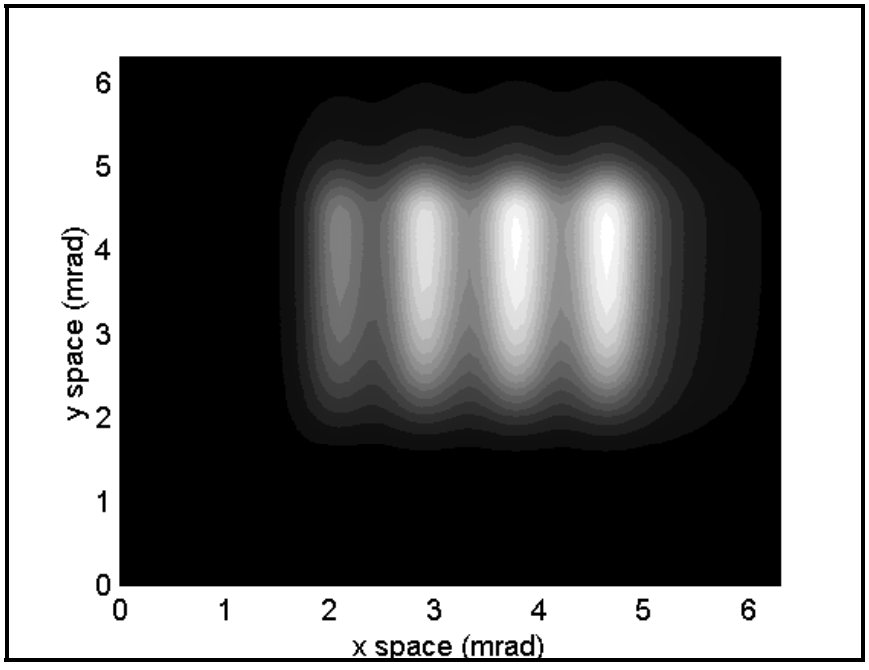

Figure 4.7. Image with Noise Only (No Aliasing): Note that the four bars are observable and the asymmetric distortion that was clearly observed in Figure 4.6 is not present.

All these results suggest that aliasing cannot be adequately modeled as noise. The method for calculating aliasing has to account for the fact that aliasing may have visual enhancing effects (Figure 4.6) and therefore cannot assume aliasing to be a contrast-degrading factor. The proposed method calculates the image contrast directly from the aliased output image and hence any contrast enhancing effect of aliasing is automatically accounted for.

Appendix C will provide an assessment of the MTF Squeeze approach that is used in the NVTherm model to account for sampling and aliasing effects. In the appendix, a qualitative comparison between the NVTherm and VISMODII approaches will also be presented.

A second major issue relates to the spatial shifts in the four-bar image location. Figure 4.8 shows the spatial shift in the image due to the phase transfer function of the electronics.

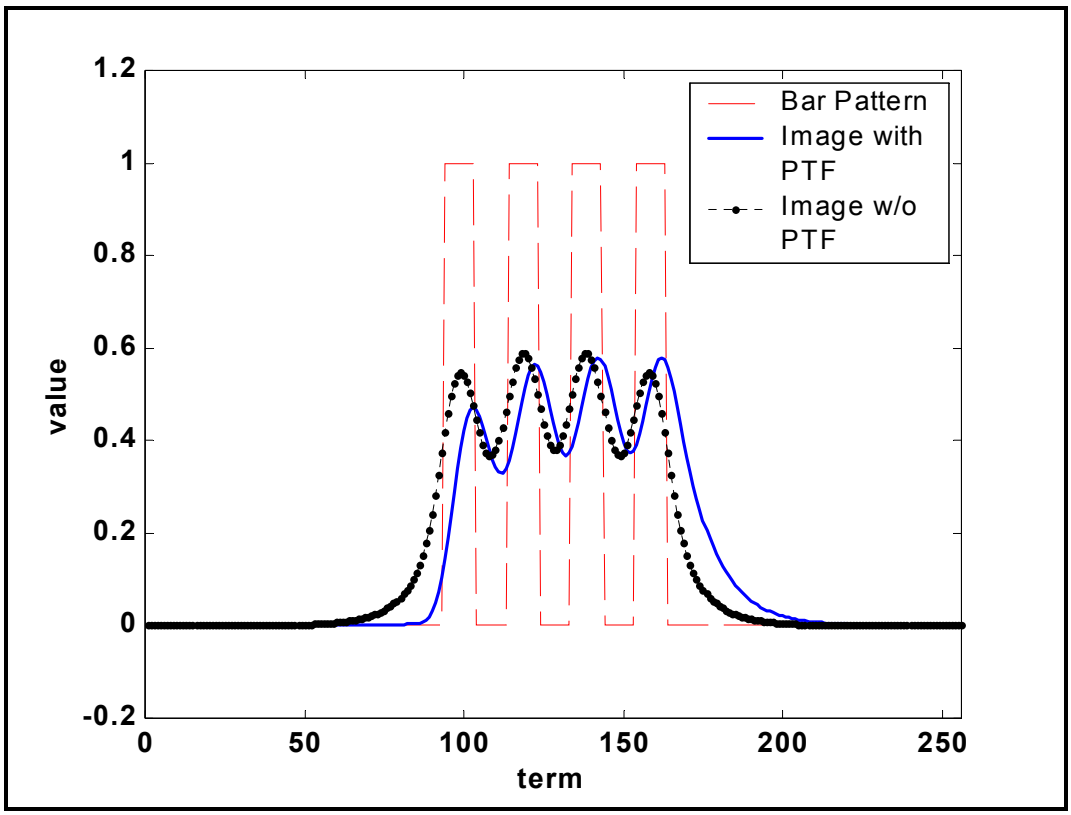

Figure 4.8. Spatial Shift in the Image due to Electronics PTF.

An algorithm is included in the code that finds the exact location of the bar pattern and calculates the contrast on this shifted pattern. The new approach for calculating contrast is depicted in Figure 4.9. Note that unlike the original algorithm explained in Chapter III, the new algorithm uses all four bars instead of using one bar and one space on the pattern to evaluate image contrast. The method finds the maximum value over the bars and minimum values over the spaces. The algorithm then does a comparison between the maximum value on each bar and the minimum values over adjacent spaces. The minimum value obtained by this comparison process determines the contrast in the image. The formulation given by Equation 4.7 has intuitive appeal since MRTD experiments require that all four bars be resolvable, and we expect that if any of the individual bars is not distinguishable from the adjacent spaces, four-bar pattern cannot be called fully "resolved".

$$Contrast(f_s) = \min\begin{pmatrix} Max1 - Min1,\ Max2 - Min1,\ Max2 - Min2, \\ Max3 - Min2,\ Max3 - Min3,\ Max4 - Min3 \end{pmatrix} \tag{4.7}$$

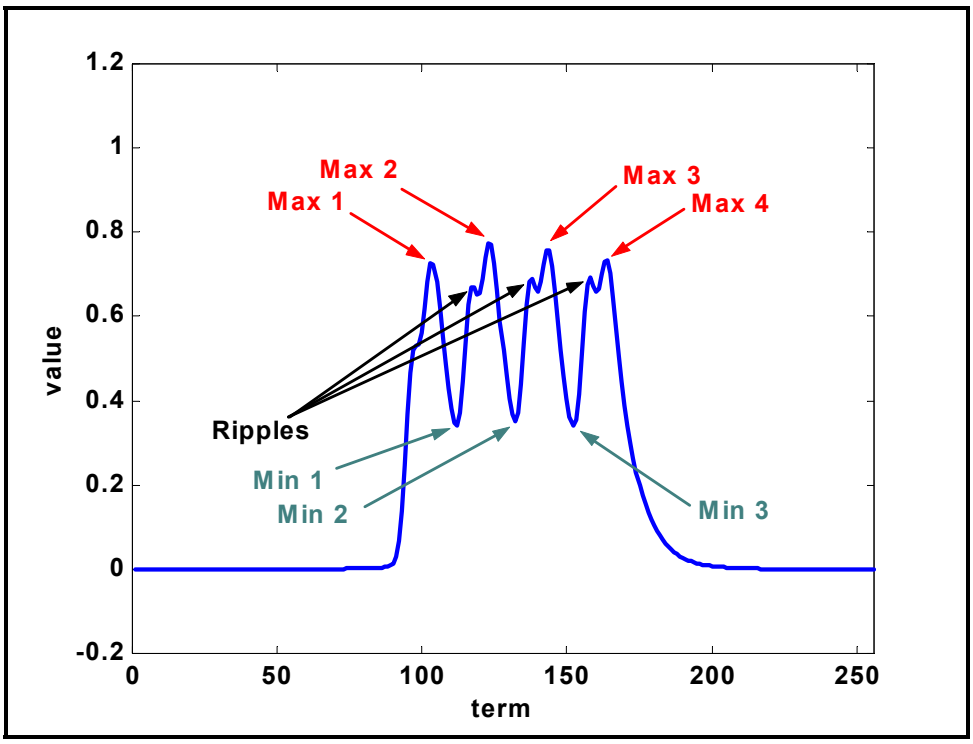

Figure 4.9. Calculation of Contrast in the Image.

Figure 4.10 shows the logical flow of the VISMODII program.

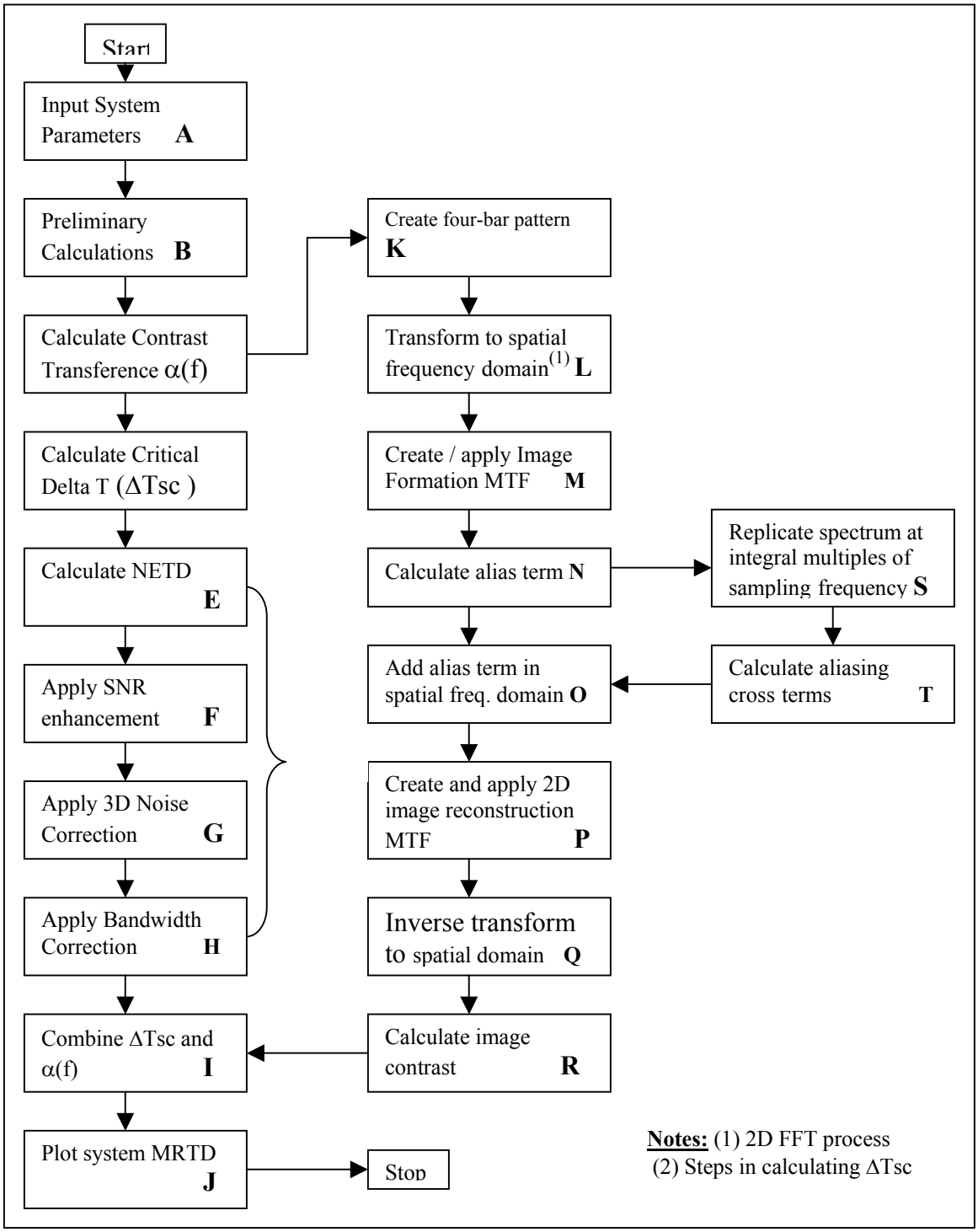
Start
Input System Parameters A
Preliminary Calculations B
Calculate Contrast Transference α(f)
Calculate Critical Delta T (ΔTsc)
Calculate NETD E
Apply SNR enhancement F
Apply 3D Noise Correction G
Apply Bandwidth Correction H
Combine ΔTsc and α(f) I
Plot system MRTD J
Stop
Create four-bar pattern K
Transform to spatial frequency domain(1) L
Create / apply Image Formation MTF M
Calculate alias term N
Replicate spectrum at integral multiples of sampling frequency S
Calculate aliasing cross terms T
Add alias term in spatial freq. domain O
Create and apply 2D image reconstruction MTF P
Inverse transform to spatial domain Q
Calculate image contrast R
Notes: (1) 2D FFT process
(2) Steps in calculating ΔTsc

Figure 4.10. VISMOD II Block Diagram.

On the flowchart, every step is labeled with a capitalized letter. Table 4.1 lists where in the thesis the corresponding calculation or step is explained. The table is intended to help the reader refer to each step conveniently.

STEP	CORRESPONDING THESIS CHAPTER/SECTION/SUBSECTION AND/OR APPENDICES
A	Appendix A
B	Chapter II Section D/1, Appendices B and E
C	Chapter III Section C/4 and Chapter IV Section B
D	Chapter III Section C/2 and Chapter IV Section A
E	Chapter III Section C/2 and Chapter IV Section A
F	Chapter III Section C/2 and Chapter IV Section A/1
G	Chapter III Sections B/1 and C/2, Chapter IV Section A/1
H	Chapter III Section B/1 and Chapter IV Section A/2
I	Chapter III Section C/1
J	Appendix E
K	Appendix E
L	Chapter IV Section B/3 and Appendix E
M	Chapter III Section C/5, Chapter IV Section B/1 and Appendix B
N	Chapter III Section C/4 and Chapter IV Section B/2
O	Chapter III Section C/4 and Chapter IV Section B/2
P	Chapter III Section C/5, Chapter IV Section B/1 and Appendix B
Q	Chapter IV Section B/3 and Appendix E
R	Chapter IV Section B/3
S	Chapter III Section C/4 and Chapter IV Section B/2
T	Chapter III Section C/4 and Appendix E

Table 4.1. Steps in the VISMODII Program and Corresponding Chapters/Sections/Subsections and/or Appendices.

Simulation starts with inputting the basic parameters of the TIS being modeled. Preliminary calculations are then performed which include the detector angular

subtenses, sampling frequencies, etc. that are relevant to the following steps. Spatial frequency dependent contrast transference parameter ($\alpha(f)$) calculation includes the frequency domain MTF/PTF analysis and the sampling/aliasing simulations. First, a two-dimensional bar pattern is created in the space domain. A two-dimensional FFT process transforms the pattern into the spatial frequency domain. Then a two-dimensional image formation MTF is created and applied to the input spectrum. Sampling and aliasing is simulated then by replication of the spectrum at sampling frequency intervals. Following the application of the two-dimensional image reconstruction MTF, the spectrum is transformed back into the spatial domain where image contrast is calculated. As a preliminary step for the calculation of the minimum threshold input contrast (ΔT_{sc}), the system NETD is calculated. This is followed by the application of the SNR enhancement factor corresponding to the eye temporal filtering effect and bandwidth correction factor. Then, three-dimensional noise effects are included. The program finally combines ΔT_{sc} with $\alpha(f)$ to obtain the system MRTD as a function of four-bar pattern spatial frequency.

THIS PAGE INTENTIONALLY LEFT BLANK

V. SUBJECTIVE MRTD

MRTD experiments have been reported in the literature [Refs. 29 through 35]. Although the reported results give a considerable amount of insight into testing methodology, specific information on the thermal imaging systems being tested and the complete test results are not satisfactory to be used for the purposes of this thesis.

In order to evaluate the validity of the VISMODII predictions, experiments have been conducted to measure MRTD using a staring FPA imager at the Naval Postgraduate School Electro-optics Laboratory. Experimental results were also used to make a quantitative comparison between the VISMODII and the FLIR92 model MRTD predictions. This chapter describes the experimental setup, procedure and results along with the comparisons of laboratory measured MRTD with the predicted values from the two models.

A. EXPERIMENTAL SETUP

Figure 5.1 demonstrates the experimental setup for subjective MRTD measurements. Target apparatus consisted of a back plate and a front plate made of aluminum and painted in non-reflective black to obtain uniform emissivity. Various size MRTD targets were cut through the front plate. The two plates were separated by a distance of 10 cm to ensure minimal heat transfer. A variable heating unit was used to control the back plate temperature by changing the voltage applied to a resistance installed on the plate. Two digital thermocouples were attached to the front and the back plates to allow reading the temperature. The thermometers were capable of displaying either Centigrade or Fahrenheit values, each with 0.1 degree accuracy. For better precision in measurement the Fahrenheit mode was used which yielded approximately 0.0556 degrees Celsius tolerance.

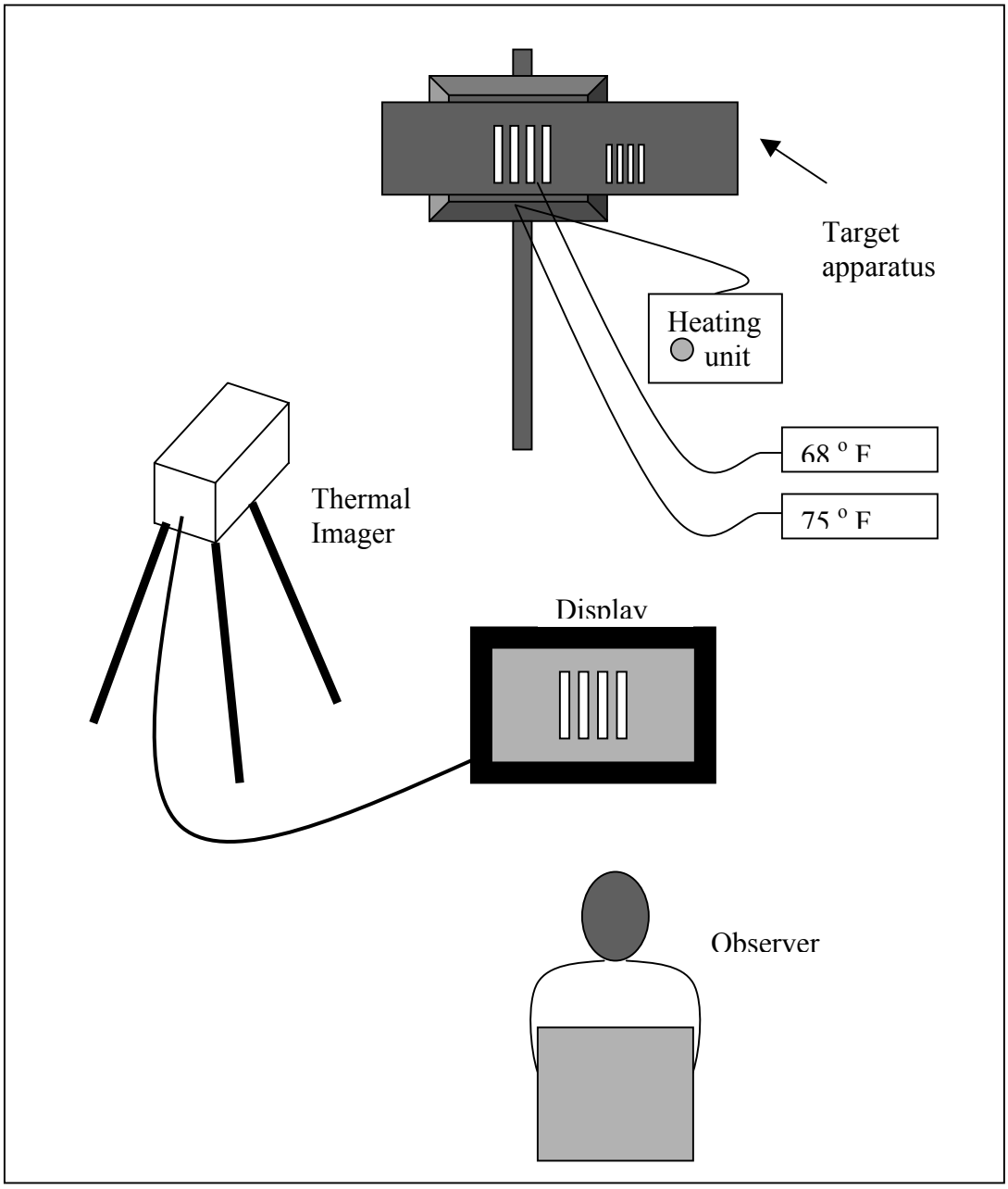

Figure 5.1. Subjective MRTD Experimental Setup.

A Mitsubishi Electronics IR-M500 staring thermal imager was utilized in the experiment. The system operates in the 3-5 micrometer range and incorporates a PtSi staring FPA with 512x512 detector elements. Figure 5.2 shows a picture of the imaging system. A detailed description of the system is given in Appendix A.

Figure 5.2. Mitsubishi IR-M500 Thermal Imaging System.

A display was used to present the four-bar target image to the observer for resolution decision.

B. PROCEDURE

The MRTD experiment basically is the measurement of the imaging system response to four-bar targets of increasingly higher spatial frequencies. For subjective MRTD this process includes the display of the image and an observer who decides whether the resolvability criterion is achieved or not.

Prior to measurements the following preparatory steps were conducted. First, the imaging system was aligned with the target apparatus such that the four-bar target was imaged at the center of the sensor FOV. Second, the distance from the target board to the imaging system entrance aperture was checked. Third, the imaging system optics focus was optimized to give the best result for the target distance. Then the imaging system was calibrated.

The observers were trained in the recognition criteria. The four-bar target pattern was called "resolved" when all observers could see the presence of four bars in the image. Also, each observer was allowed to become familiar with the equipment and was allowed to adjust display settings for optimal viewing. Any external noise and light sources were turned off to reduce potential interference with the experiment. Observers were given enough time to adapt to darkness. During the experiments, observers were allowed head movements and unlimited time to resolve the pattern.

The target board, i.e. the front plate, was positioned such that the bars were oriented vertically to obtain the horizontal MRTD and horizontally to obtain the vertical MRTD. Optimum scene phasing was determined subjectively by moving the MRTD target pattern across the FOV and selecting the position that yields the best representation of the four-bar target.

Two sets of measurements were taken for each case. First, the temperature difference was set to a value at which the bar pattern could not be resolved. Then the back plate was heated (increasing delta T) until all four bars became resolvable. Second, the temperature difference was set to a value at which the bar pattern could clearly be resolved. Then the back plate was cooled (decreasing delta T) to the point where resolution was lost. In both, the temperature difference was recorded at which all four bars were just resolvable. MRTD for each spatial frequency was taken as the average value of the differential temperature values obtained by the heat-up and cool-down cycles. The same procedure was performed for all spatial frequencies of interest to obtain the MRTD curve.

C. MEASUREMENT RESULTS

The MRTD measurement results are given in Appendix D in graphical and tabular form. Figure 5.3 provides a summary of the measured MRTD values for the Mitsubishi system. Two-dimensional MRTD values were not directly measured. They were obtained for each bar spatial frequency from the geometrical mean of the vertical and horizontal MRTD values.

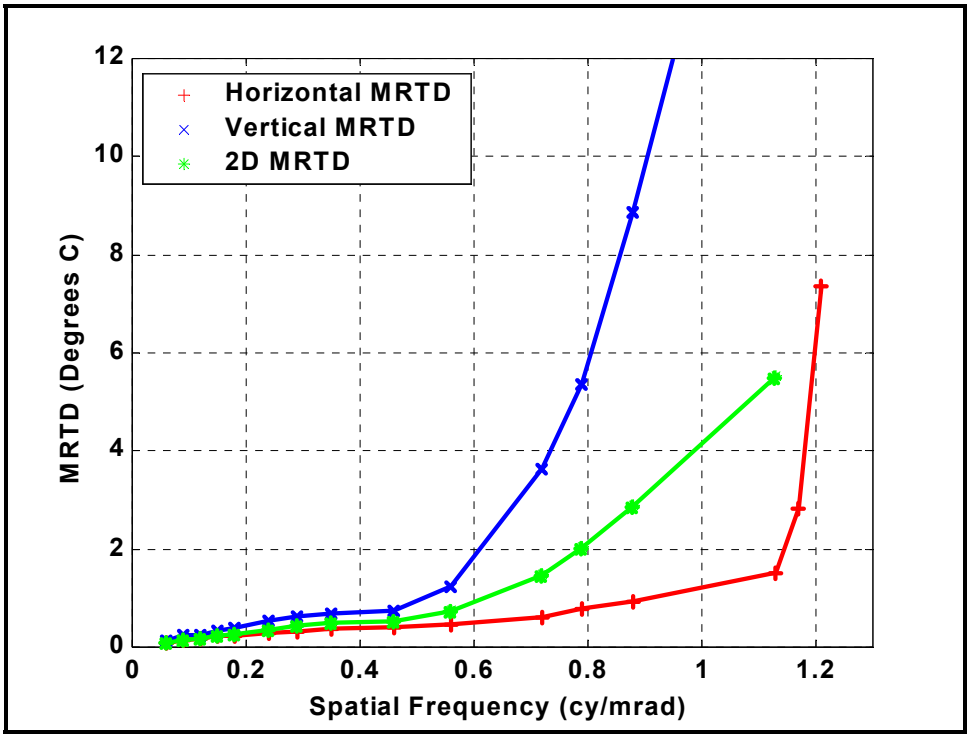

Figure 5.3. Measured Subjective MRTD.

From the experimental results, the following observations are made. The vertical MRTD values are significantly different from the horizontal MRTD, especially at high spatial frequencies. This may be a consequence of different degrees of aliasing and blurring effects in the horizontal and vertical directions.

Both vertical MRTD measurements and horizontal MRTD measurements show that the temperature difference at which all four bars are resolved is lower for the cool-down measurement cycle. This implies that for a human observer, it is easier to track an already resolved four-bar target as it becomes unresolved in noise than to recognize a 'new' target as it emerges out of noise.

There is a low spatial-frequency threshold for MRTD, which is greater than zero. This supports the visibility model's approach of defining a system- and observer-specific minimum threshold contrast.

D. COMPARISON WITH VISMODII AND FLIR92 MODEL RESULTS

Figure 5.4 shows the subjective MRTD predictions from the VISMODII code. Figure 5.5 includes the predictions from the FLIR92 model. The VISMODII MATLAB code is provided in Appendix E and Appendix F gives the short-listing output from the FLIR92 model.

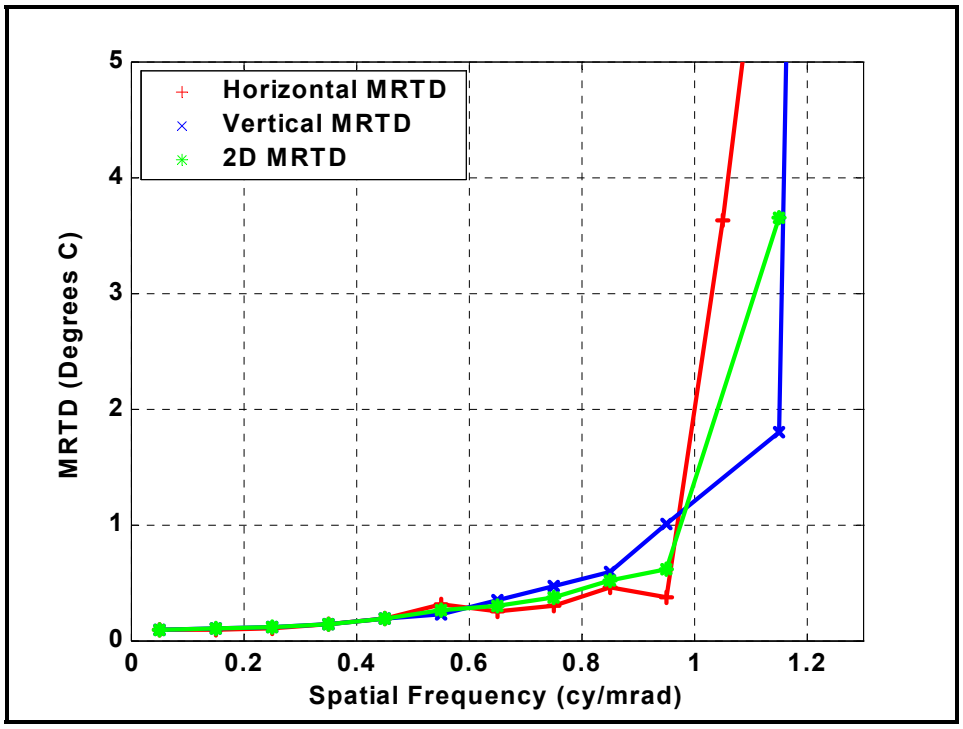

Figure 5.4. VISMOD II Subjective MRTD Predictions.

An observation from the figures is that, contrary to the experimental data, the models predict the vertical MRTD asymptote to be at a higher spatial frequency than the horizontal MRTD cutoff. This may relate to a display limitation for the vertical MRTD case that was observed during the measurements. At higher spatial frequencies the horizontal line structure on the display appeared to limit the observer's ability to resolve the bars. The line structure has a more severe effect on the vertical MRTD than it does on the horizontal MRTD. The noise-like interfering effect of this line structure on resolution has been discussed in the literature [Ref. 40]. However the display MTFs used by both VISMODII and FLIR92 models are symmetrical in horizontal and vertical directions.

This suggests that the inclusion of a non-symmetrical display MTF in the models may account for the difference between the measured and predicted MRTD values.

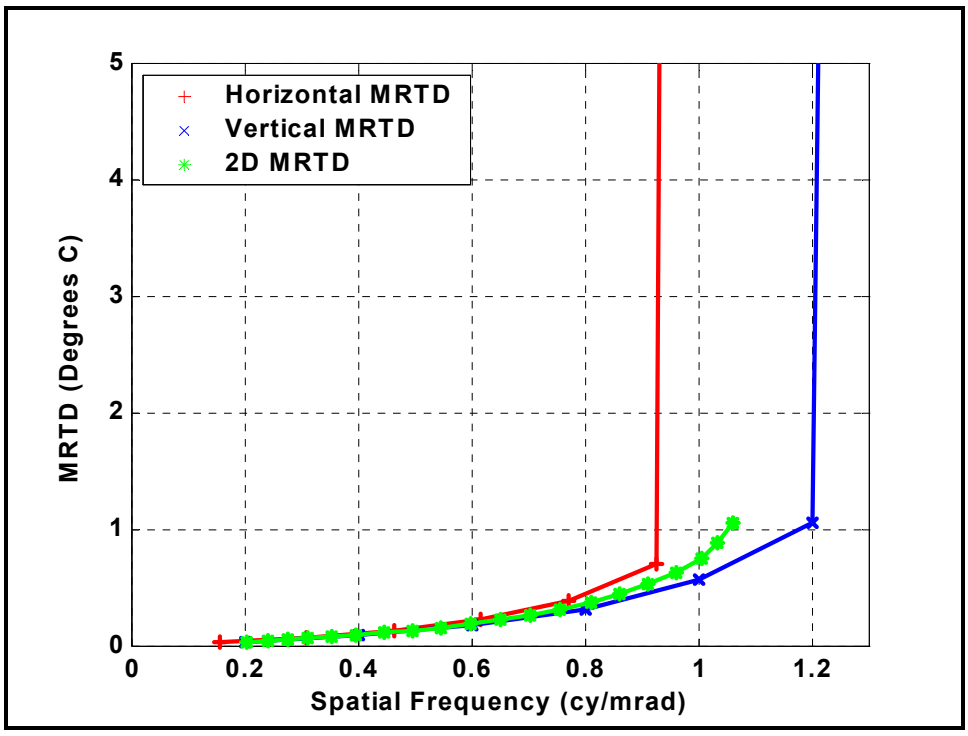

Figure 5.5. FLIR92 MRTD Predictions.

Horizontal MRTD values predicted by the two models are given in Figure 5.6 along with the measured data. VISMODII predictions are closer to the measured data than the FLIR92 predictions at both the low and the high spatial frequency ends. Notice that the FLIR92 high frequency cutoff appears at the Nyquist limit beyond which the model provides no data. Measurements and VISMODII on the other hand indicate that MRTD values can be obtained beyond this limit.

Figure 5.7 presents the predicted and measured vertical MRTD values. VISMODII predictions are again closer to the measured data. However, unlike the horizontal MRTD case the measured values are significantly higher than the predictions from the two models. The display effect previously discussed may be the origin of this discrepancy.

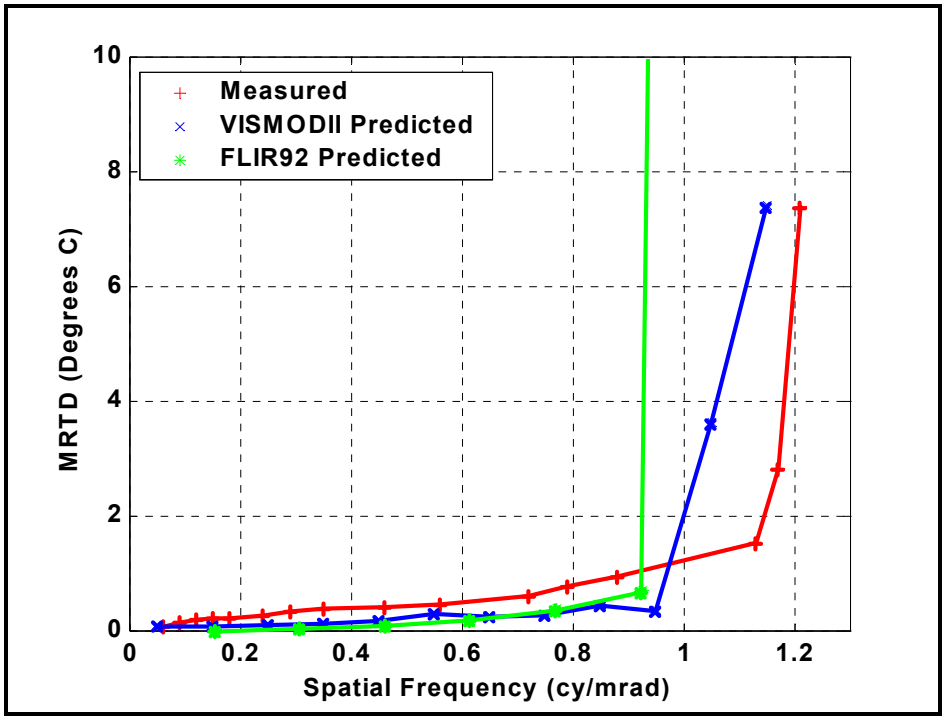

Figure 5.6. Horizontal Subjective MRTD Comparison.

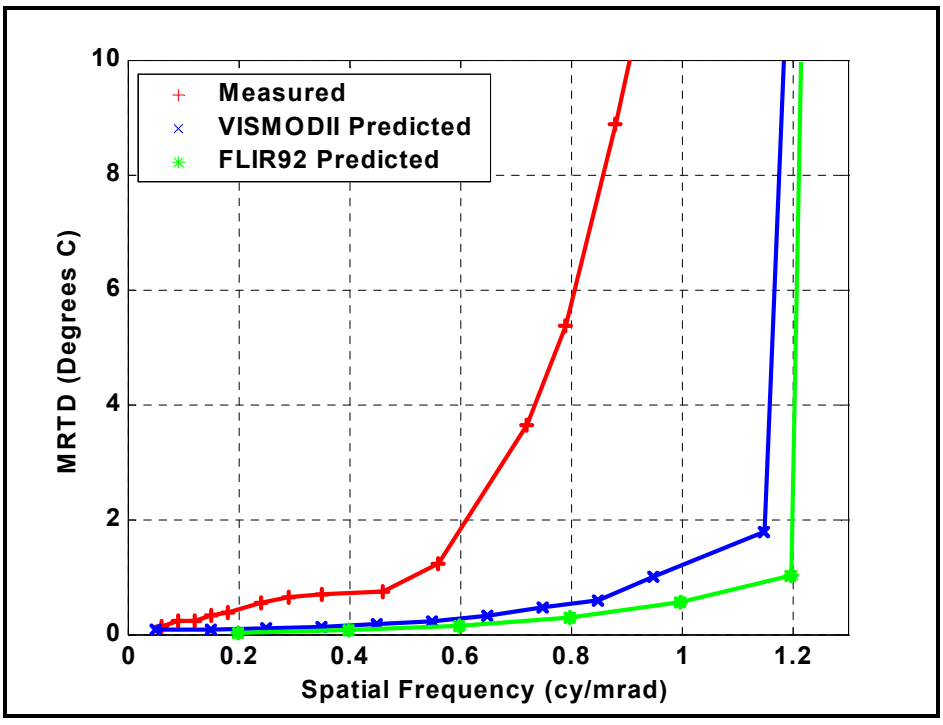

Figure 5.7. Vertical Subjective MRTD Comparison.

Two-dimensional MRTD predictions and the measured data shown in Figure 5.8 also suggest that the predictions from the VISMODII appear to be in better agreement with the measurement results.

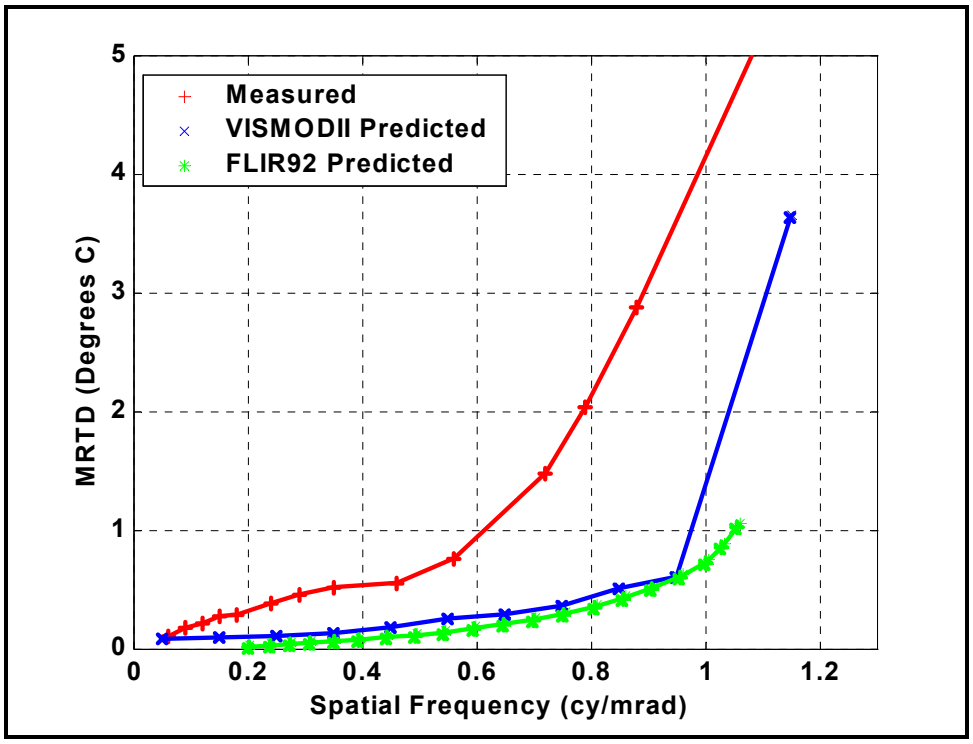

Figure 5.8. Two-Dimensional Subjective MRTD Comparison.

As previously discussed as an essential characteristic of the visibility based modeling, the VISMODII model suggests a minimum contrast threshold below which the resolution of four bars is not possible. The eye-brain spatial integration terms in the FLIR92 model MRTD equation (Equation 3.4) go to zero at the zero spatial frequency limit [Ref. 9]. The mathematical proof is given in Appendix G. Figures 5.9 through 5.11 provides more detailed presentations of the MRTD values at low spatial frequencies. For all cases, the measured data indicates a non-zero low frequency limit. The experimental error limits shown in the figures correspond to the 0.1 degrees Fahrenheit fault tolerance of the digital thermometers used in the measurements. The measured MRTD results are very close to the predictions from the VISMODII model, especially at the very low

spatial frequency limit. Another reported MRTD test performed with staring array imagers also mentions the existence of a low frequency MRTD threshold [Ref. 35]. These figures correctly suggest that VISMODII model's approach is in line with the measured trends.

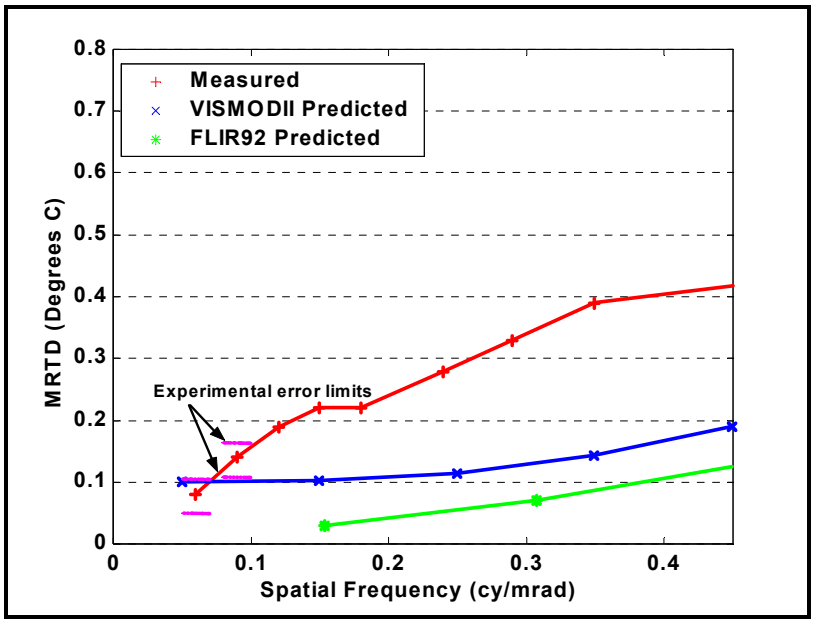

Figure 5.9. Horizontal Subjective MRTD Comparison at Low Spatial Frequencies.

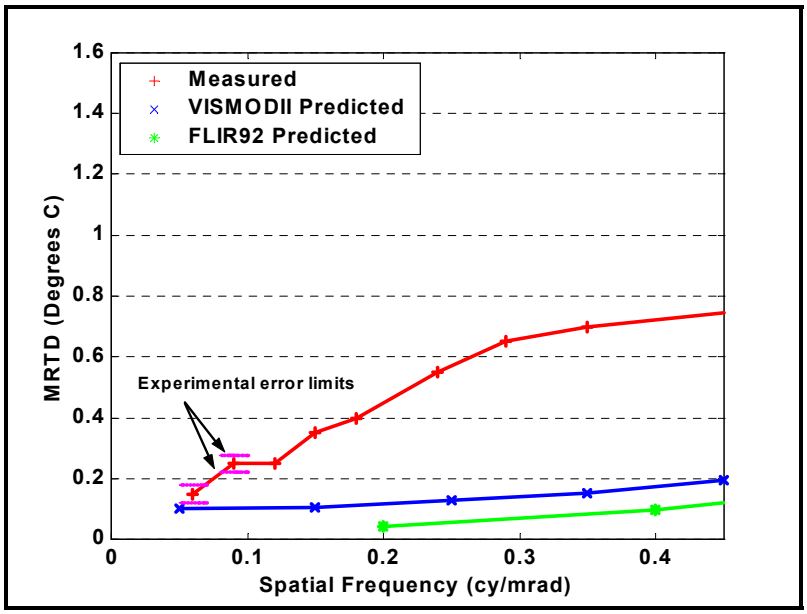

Figure 5.10. Vertical Subjective MRTD Comparison at Low Spatial Frequencies.

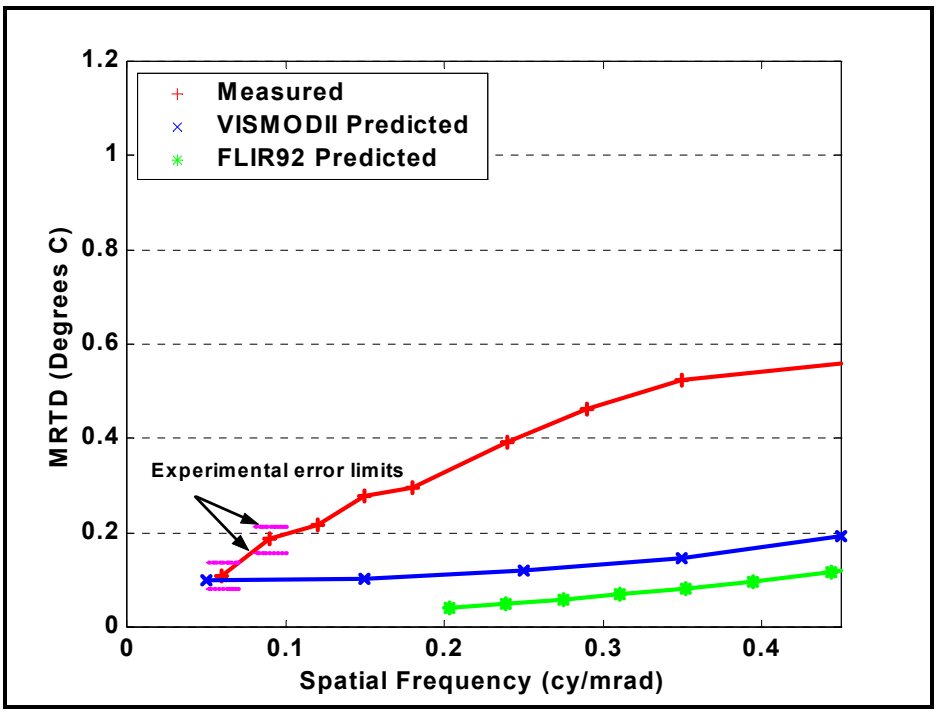

Figure 5.11. Two-Dimensional Subjective MRTD Comparison at Low Spatial Frequencies.

E. ASSESSMENT OF SAMPLING, ALIASING AND SCENE PHASING EFFECTS ON THE MRTD PREDICTIONS

One important characteristic of the VISMODII is its ability to successfully incorporate sampling, aliasing and scene phasing effects into MRTD calculation. Also, the model has the inherent flexibility that allows the user to exclude these effects and make a comparative analysis of their impacts on the MRTD. Figure 5.12 demonstrates the sampling and aliasing effects on the MRTD predictions. Several significant effects are observed from the two MRTD curves. As discussed in the previous chapter, sampling and aliasing effects are observable at four-bar spatial frequencies as low as 0.45 cy/mrad. The thermal imager used in the simulation has a Nyquist limit of 0.96 cy/mrad. This suggests that limiting the MRTD predictions to the sub-Nyquist frequencies is not an adequate approach. Second, at certain spatial frequencies below the Nyquist limit, the MRTD value with aliasing turns out to be smaller than the MRTD without the aliasing effects. This indicates that sampling generated replicas may add constructively and hence

aliasing can manifest itself as contrast enhancement. Therefore, aliasing effects cannot be simply modeled as contrast degradation. This serves as the foundation of the new contrast calculation method explained in Chapter IV and unlike NVTherm the VISMODII model has the capability of accounting for the visual enhancing effects of aliasing. Finally the curve without aliasing predicts the system MRTD cutoff to be at a higher spatial frequency indicating that a model failing to include aliasing effects may overestimate the MRTD performance of a thermal imager.

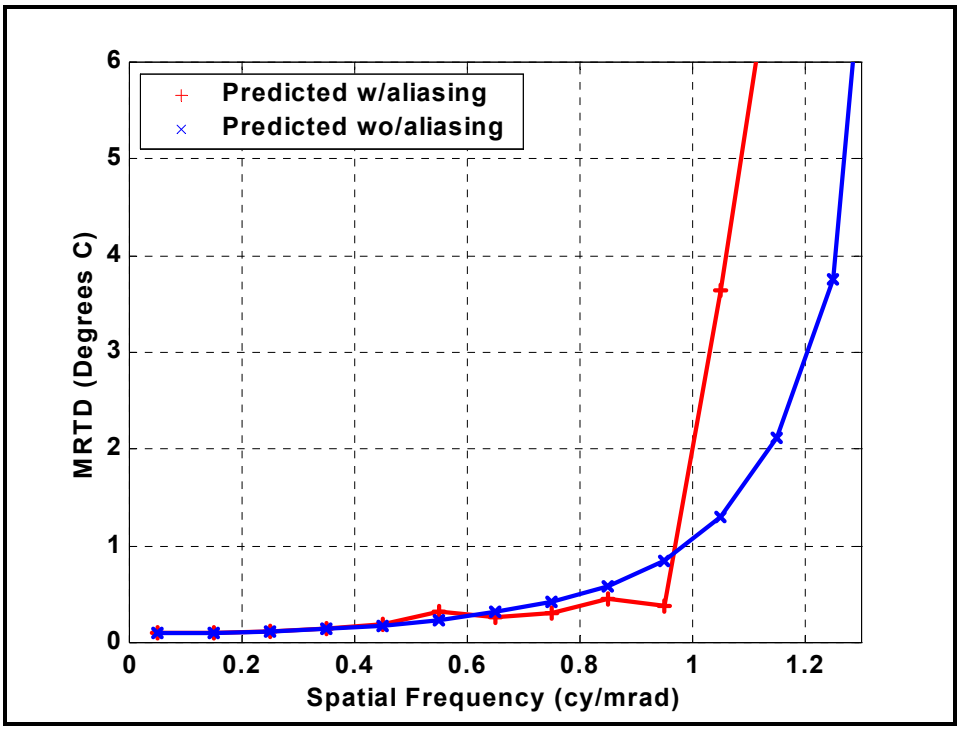

Figure 5.12. Sampling and Aliasing Effects on MRTD Prediction.

Scene phasing, as explained in Chapter III, occurs when there is misalignment between the sampling array and the scene being sampled, i.e. the four-bar pattern. Spatial sampling process can be mathematically formulated as the convolution with a two-dimensional array of delta functions given by:

$$P(f_x, f_y) = \sum_{n=-\infty}^{+\infty} \sum_{m=-\infty}^{+\infty} \delta(f_x - nf_{sx})\delta(f_y - mf_{sy}) \tag{5.1}$$

Net result of this two dimensional sampling process is the spectrum, which was filtered by the optics and the detector, repeated at integral multiples of the sampling frequency in the horizontal and vertical directions.

$$S_{sampled} = \sum_{n=-\infty}^{+\infty} \sum_{m=-\infty}^{+\infty} S(f_x - nf_{sx}, fy - mf_{sy}) \tag{5.2}$$

From Fourier theory, if we denote the Fourier transform in the following manner:

$$\Im\{s(x,y)\} = S(f_x, f_y) \tag{5.3}$$

Then, the Fourier transform of the shifted function can be written as:

$$\Im\{s(x-b_x, y-b_y)\} = S(f_x, f_y) \times e^{j2\pi(f_x b_x + f_y b_y)} \tag{5.4}$$

Scene spatial displacement, therefore, manifests itself as a phase shift in the spatial frequency domain. When the image center is shifted by a distance 'b_x' in the horizontal direction and 'b_y' in the vertical direction from the sampling element, the two-dimensional sampled spectrum will be:

$$S_{SP} = \sum_{n=-\infty}^{+\infty} \sum_{m=-\infty}^{+\infty} S(fx - nfsx, fy - mfsy) \times e^{j2\pi(f_{sx} n b_x + f_{sy} m b_y)} \tag{5.5}$$

A one-dimensional representation of this spectrum was given in Figure 3.5. The displacement 'b' can be in the range between zero and one detector pitch (Λ). When b is equal to zero, the phase term disappears, which is the optimum condition meaning that the scene is perfectly aligned with the detector elements. When b is one quarter of the detector pitch, we have the maximum scene phasing. Effects of scene phasing on MRTD are demonstrated in Figure 5.13. The two curves lie on top of each other up to 0.55 cy/mrad. This suggests that, at lower spatial frequencies the bar patterns are larger and the relative positions of the bar pattern and the detector elements are not very critical. At higher spatial frequencies, the scene phasing does affect the MRTD curve.

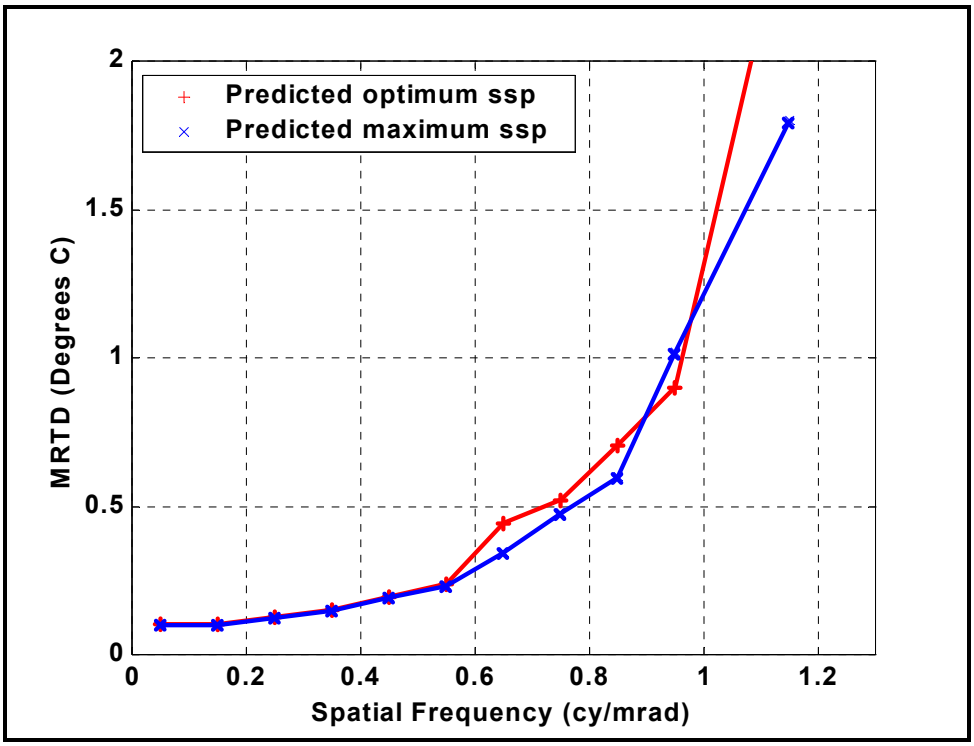

Figure 5.13. Sample Scene-phasing (ssp) Effects on MRTD Prediction.

VI. OBJECTIVE MRTD

Although subjective MRTD has been the most common parameter to specify thermal imaging system performance, the existence of the human observer in the loop makes measurement results subjective and limits repeatability. Objective measurement of MRTD has appeal for the applications in which automatic target recognizers are used. Therefore, an experimental method to measure and a performance model to predict objective MRTD needed to be developed. Several experimental and modeling efforts have been reported in the literature related to automated and/or objective procedures to obtain MRTD [Refs. 36 through 39].

The Visibility model concepts were extended to the case where the resolvability decision is not related to a human observer's ability to resolve four bars. This chapter will cover the experimental design for objective MRTD, the objective MRTD modeling concepts and a comparison between the experimental results and the MRTD model predictions.

A. EXPERIMENTAL SETUP

The objective MRTD measurement scheme is fundamentally similar to the subjective MRTD method as demonstrated in Figure 6.1. An oscilloscope that was synchronized to one horizontal video line across the image was used to simulate an ATR device. The oscilloscope enables the measurement of the voltage level along the image. Notice that the display and the human observer are no longer present in the measurement process. Although a human observer is still needed in this simple scheme to read the SNR level from the oscilloscope display, no subjective decision of resolvability is required. It is expected at any given time any knowledgeable observer would read the same SNR given the same level of signal and noise.

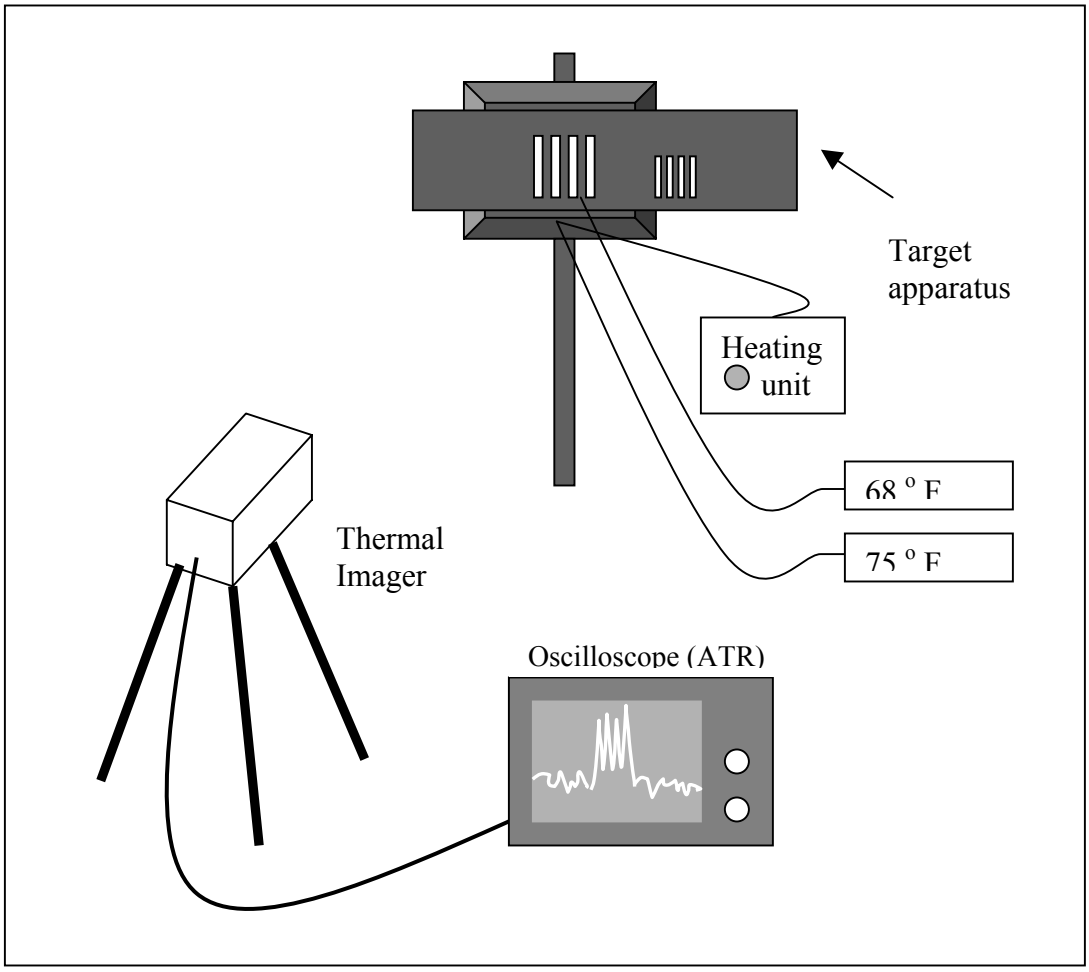

Figure 6.1. Objective MRTD Experimental Setup.

B. PROCEDURE

One fundamental part of the objective MRTD experiment is the noise analysis. The noise measurement procedure is shown in Figure 6.2. The detectors were uniformly illuminated by a large target. The target covered the entire FOV of the TIS, which ensured that any variation in the received signal was due to the noise added in the imaging system.

Figure 6.3 is a snapshot of noise as it is seen on the oscilloscope display. Fifty equally spaced samples were taken on this noise waveform. Assuming that the noise was random and has a mean value of zero, the rms value of the noise was found to be 8.1 mV.

This rms noise value was then used in SNR calculations both in the experiments and in the simulation. A noise sample data set is given in Appendix H.

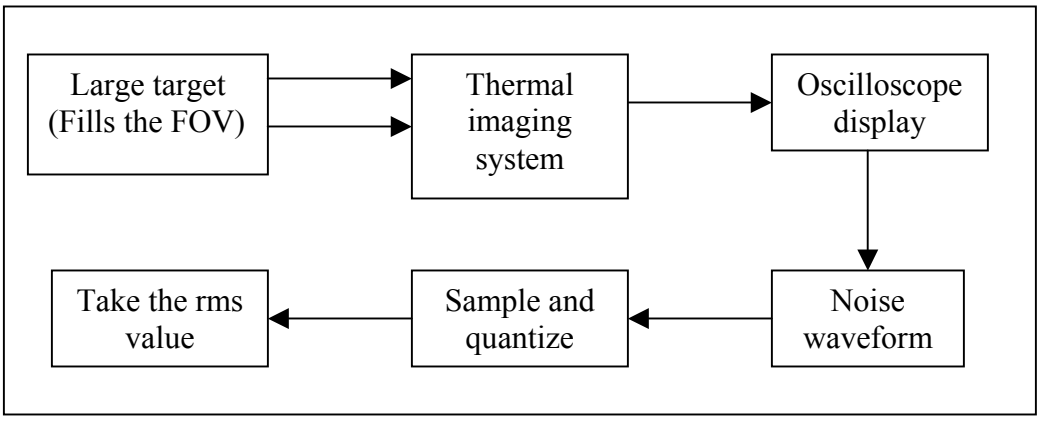

Figure 6.2. Noise Measurement Procedure.

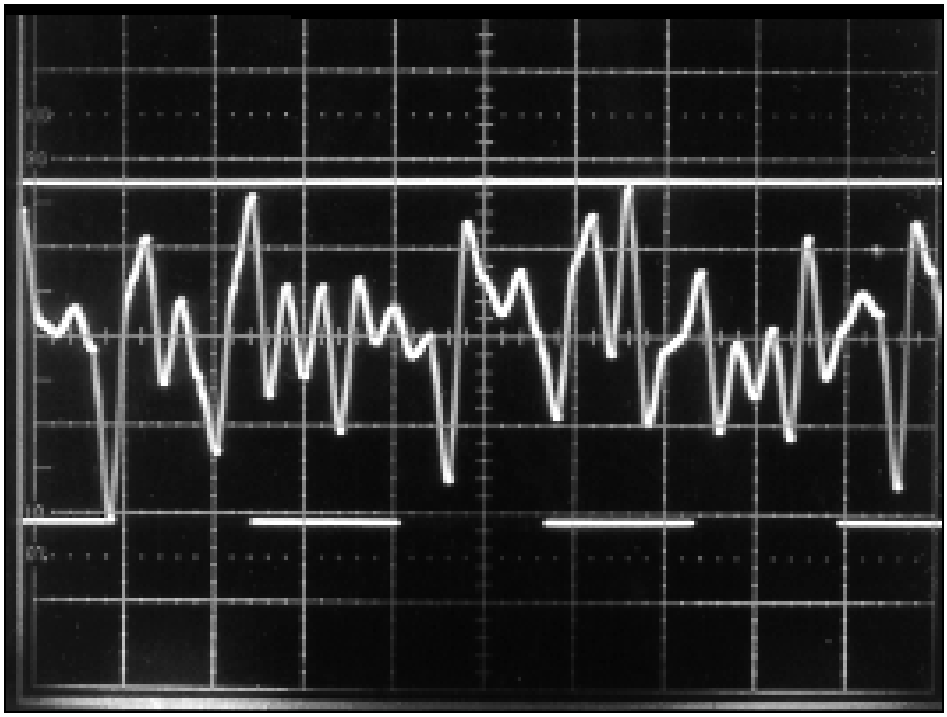

Figure 6.3. Snapshot of Noise Taken from the Oscilloscope Display (Vertical axis is 10 milliVolts per division).

Two different objective MRTD measurement schemes were used. First, the SNR measured on the oscilloscope display was held constant and the temperature difference

that gives a SNR value of 6.0 was recorded for varying spatial frequencies. This measurement scheme is conceptually very similar to the typical subjective MRTD test in that for each spatial frequency a minimum temperature differential is determined at which a given criterion, in this case an SNR value, is achieved. A sample four-bar representation on the oscilloscope display is given in Figure 6.4.

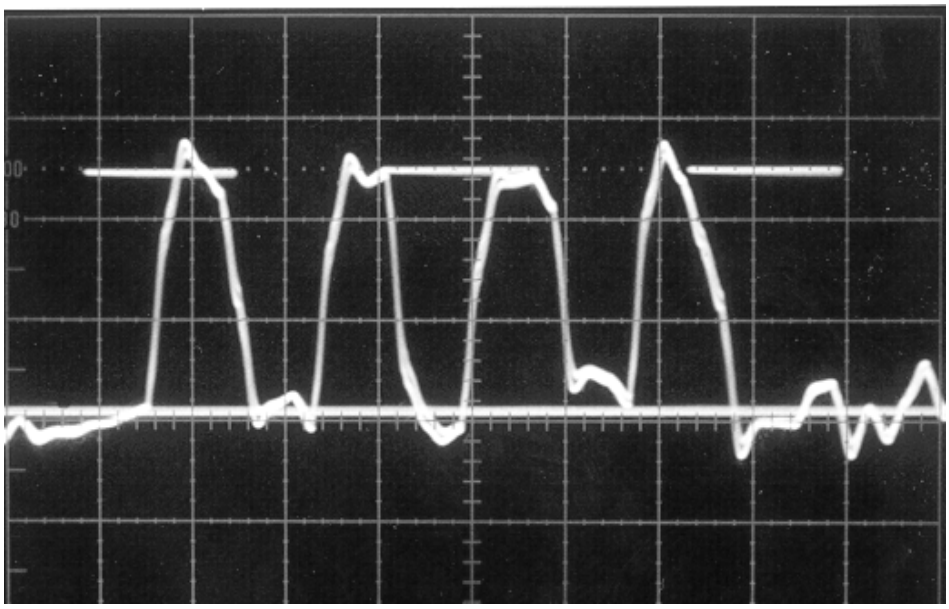

Figure 6.4. Four-Bar Target Representation on the Oscilloscope Display (Vertical Axis is 20 milliVolts per Division).

In the second set of measurements, spatial frequency was held constant and the required SNR was varied. In this scheme, the temperature difference that provided the required SNR was recorded. This was repeated for four different target bar frequencies. The main objective was to measure the dependence of the MRTD on the required SNR for different spatial frequencies.

C. MEASUREMENT RESULTS

The results from the two different sets of measurements are presented in Figures 6.5 and 6.6. Appendix D gives these results in a tabular form. The following observations are made from Figure 6.5. An MRTD trend similar to the ones obtained in subjective measurements is noticeable. However MRTD cuts off at a significantly lower spatial frequency compared to the subjective MRTD cutoff. Objective MRTD values are higher

for all spatial frequencies than the subjective MRTD values. This indicates that the human eye-brain is a very efficient combination to pick out signals in a noisy environment. Although there is not an observable asymptotic behavior at the low spatial frequency end, the curve indicates that a non-zero low frequency threshold for MRTD does exist, which supports the visibility concept approach.

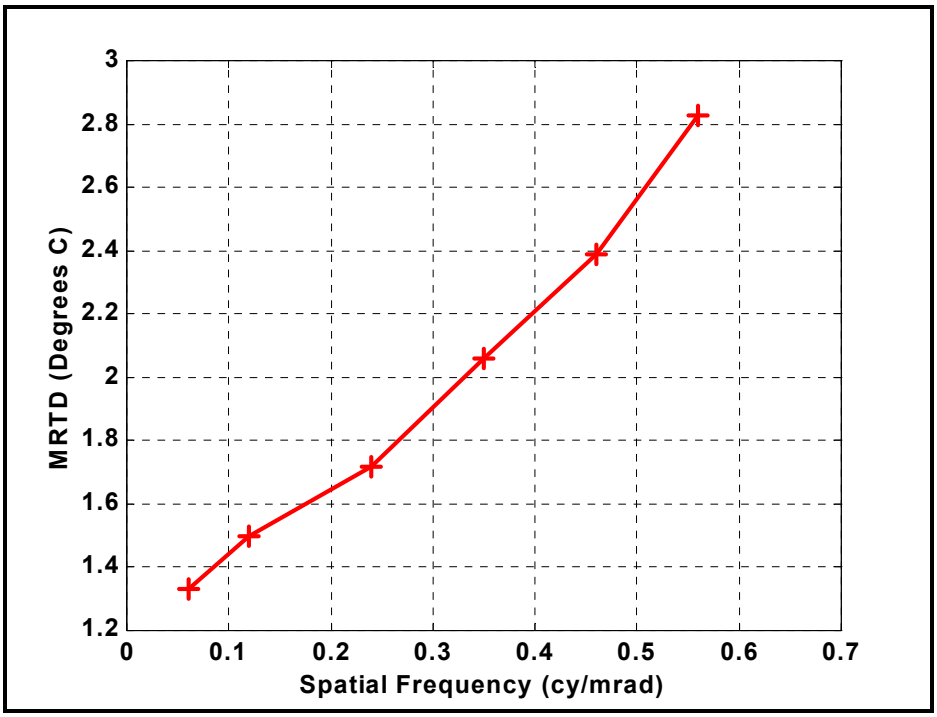

Figure 6.5. Measured Objective MRTD (SNR=6.0).

The family of curves given in Figure 6.6 suggests the following expected but useful conclusions. First, an increase in the temperature difference between the bars and the background of the MRTD pattern translates to an approximately equal increase in the observed voltage difference between the signal corresponding to the bars and the background, such that the ratio of delta T to delta V remains approximately constant. Second, for any given spatial frequency, the temperature difference required to 'see' four bars in the signal increases approximately linearly as the SNR requirement is increased.

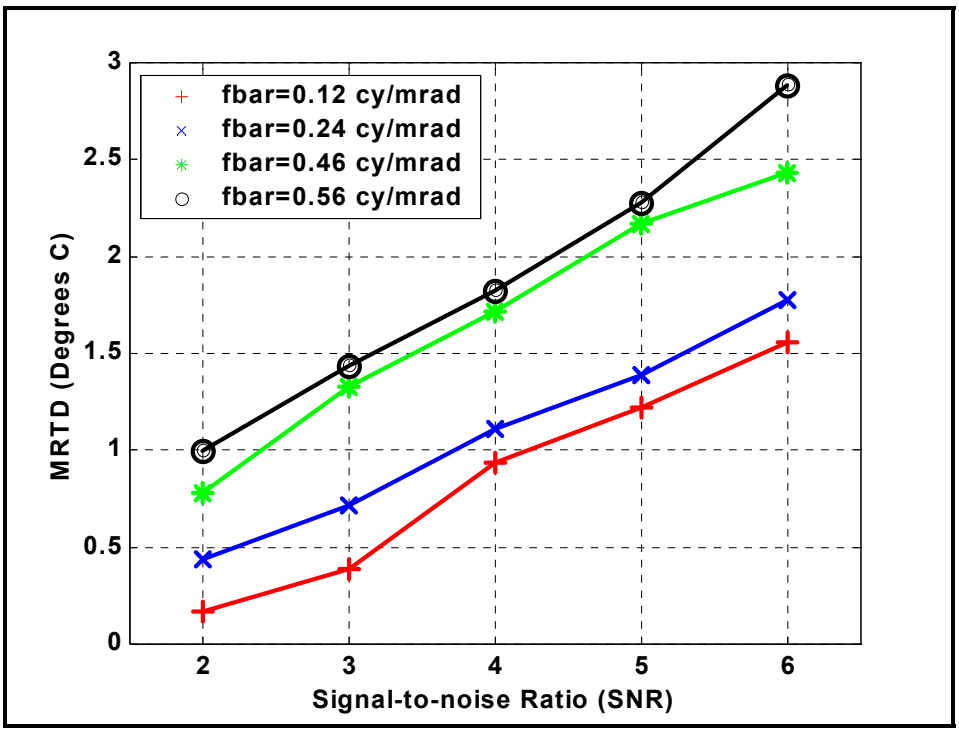

Figure 6.6. Measured Objective MRTD vs. Required SNR for Various Four-Bar Spatial Frequencies.

The data obtained in the second set of measurements can be interpreted in a different way. The second interpretation gives a new set of curves depicted in Figure 6.7 that demonstrate the measured MRTD values as a function of spatial frequency for various SNR values. The curves show that for all SNR values the MRTD values increase with the increasing spatial frequencies.

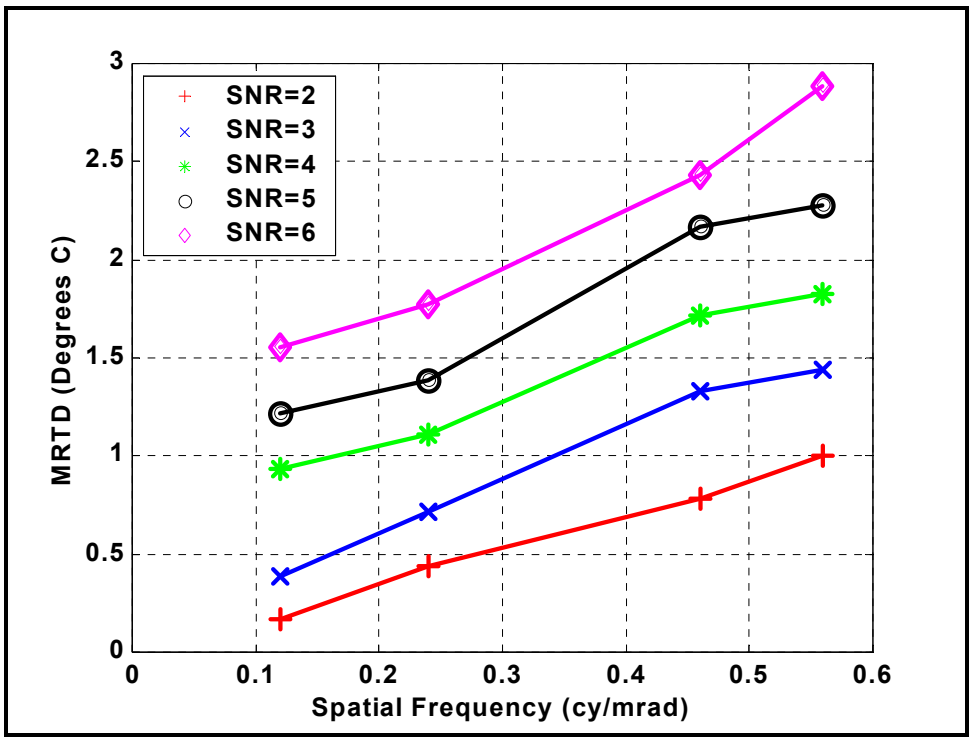

Figure 6.7. Measured Objective MRTD for Various Required SNR Values.

D. OBJECTIVE MRTD MODELING CONCEPTS

The results from the previous section indicated the presence of an objective minimum threshold contrast specific to the ATR device used and a spatial-frequency-dependent contrast transference parameter. These suggested the applicability of the subjective MRTD formulation given by Equation 6.1 to the objective MRTD scheme.

$$MRTD(f_z) = \frac{\Delta T_{sco}}{\alpha(f_z)} \tag{6.1}$$

Then, objective MRTD modeling is conceptually identical to the subjective MRTD case, with the appropriate values calculated for the minimum threshold contrast and the contrast transference parameter.

Based on the results from the laboratory experiments the following heuristic formulation for objective minimum threshold contrast is proposed.

$$\Delta T_{sco} = SNR_{thr} \frac{\Delta T}{\Delta V} V_n \tag{6.2}$$

where:

SNR_{thr} is the required signal-to-noise ratio,

ΔT is the temperature difference between the target and background,

ΔV is the change in voltage in Volts due to ΔT, and

V_n is the measured rms noise voltage in Volts.

Although simpler in nature, this formulation is compatible with its subjective counterpart (Equation 4.2). Note that the measured rms noise value replaces the three-dimensional noise values and SNR enhancement due to eye temporal integration is not applicable. This formula assumes that the ratio $\Delta T/\Delta V$ is approximately constant and suggests that the minimum threshold input contrast increases if there is more low-spatial-frequency noise present. As the curves from Figure 6.6 and the subjective ΔT_{sc} formulation suggest, the form proposed for the objective minimum threshold contrast accounts for the increase in input threshold with increasing SNR_{thr}. Given the measured values of the rms noise voltage, and the differential signal voltage created by a differential temperature at the low spatial frequency limit, the minimum threshold contrast can be calculated for any given threshold SNR requirement using Equation 6.2. For the Mitsubishi system, this value was calculated to be 1.33 degrees Celsius for a threshold SNR value of 6.0, which is approximately 15 times higher than the subjective minimum threshold contrast corresponding to the same threshold SNR condition.

Having established a method for predicting ΔT_{sco}, we continue with the calculation of the other essential part of the MRTD formulation, i.e. the objective contrast transference parameter. This parameter remains conceptually the same for objective MRTD except for the fact that the display is not a part of the MRTD measurement process, hence the display MTF is no longer required in the reconstruction MTF. All other blurring effects due to the thermal imaging sub-system transfer functions and the

aliasing effects due to the sampling in the detector array are equally relevant for objective MRTD predictions.

E. COMPARISON OF MODEL RESULTS WITH MEASURED DATA

The VISMODII model objective MRTD prediction for a constant SNR value of 6.0 is given in Figure 6.8 and this data is plotted together with the measured objective MRTD values in Figure 6.9. Two curves are very close together at the low spatial frequency limit; the results are encouraging and demonstrative of the accuracy of the model concepts.

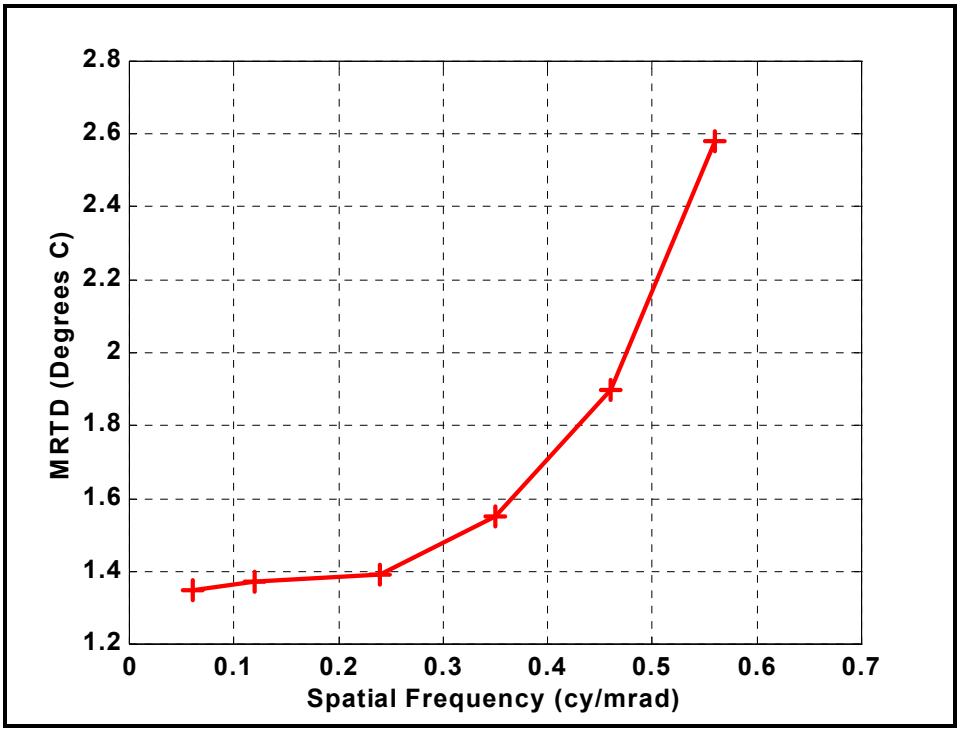

Figure 6.8. VISMODII Objective MRTD Predictions (SNR=6.0).

Figure 6.10 demonstrates the model outputs for MRTD versus the required SNR for four different spatial frequencies. Note the linear increase in MRTD with increases in the required SNR, consistent with the measured trend (Figure 6.6). The two curves at the lower section of the figure are very close together indicating the low spatial frequency asymptote in the predicted MRTD curves. The predictions are plotted together with the measured data in Figures 6.11 through 6.14.

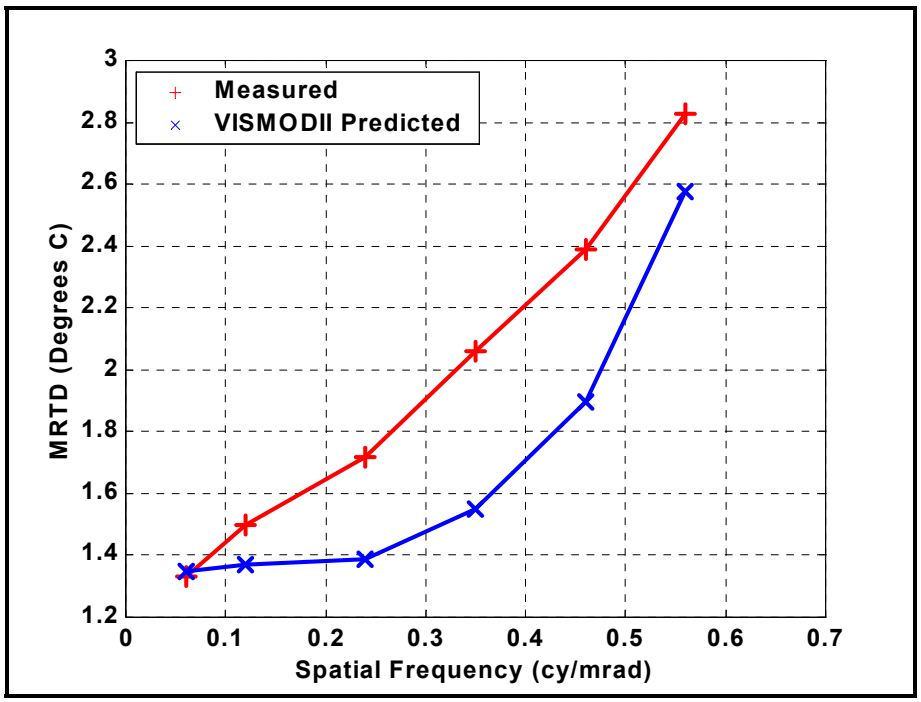

Figure 6.9. Objective MRTD Comparison (SNR=6.0).

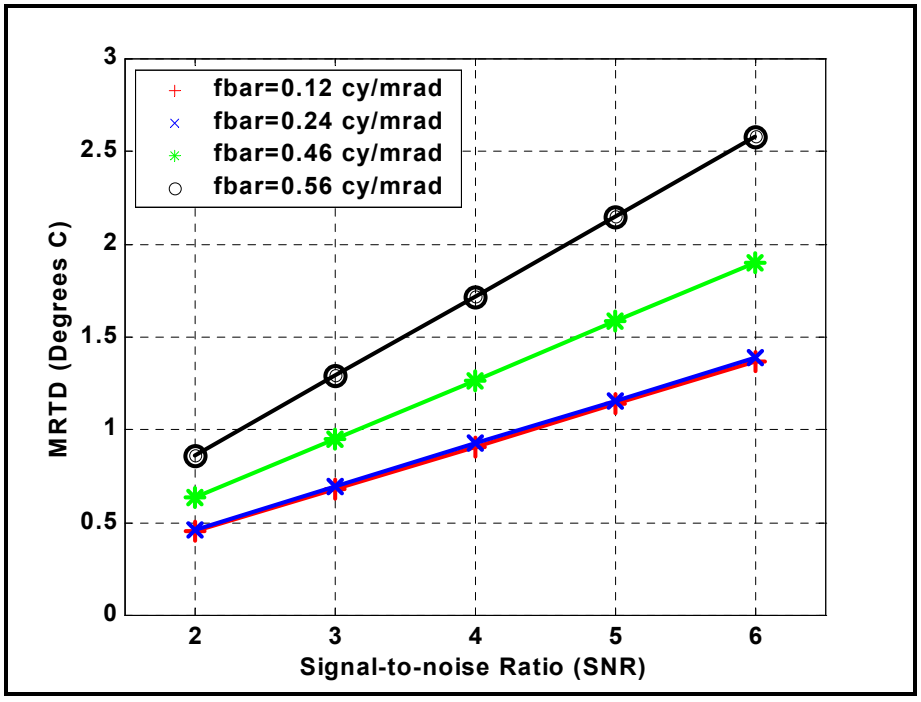

Figure 6.10. VISMOD II Predicted MRTD vs. Required SNR for Various Four-Bar Spatial Frequencies.

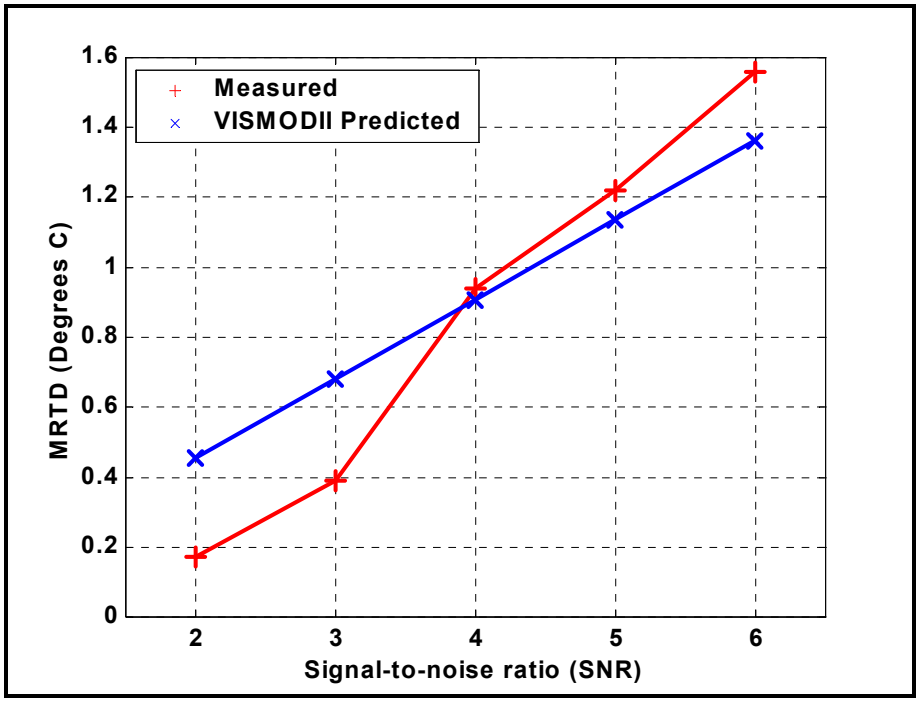

Figure 6.11. Objective MRTD vs. Required SNR Comparison (f_s=0.12 cy/mrad).

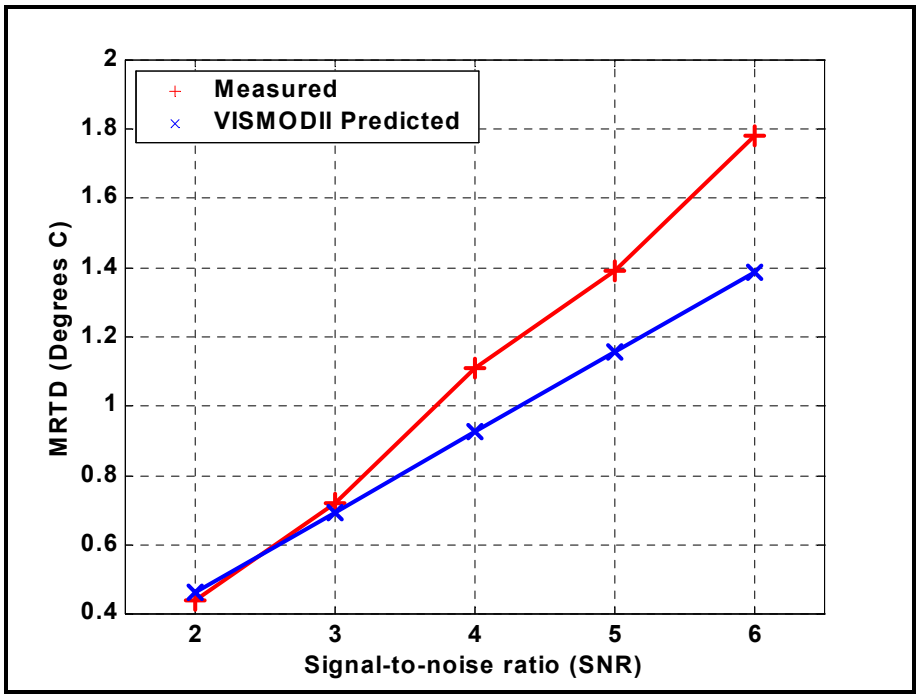

Figure 6.12. Objective MRTD vs. Required SNR Comparison (f_s=0.24 cy/mrad).

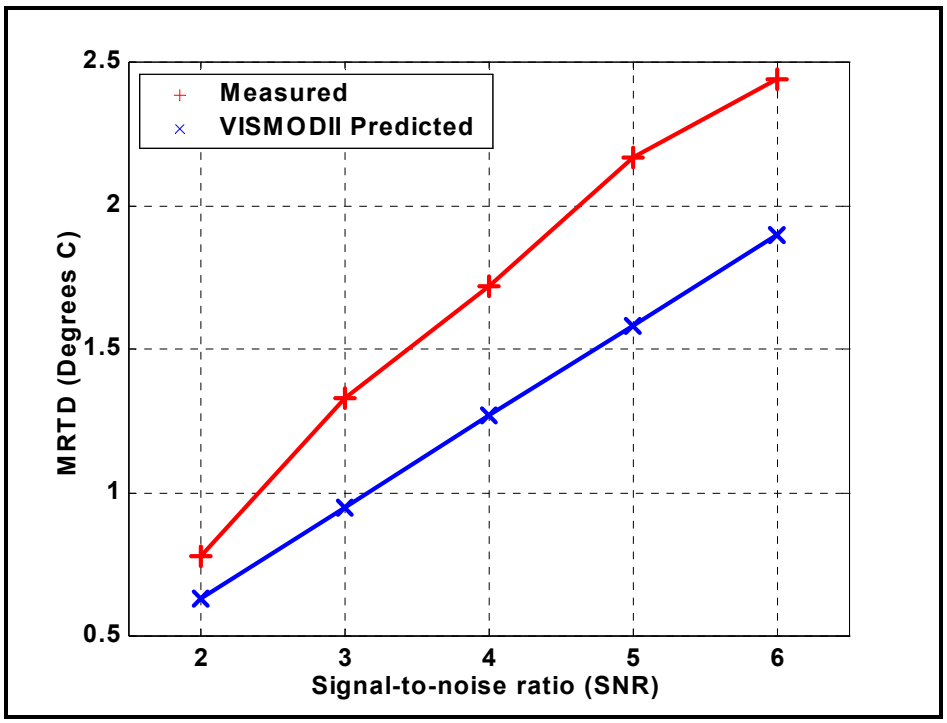

Figure 6.13. Objective MRTD vs. Required SNR Comparison (f_s=0.46 cy/mrad).

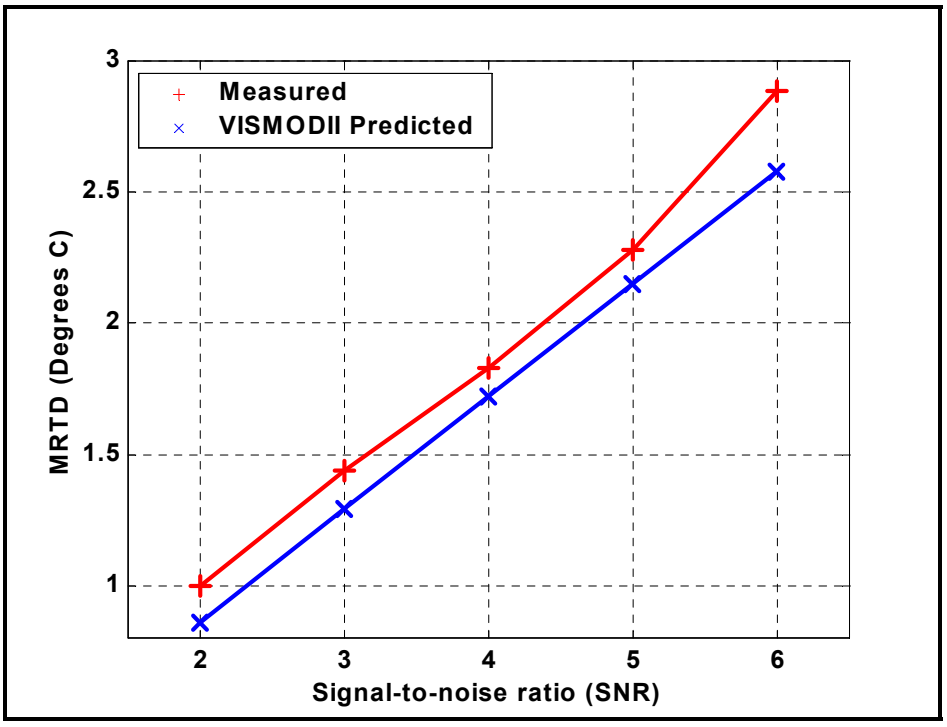

Figure 6.14. Objective MRTD vs. Required SNR Comparison (f_s=0.56 cy/mrad).

The differences observed between the predictions and the measured data may be attributable to the difficulties in thresholding during the measurements. The equipment precision is also an important issue in the measurements. The measured MRTD values seem to be higher than the simulated results suggesting that a contrast-degrading factor may be introduced in the measurement process, such as an oscilloscope MTF, that is not included in the model. Follow-up work in this area may pursue an additional MTF corresponding to this contrast degradation.

VISMODII objective MRTD values for different values of threshold SNR are presented in Figure 6.15. For each value of SNR, the typical MRTD curve trend is observable.

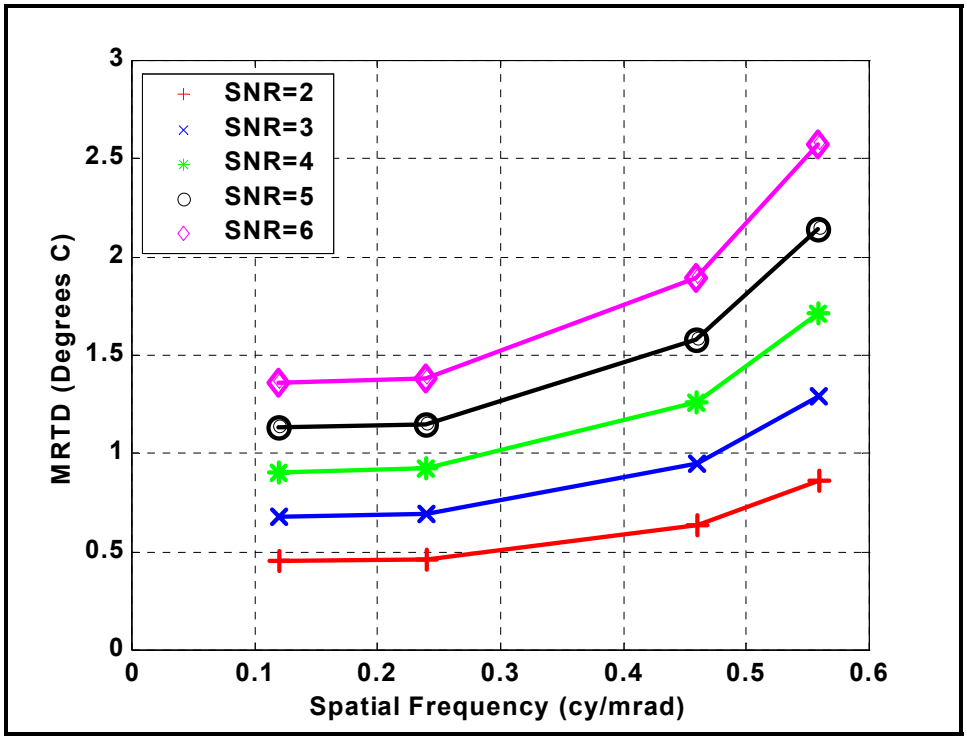

Figure 6.15. VISMOD II Objective MRTD vs. Spatial Frequency Predictions for Various Required SNR Values.

Comparisons of this data with the measured MRTD curves are provided in Figures 6.16 through 6.20. On the figures, the average percent error between the predicted and measured values is written. The error is significantly higher at the smaller

SNR values of 2.0 or 3.0. The level of agreement between the measured and the predicted MRTD values increases along with increases in the SNR. For an SNR of 2.0, the error is 25 percent, however this value drops approximately by a factor of two when the required SNR is 4.0. This may be due to the difficulty in measuring the signal level when the signal is barely distinguishable in noise.

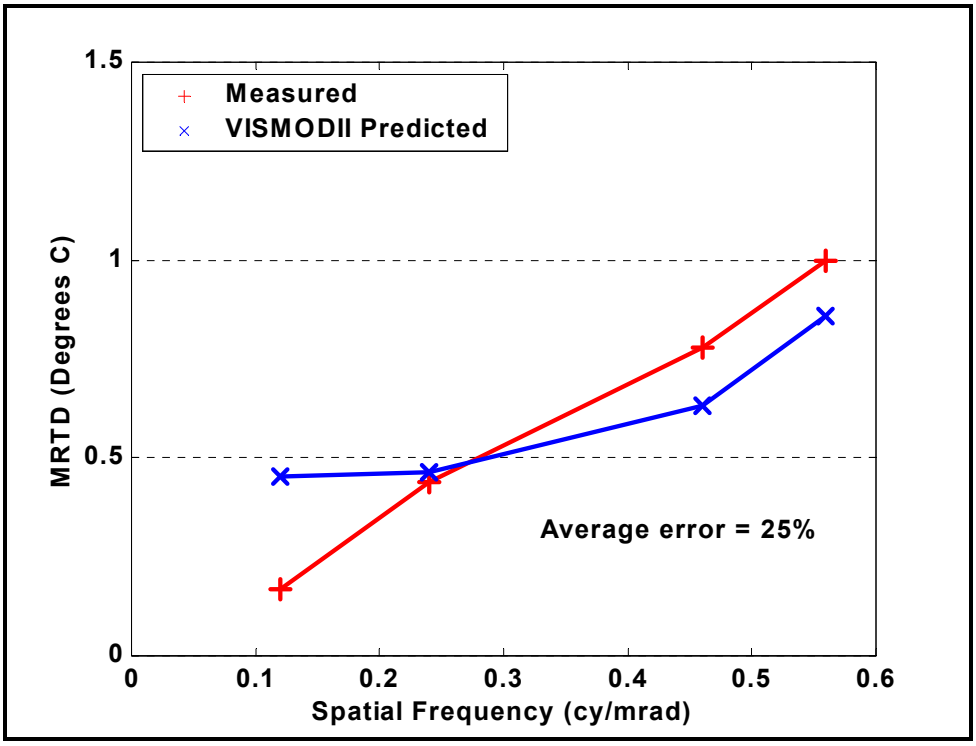

Figure 6.16. Objective MRTD vs. Spatial Frequency Comparison (SNR=2).

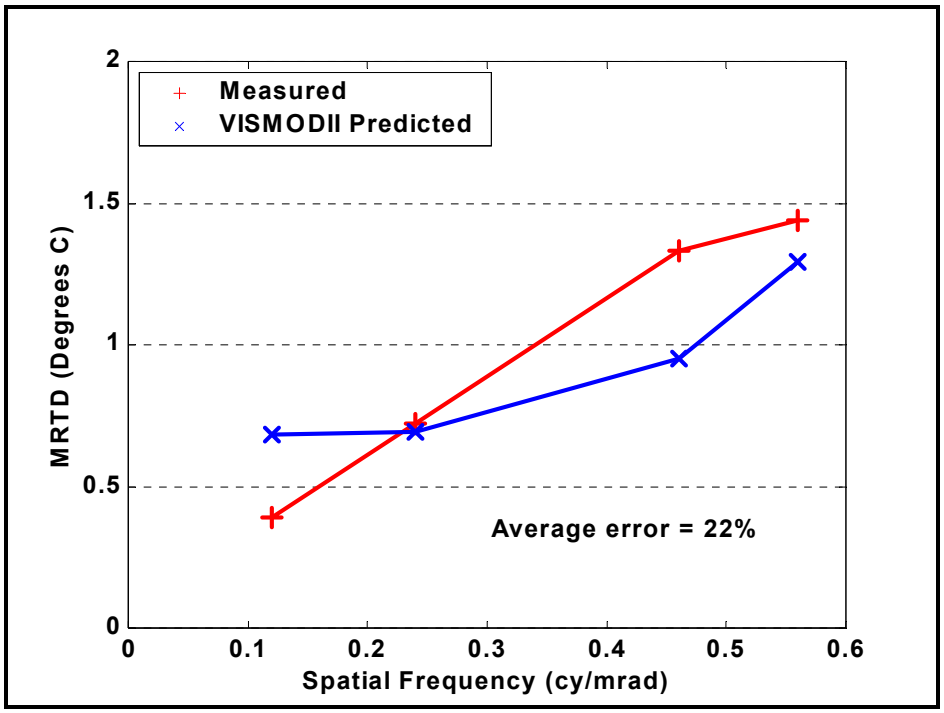

Figure 6.17. Objective MRTD vs. Spatial Frequency Comparison (SNR=3).

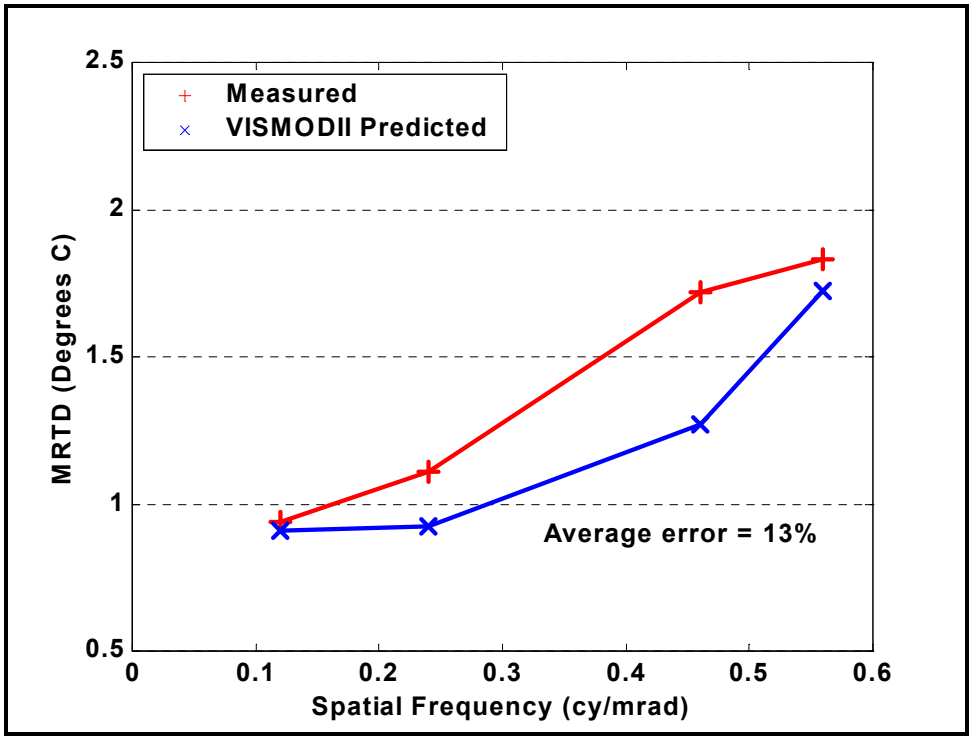

Figure 6.18. Objective MRTD vs. Spatial Frequency Comparison (SNR=4).

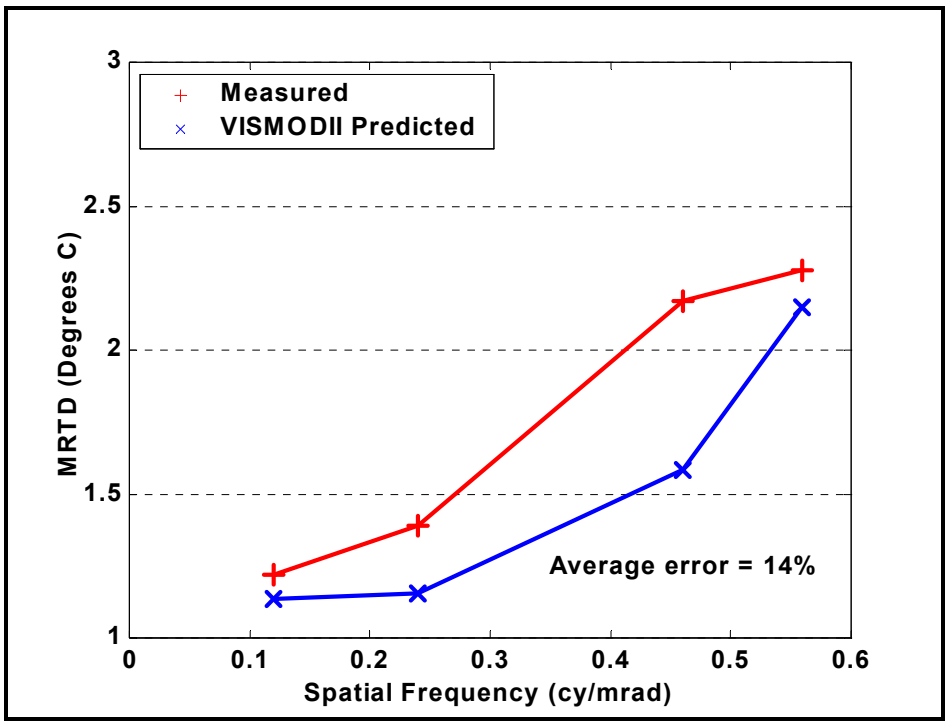

Figure 6.19. Objective MRTD vs. Spatial Frequency Comparison (SNR=5).

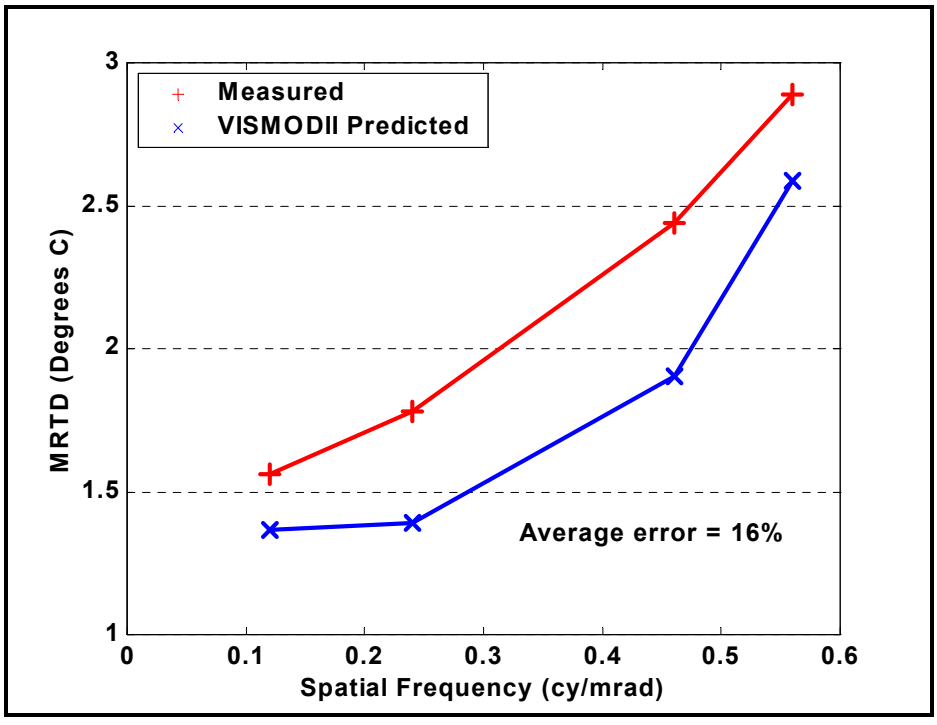

Figure 6.20. Objective MRTD vs. Spatial Frequency Comparison (SNR=6).

VII. CONCLUSIONS AND RECOMMENDATIONS

The main objective of this thesis was to improve the VISMODII model and to extend it to predict objective MRTD. This chapter will highlight the conclusions reached during this work and will provide recommendations for further research.

A. CONCLUSIONS

In this thesis, the VISMODII model has been improved to obtain more accurate predictions. In particular, the analysis of contrast transfer and the formulation of minimum input threshold have been refined. The improved version of VISMODII treats the aliasing issue in such a way that the contrast enhancement due to aliasing below the Nyquist limit is accounted for. The model also has the capability of incorporating scene-phasing effects. As demonstrated in Chapter V the effects of sampling, aliasing and scene phasing have an important impact on the MRTD performance of a thermal imager.

The laboratory experiments provided the data to compare the predictive results from VISMODII with the FLIR92 model outputs and the measurement results. The comparisons presented in Chapter V demonstrated that the improved VISMODII gives results that are in better agreement with the measured data than predictions from the FLIR92 model.

The modeling concepts of the improved VISMODII model have been recognized by the community outside the NPS. Appendix I will provide a pre-print of the paper that was accepted for presentation at the Thirty-Fifth Asilomar Conference on Signals, Systems, and Computers on November 4 – November 7, 2001.

The extension of VISMODII to predict objective MRTD discussed in Chapter VI is an important accomplishment. The visibility concept has been demonstrated to be applicable in predicting the objective MRTD. The laboratory measurement of objective MRTD provided the data to evaluate the performance of the 'Objective VISMODII' model. Although the measurements are limited in scope, they do demonstrate that the VISMODII predictive model can also be applied to objective MRTD measurements.

B. DIRECTIONS FOR FURTHER RESEARCH

The differences between the predicted and measured values for the vertical MRTD indicate the need to analyze the asymmetrical effects of the display [Ref. 40] on MRTD results. In particular the different effects of the display on resolution in the horizontal and vertical directions need further analysis. The inclusion of a non-symmetrical display MTF may be considered in this regard.

The simulation results given in Chapter VI suggest a consistent trend for the predictive objective MRTD values to be lower than those measured. This indicates that the model may not reflect some contrast-degrading effect introduced in the measurement process. Inclusion of the oscilloscope in the measurements may require the introduction of an additional unknown MTF that will account for the contrast degradation in the output signal. A more detailed analysis of the device properties and the contrast transference parameter for the objective MRTD may lead to an improved level of agreement between the measured and predicted results.

The current version of VISMODII uses a heuristic formulation (Equation 6.2) for objective threshold input contrast. This formula requires the measured values of the RMS noise voltage and the differential signal voltage created by a differential temperature at the low spatial frequency limit. Development of an analytic prediction for objective threshold input contrast would be an important enhancement.

VISMODII predicts the MRTD for the two orthogonal, i.e. horizontal and vertical directions. It has been suggested that this approach may not be appropriate in assessing the performance of thermal imaging systems incorporating more complex sampling schemes [Ref. 3]. A more complete two-dimensional model should have the ability to provide the MRTD values along any intermediate orientation of the bar pattern. This would be a valuable contribution to the VISMODII model.

VISMODII currently uses the 256-point 2D FFT process to convert from the spatial domain to the spatial frequency domain. The number of points in the FFT process imposes a limitation on spatial frequencies that can be represented in the spectrum. The

model can be modified in such a way that gives the user the flexibility to use 'N' point FFT.

More experiments using a different thermal imaging system could provide additional data to evaluate the simulation results. Finally, the equipment precision proved to be a limiting factor in the laboratory experiments. More measurements can be taken using different digital thermometers and heating units with better accuracy.

THIS PAGE INTENTIONALLY LEFT BLANK

APPENDIX A. TIS PARAMETERS

This appendix lists the parameters of the Mitsubishi Electronics IR-M500 thermal imaging system [Ref. 41] that was used in the laboratory measurements. These parameters are used in FLIR92 and VISMODII model simulations.

MITSUBISHI IR-M500 THERMAL IMAGING SYSTEM

BLIP Performance ..... YES
Spectral cut-on [V] ..... 3.0 micrometers
Spectral cut-off [V] ..... 5.0 micrometers
F/number [V] 1.4
Focal length [V] ..... 5.0 cm
Optical transmittance [V] 0.95
Frame rate [V] ..... 60 Hz
Detector active horizontal dimension [V] ..... 16.24 micrometers
Detector active vertical dimension [V] ..... 12.49 micrometers
D* [V] ..... 5.0×10^{10} cmHz $^{1/2}$ /W
Integration time [V] ..... 16145.833 microseconds
Number of horizontal detector elements [V] 512
Number of vertical detector elements [V] 512
Detector cell horizontal dimension [V] ..... 26 micrometers
Detector cell vertical dimension [V] ..... 20 micrometers
PtSi emission coefficient 0.16 1/eV
Schottky barrier height ..... 0.22 eV
Number of active CRT lines 480
Display brightness ..... 10.0 milliLamberts
Display height ..... 27.94 cm
3D noise level ..... MOD

[V] indicates that the parameter is used in the VISMODII model.

THIS PAGE INTENTIONALLY LEFT BLANK

APPENDIX B. DETAILED SPATIAL FREQUENCY ANALYSIS IN VISMODII

In this appendix, we provide detailed explanations on a few topics related to the spatial frequency analysis in the VISMODII model.

Using the thermal imaging system parameters given in Appendix A, the following calculations can be made. Detector cell horizontal dimension is given as 26 micrometers. Using the focal length of 5 centimeters, the spatial sampling period in the horizontal direction can be calculated as:

$$\Lambda = \frac{\Delta x}{F} = \frac{26\ \mu m}{50\ mm} = 0.52\ mrad \tag{B.1}$$

The spatial sampling frequency is the reciprocal of the sampling period:

$$f_{sx} = \frac{1}{\Lambda} = \frac{1}{0.52\ mrad} = 1.92\ cycles/mrad \tag{B.2}$$

The Nyquist frequency limit in the horizontal direction is defined as half the horizontal spatial sampling frequency:

$$f_{NX} = \frac{f_{sx}}{2} = \frac{1.92\ cycles/mrad}{2} = 0.96\ cycles/mrad \tag{B.3}$$

Equation B.4 gives the horizontal MRTD target spectrum, which is the two-dimensional Fourier transform of the four-bar pattern.

$$I(f_x, f_y) = \left[\left(\frac{1}{\pi f_x}\right)\left(-\sin(\pi f_x d) + \sin(3\pi f_x d) - \sin(5\pi f_x d) + \sin(7\pi f_x d)\right)\right] \times \left(\frac{1}{\pi f_y d}\right)\sin(7\pi f_y d) \tag{B.4}$$

where f_x and f_y are the spatial frequencies along the horizontal and vertical directions and d is the width of one bar. A plot of this spectrum along the x-axis (f_y=0) is given in Figure B.1 for a four-bar target spatial frequency of 0.65 cycles/mrad. Note the repetition

of the spectrum at intervals of the sampling frequency. The figure shows that the sample-generated replicas of the original spectrum overlap with the target spectrum (baseband) and aliasing occurs. The figure clearly suggests that aliasing is an issue for bar-targets at four-bar spatial frequencies below the Nyquist limit (B.3).

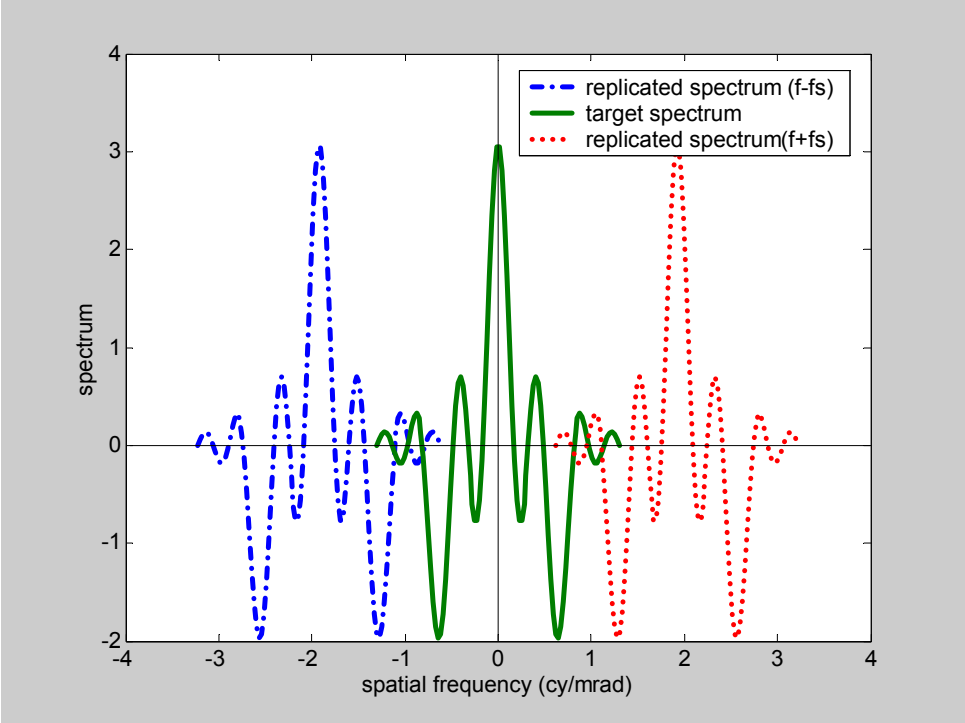

Figure B.1. Horizontal MRTD Bar-Pattern along the x-Axis ($f_y = 0$) (Four-Bar Target Frequency: 0.65 cy/mrad).

VISMODII uses the 2D FFT process to convert from the spatial domain to the spatial frequency domain. Each bar on the target pattern is represented by 10 elements in width and 70 elements in height (7:1 aspect ratio) in a two-dimensional matrix. The number of points that represents each bar imposes a limitation on the maximum spatial frequency that can be represented in the 2-D FFT spectrum. The angular separation Δw corresponding to two adjacent elements in the matrix can be related to the width of one-bar in the following manner:

$$\Delta w = \frac{d\ (mrad)}{10} \tag{B.5}$$

Four-bar target angular spatial frequency can be written in terms of the angular bar width as:

$$f_s = \frac{1}{2d} \quad cy/mrad \tag{B.6}$$

Equation B.7 gives the maximum frequency that can be accurately represented by the FFT process [Ref 42].

$$f_{\max} = \frac{1}{2\Delta w} = \frac{10}{2d} = 10 \times f_s \tag{B.7}$$

In VISMODII, the bar pattern is created only once, and in the program the spatial frequencies that are used in creating the MTF/OTFs are scaled according to the four-bar target spatial frequency. The spatial frequency matrices used in creating the MTF/OTFs are of 256x256 elements and take values between $-f_{max}$ and f_{max}. The DC term in the matrices correspond to the 129,129 th element in the matrix as shown in Figure B.2. Therefore, the negative frequency spectrum is represented by 128 elements and the positive spatial frequency spectrum is represented by 127 elements.

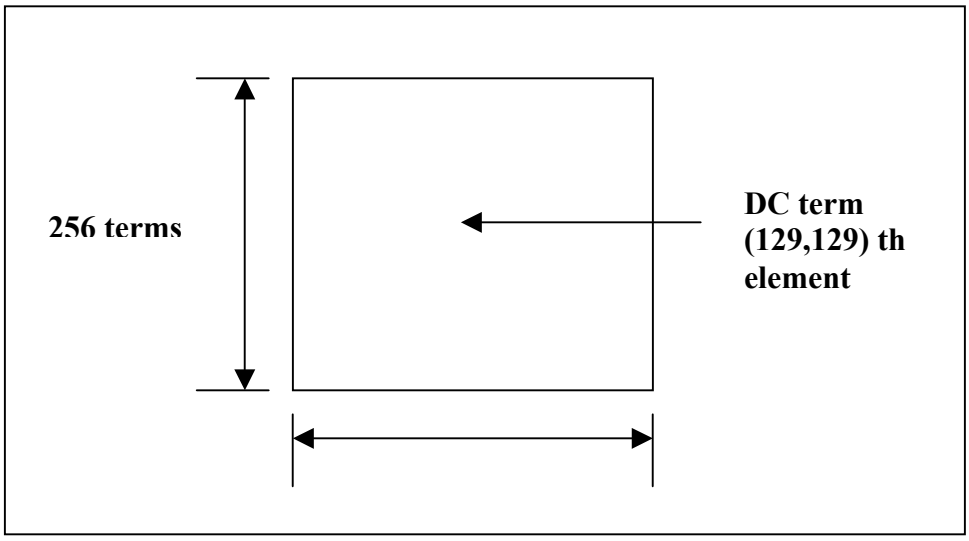

Figure B.2. Spatial Frequency Matrix Demonstrating the DC Term.

The spatial frequency matrix is created separately for the horizontal and vertical directions. Two-dimensional spatial frequency is obtained by using Equation B.8. In creating the detector MTF (Equations 3.29 and 3.30) one-dimensional spatial frequencies need to be used. In the diffraction-limited optics MTF (Equation 3.27), optics geometric blur MTF (equation 3.28) and display MTF (Equation 3.32), two-dimensional spatial frequency is used.

$$f = \sqrt{f_x^{\,2} + f_y^{\,2}} \tag{B.8}$$

The model does not use the spatial frequencies described above in creating the electronics OTF, as the OTF is obtained directly from the exact two-dimensional Fast Fourier Transform (FFT) of the impulse response of the RC filter. The form used for the impulse response is repeated here for convenience:

$$h_{xy}(x,y) = e^{-2\pi f_{3dB} x} \times e^{-2\pi f_{3dB} y} \tag{B.9}$$

where:

f_{3dB} is the electronics 3dB cutoff frequency in cy/mrad,

x and y are the space variables in the horizontal and vertical directions in mrad. The variables x and y are obtained in the following manner. The incremental distance in mrad between the elements in the matrix (256x256 matrix representing the spatial domain) is given by:

$$\Delta w = \frac{1}{2 f_{\max}} \tag{B.10}$$

Then, the variables x or y, corresponding to a specific point in space is given by the incremental distance between elements multiplied by the index corresponding to the particular point.

$$x = (Index) \times \Delta w \tag{B.11}$$

where Index is an integer between 1 and 256.

APPENDIX C. ASSESSMENT OF MTF SQUEEZE MODEL FOR ACCOUNTING FOR ALIASING EFFECTS

In this appendix, the MTF Squeeze approach that has been developed to account for sampling and aliasing effects in the NVTherm model is presented.

In Chapter III we have looked at FLIR92 briefly, and noted that FLIR92 limits MRTD predictions to the Nyquist frequency. Laboratory measurements, however, indicated that with sampled sensors it is possible to measure MRTD beyond the sensors half sample rate [Ref. 23]. The MTF squeeze approach is used in the NVTherm model to account for sampling and aliasing artifacts and to extend the MRTD predictions beyond the half sampling frequency.

Perception experiments were conducted with the objective to determine the effects of sampling on human performance of visual tasks. Probability of recognition and identification of military targets were measured using various levels of blur and undersampling. The results of these measurements have been used in developing the "MTF Squeeze" model [Ref. 27].

Sampling introduces an additional blurring effect since it creates ambiguity in the target edge location. The image appears wider than the object. The scaling property of the Fourier transform determines the relationship between space domain and spatial frequency domain such that an expansion in space domain corresponds to a contraction in image spectrum or vice versa. Therefore the additional blur appears as if the system has a narrower MTF. This phenomenon is called the MTF Squeeze [Ref. 4].

A. SPURIOUS RESPONSE TERM USED IN THE MTF SQUEEZE MODEL

The entire part of image spectrum other than the baseband is referred to as spurious response. Aliasing causes spurious response; the amount of spurious response depends on object spectrum, image formation MTF (pre sample blur), sampling frequency and image reconstruction filter (post sample blur). Spurious response capacity of an imager can be determined from the system's response to a point source in the same way the MTF is defined for a continuous system [Ref. 27].

Considering a sampled imaging system, the response function of the imager in one dimension is formulated as follows:

$$R_{sp} = \left[\sum_{n=-\infty}^{\infty} H_i(f_x - nf_{sx}) e^{-j(f_x - nf_{sx})b} \right] H_r(f_x) \tag{C.1}$$

We can extract the n=0 term from the summation and write

$$R_{sp} = H_i(f_x) e^{-jf_x b} H_r(f_x) + \left[\sum_{\substack{n=-\infty \\ n \neq 0}}^{\infty} H_i(f_x - nf_{sx}) e^{-j(f_x - nf_{sx})b} \right] H_r(f_x) \tag{C.2}$$

where

$H_i(f_x)$ is the image formation MTF (optics and detector MTFs)

$H_r(f_x)$ is the image reconstruction MTF(display and eye MTFs)

f_{sx} is the sampling frequency in cycles/mrad

f_x is the spatial frequency in cycles/mrad

b is the spatial offset of origin from a sample point

In this form the n=0 term is defined as the transfer response or the baseband response and is equivalent to the total system MTF, and the right side of the equation is defined as the spurious response function. Transfer response has no dependence on sampling properties. In the limit when sample spacing goes to zero, the response function will be equal to the transfer response. A sampled imager always has the spurious response terms. These terms are the sampling-generated replicas of the image formation filter multiplied by the image reconstruction filter. If horizontal and vertical system MTFs are not identical, spurious responses for horizontal and vertical directions can be different [Ref. 27].

The sampling frequency determines the position of the spurious response terms on the spatial frequency axis. An effective reconstruction filter can remove high frequency

spurious signal, however some spurious spectrum is always present in undersampled imagers. The spatial offset of the origin from a sample point (sample phase) defines the phase relationship between the transfer response and the spurious response [Ref. 27].

Integrated spurious response to transfer response ratio (SR) is the term used to relate sampling effects to performance of the imager. Total spurious response is made up of in-band spurious response and out-of band spurious response. Figure C.1 illustrates this concept.

Total and in-band spurious responses are calculated using the equations:

$$SR = \frac{\int_{-\infty}^{\infty} (Spurious\ response)df}{\int_{-\infty}^{\infty} (Transfer\ response)df} \tag{C.3}$$

$$SR_{in-band} = \frac{\int_{-f_{sx}/2}^{f_{sx}/2} (Spurious\ response)df}{\int_{-\infty}^{\infty} (Transfer\ response)df} \tag{C.4}$$

Out-of-band spurious response is determined from the relationship

$$SR = SR_{in-band} + SR_{out-of-band} \tag{C.5}$$

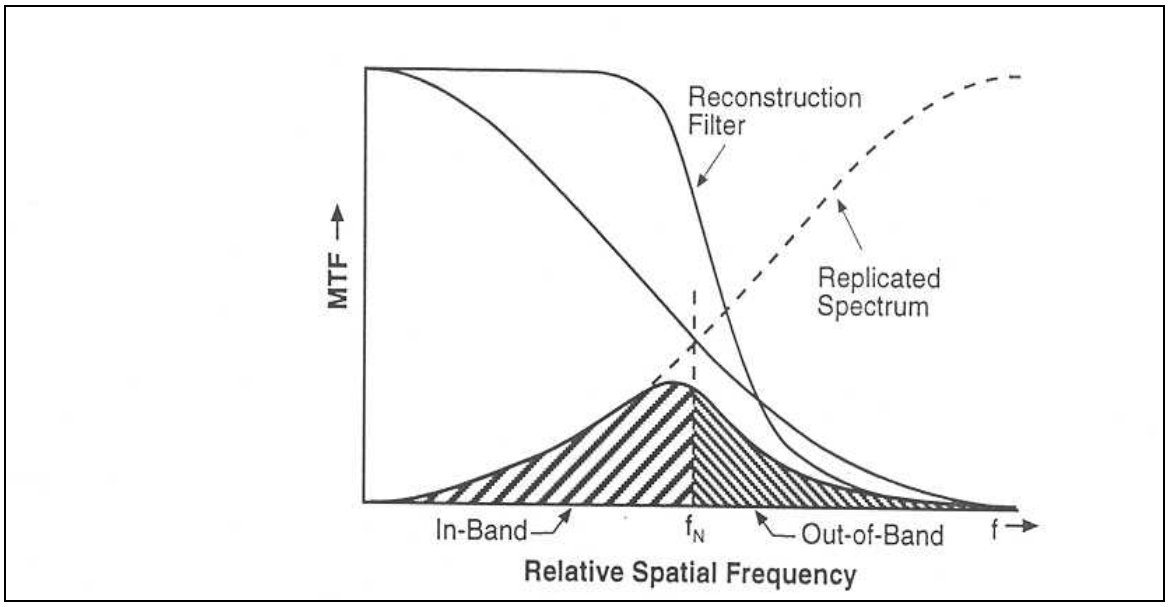

Figure C.1. Definition of In-Band and Out-of Band Spurious Response "From [Ref. 4]".

Ideally, out-of-band spurious response can be removed by reconstruction filter. However, ideal filters are difficult to realize and removing out-of-band spurious response comes with the penalty of removing baseband spectrum also. Therefore both in-band and out-of band spurious responses exist and degrade performance [Ref. 28].

B. MTF SQUEEZE FACTORS

There are a number of theories that relate sampling-aliasing effects to performance. One theory treats spurious response effects as temporally coherent fixed pattern noise. Another theory suggests a change in Johnson's criteria of resolvable cycles to account for the differences observed between staring and scanning sensors. MTF Squeeze models the performance degradation due to undersampling by reducing the MTF. A squeezed MTF is used in the sensor model to quantify the effects of aliasing [Ref. 28].

Two perception experiments were conducted at NVESD in order to assess the impacts of sampling and aliasing on target recognition and identification. One was a recognition and the other was an identification test [Ref. 27]. In the experiments, the

amount of spurious response was controlled by sample spacing [Ref. 28]. The data from these tests revealed that performance degradation due to sampling is equivalent to an additional blur in the image [Ref. 27]. The two-dimensional relative blur increase RI for recognition was found to be:

$$RI = \frac{1}{1 - 0.32SR} \tag{C.6}$$

If sampling and thus spurious response is present in only one direction, blur increase becomes:

$$RI = \frac{1}{\sqrt{1 - 0.32SR_{v\,or\,h}}} \tag{C.7}$$

The scaling property of the Fourier transform allows the representation of the added blur as a contraction in MTF. MTF squeeze factor is defined as the reciprocal of the blur increase:

$$MTFsqueeze = \sqrt{1 - 0.32SR_v} \times \sqrt{1 - 0.32SR_h} \tag{C.8}$$

If the spurious responses in the two directions are equal, squeeze factor becomes:

$$MTFsqueeze = 1 - 0.32SR \tag{C.9}$$

MTF squeeze is applied as depicted in Figure C.2 separately to the horizontal and the vertical MTFs. At each point on the MTF curve, frequency is scaled by the squeeze factor [Ref. 28]. Therefore, modulation transfer at a spatial frequency degrades depending on the amount of spurious response [Ref. 26].

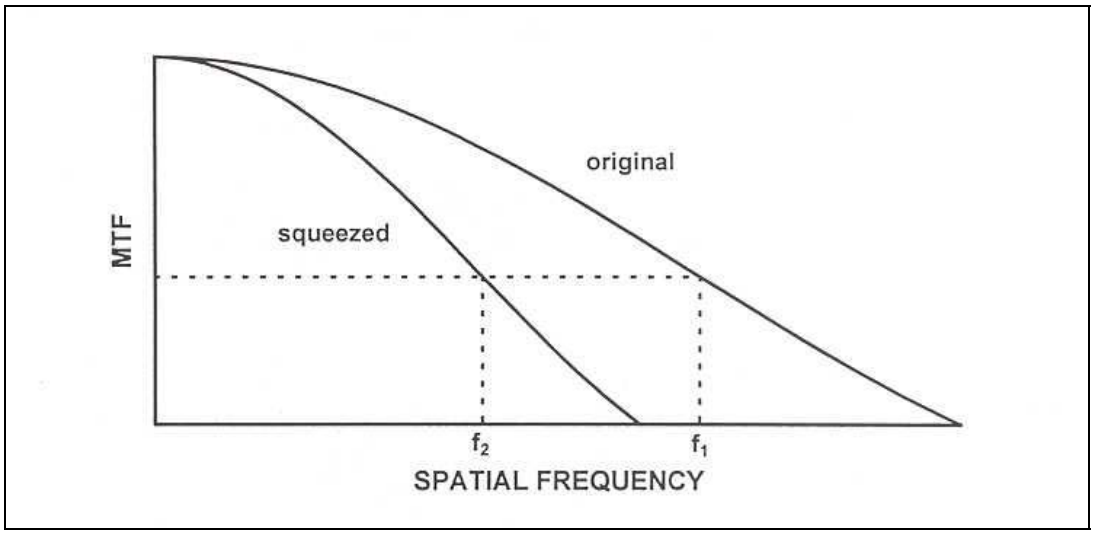

Figure C.2. MTF Squeeze. For recognition f_2=(1-0.32SR) f_1 "From [Ref. 4]".

Similarly, the experiment conducted for identification performance yielded the squeeze factor for identification as

$$MTFsqueeze = \sqrt{1-2SR_{v-out-of-band}} \times \sqrt{1-0.32SR_{h-out-of-band}} \qquad (C.10)$$

and if the spurious response is the same in the two directions

$$MTFsqueeze = 1-2SR_{out-of-band} \qquad (C.11)$$

The results of the experiments suggest the relationships between spurious response and performance as explained in Table C.1.

Task	**In-Band SR** (Edge shifting, line width variations, other local artifacts)	**Out-of-Band SR** (Raster, sharply demarcated pixels)	**MTF Squeeze**
Hot-Spot Detection	Moderate to Large Dependence	Small Dependence	Speculation
Recognition	Moderate Dependence	Moderate Dependence	1-0.32SR
Identification	Small Dependence	Large Dependence	1-2SRout-of-band

Table C.1. Performance Dependence on Spurious Response "From [Ref. 28]".

It is important to note that the MTF Squeeze model applies only to static field performance [Ref. 28], since sampling rate changes when there is relative scene-sensor motion; and sampling rate is the controlled variable in the experiments conducted to obtain MTF squeeze factors.

C. COMPARISON WITH VISMODII APPROACH

In this section we make a qualitative comparison between the NVTherm and Visibility models' approaches for accounting for aliasing effects. Both methods are similar in that they treat sampling in the spatial frequency domain as the replication of the filtered scene spectrum at integral multiples of sampling frequency, and they relate aliasing to the additive spurious spectrum that overlaps the baseband.

However, there are two important distinctions between the two treatments. First, the MTF Squeeze model inherently assumes aliasing to be a contrast-reducing factor. As demonstrated in the previous section aliasing can have a contrast enhancing effect below the Nyquist limit. The second important issue relates to subjectivity. MTF squeeze factors used in the NVTherm model are derived semi-empirically. Experiments involve human observers and therefore the resulting squeeze factors are subjective. The Visibility model's approach on the other hand is totally based on a frequency domain analysis of the sampling and aliasing effects. As is demonstrated in Chapter VI, the VISMODII approach is equally applicable to an objective MRTD scheme.

THIS PAGE INTENTIONALLY LEFT BLANK

APPENDIX D. MEASUREMENT RESULTS

This appendix presents the measured data in tabular and graphical form. First subjective measurements are given. These are followed by the objective MRTD measurement results.

A. SUBJECTIVE MRTD MEASUREMENTS

Spatial frequency (cy/mrad)	MRTD (C) Heat up cycle (Trial 1)	MRTD (C) Cool down cycle (Trial 2)	MRTD (C) Average
0.06	0.11	0.06	0.08
0.09	0.22	0.06	0.14
0.12	0.28	0.11	0.19
0.15	0.28	0.17	0.22
0.18	0.28	0.17	0.22
0.24	0.33	0.22	0.28
0.29	0.39	0.28	0.33
0.35	0.44	0.33	0.39
0.46	0.50	0.33	0.42
0.56	0.56	0.39	0.47
0.72	0.72	0.50	0.61
0.79	0.83	0.72	0.78
0.88	1.06	0.83	0.94
1.13	2.06	1.00	1.53
1.17	2.83	2.83	2.83
1.21	8.00	6.78	7.39

Table D.1. Horizontal MRTD Measurements.

Spatial frequency (cy/mrad)	MRTD (C) Heat up cycle (Trial 1)	MRTD (C) Cool down cycle (Trial 2)	MRTD (C) Average
0.06	0.21	0.09	0.15
0.09	0.29	0.21	0.25
0.12	0.29	0.21	0.25
0.15	0.40	0.30	0.35
0.18	0.42	0.38	0.40
0.24	0.61	0.50	0.55
0.29	0.68	0.53	0.65
0.35	0.74	0.66	0.70
0.46	0.76	0.75	0.75
0.56	1.40	1.10	1.25
0.72	4.25	3.05	3.65
0.79	6.20	4.60	5.40
0.88	10.40	7.40	8.90
1.13	24.00	16.00	20.00

Table D.2. Vertical MRTD Measurements.

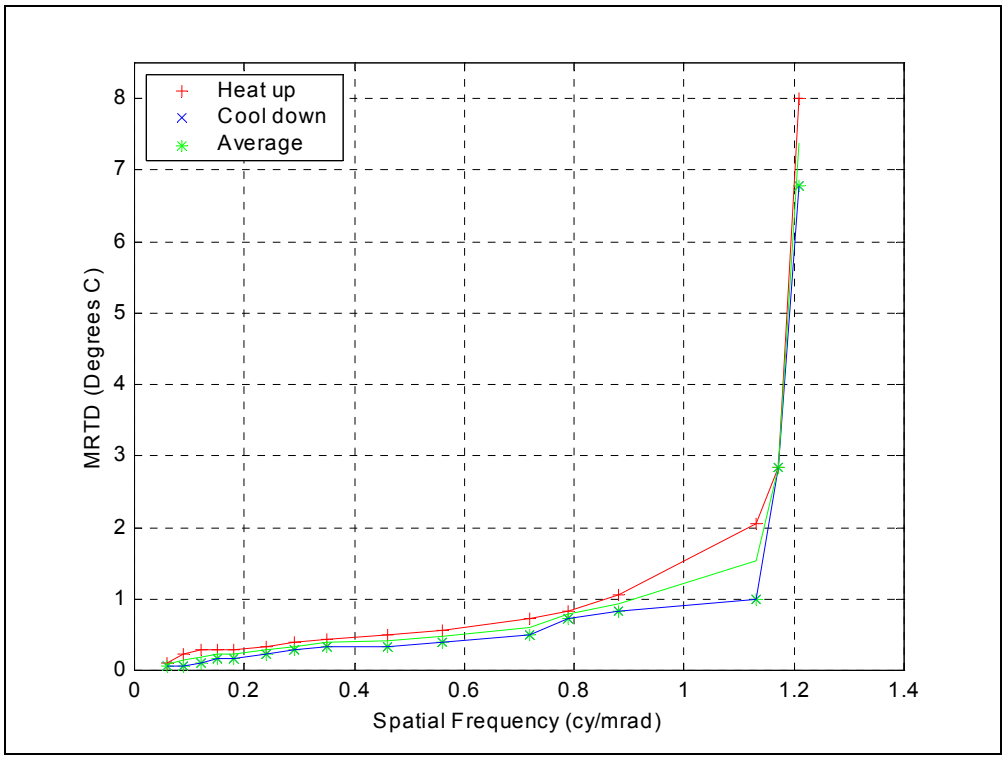

Figure D.1. Horizontal MRTD Measurements.

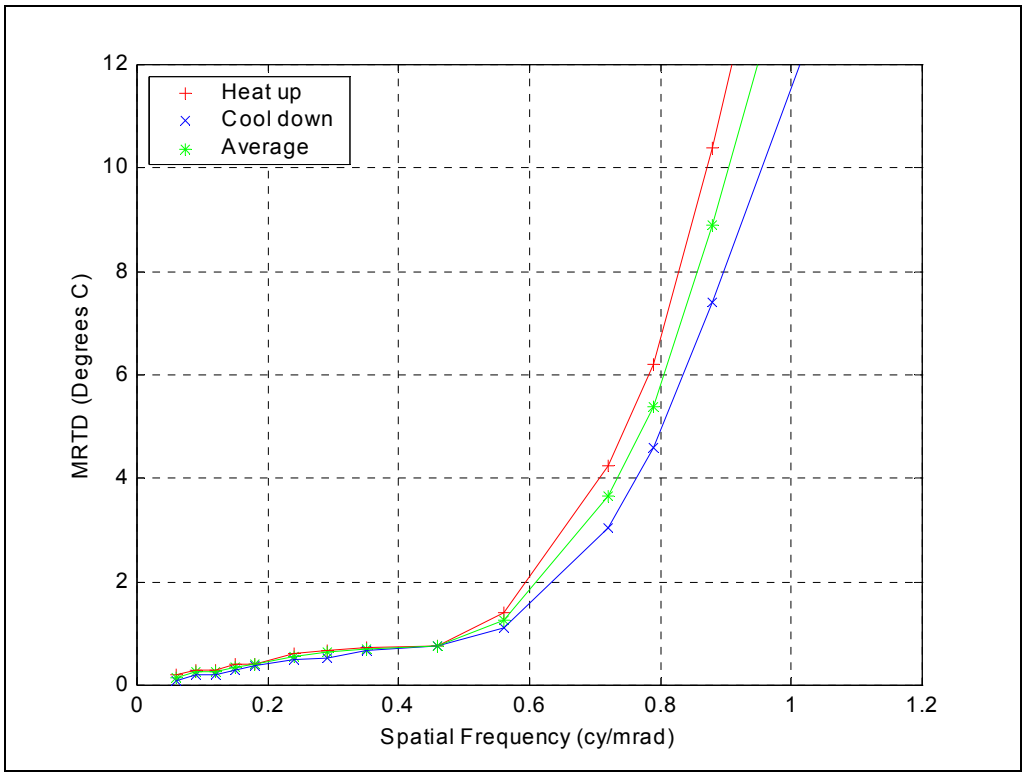

Figure D.2. Vertical MRTD Measurements.

B. SUBJECTIVE MRTD MEASUREMENTS

Spatial Frequency (cycles/mrad)	MRTD (Degrees C)
0.06	1.33
0.12	1.50
0.24	1.72
0.35	2.06
0.46	2.39
0.56	2.83

Table D.3. Objective MRTD (Constant SNR=6.0).

(SNR)	MRTD (fs=0.12 cy/mrad)	MRTD (fs=0.24 cy/mrad)	MRTD (fs=0.46 cy/mrad)	MRTD (fs=0.56 cy/mrad)
2	0.17	0.44	0.78	1.00
3	0.39	0.72	1.33	1.44
4	0.94	1.11	1.72	1.83
5	1.22	1.39	2.17	2.28
6	1.56	1.78	2.44	2.89

Table D.4. Objective MRTD (Constant Spatial Frequency).

APPENDIX E. VISMODII SOURCE CODE

VISMODII MATLAB code is provided in this appendix. There are three files under the subjective MRTD code section. Mitsv2.m is the main program that has the input data and preliminary calculations. It calls the Meffcnt.m function that calculates the contrast transference parameter. Alias.m is the function that calculates the aliasing terms and returns to the Meffcnt.m. Mitsv2.m then calculates the minimum threshold contrast and combines it with the contrast transference parameter to obtain the MRTD curve. In the objective MRTD code, only two files are included since the Alias.m is the same for both subjective and objective MRTD. The operations performed by Mitsv2obj.m and Meffcntobj.m are essentially identical to those performed by their subjective counterparts. However, the code is different, as different formulations are used for objective minimum threshold contrast and the objective contrast transference parameter.

A. SUBJECTIVE MRTD SOURCE CODE

1. Mitsv2.m

```
%%%%%%%%%%%%%%%%%%%%%%%%%%%%%%%%%%%%%%%%%%%%%%%%%%%%%%%%%%%%%%%%%%%%%%%%
%
%  Program     : VISMODII
%  Author      : Mike Groen
%  Date        : 11/01/95
%  Description: Given system parameters, this script file will predict
%                  MRTD curves for staring arrays
%  Subroutines: meffcnt.m, alias.m, qs2var.m, quad2var.m and sre.m
%
%  This version dated July 25 2001 has been modified by Mustafa Celik
%%%%%%%%%%%%%%%%%%%%%%%%%%%%%%%%%%%%%%%%%%%%%%%%%%%%%%%%%%%%%%%%%%%%%%%%

clear;
clf;

%%%%%%%%  Define spatial frequencies of interest (cy/mrad)  %%%%%%%%

fbar = [0.05:0.1:1.15];
```

```
%%%%%%%%%%%%%%%%%%%%%%%%%%%%%%%%%%%%%%%%%%%%%%%%%%%%%%%%%%%%%%%%%%%%%%%
%%%%%%%%%%%%%%%%%% Define system parameters
%%%%%%%%%%%%%%%%%%%%%%%%%%%%%%%%%%%%%%%%%%%%%%%%%%%%%%%%%%%%%%%%%%%%%%%

nh=512;         % number of horizontal detector elements
nv=512;         % number of vertical detector elements
a=16.24;        % detector active horizonal dimension (micrometers)
b=12.49;        % detector active vertical dimension (micrometers)
hpitch=26;      % detector pitch (center-to-center spacing), horizontal (micrometers)
vpitch=20;      % detector pitch (center-to-center spacing), vertical (micrometers)
fnumber=1.4;    % system f-number
focal=50;       % effective focal length (mm)
Fdot=60;        % frame rate (Hz)
clock=.97;      % clock-out factor (determines integration time)
Dstarp=5e10;    % peak specific detectivity (D-star) (cm-Hz^1/2/Watt)
lambdap=5.0;    % peak wavelength (micrometers)
lambda1=3.0;    % wavelength band lower limit (micrometers)
lambda2=5.0;    % wavelength band upper limit (micrometers)
fxec=2.3e6;     % electronic cut off (Hz)
monfac=.25;     % monitor gaussian rms factor normalized by alpha
poles=1;        % number of poles for electronic filter
blurspot=0;     % standard deviation of blur spot diameter (mrad)
theh=0;         % average angle off array center image is (rad) [usually zero or .785]
thev=0;         % ditto, vertical (rad)   [usually zero or .785]
lloydc2 = 1.4388e4; % c2 constant in Planck's blackbody equation (used in calculating
delta Tsc)
Tbg=300;        % background temperature (Kelvin)
To=.95;         % optical transmission
sigmavh=.4;     % fixed pattern noise (given as percent of sigma tvh)
SNRthr=6.0;     % threshold signal-to-noise ratio
te=.2;          % eye integration time
fpeye =0.4;     % peak response frequency for the eye (0.1-0.4) cy/mrad
Deye =3.3;      % diameter of the eye pupil (mm)
monwave=0.55;   % monitor wavelength (microns) nominal 0.5 micrometers


%%%%%%%%%%%%%%%%%%%%%%%%%%%%%%%%%%%%%%%%%%%%%%%%%%%%%%%%%%%%%%%%%%%%%%%
%%%%%%%%%%%%%%%%%% Preliminary Calculations
%%%%%%%%%%%%%%%%%%%%%%%%%%%%%%%%%%%%%%%%%%%%%%%%%%%%%%%%%%%%%%%%%%%%%%%

avglambda=0.5*(lambda1+lambda2);  % average (diffraction) wavelength
opdia=focal/fnumber;      % optical diameter(mm)
alpha=a/focal;            % horizontal detector angular subtense (DAS) in mrad
beta=b/focal;             % vertical DAS in mrad
```

```
sih=hpitch/focal;          % horizontal sampling interval in mrad
siv=vpitch/focal;          % vertical sampling interval in mrad
ao=pi*(opdia/2)^2;         % area of collecting lens (mm^ 2)
td=clock/Fdot;             % detector dwell time (sec)
fopt=opdia/avglambda;      % optical cut off in cy/mr
fsh=focal/hpitch;          % horizontal sampling frequency (cy/mr)
fsv=focal/vpitch;          % vertical sampling frequency (cy/mr)
tclock=nh*nv*Fdot;         % clock-out frequency (in Hz)
fth=sih*tclock;            % clock-out frequency conversion factor
fehis=fxec/fth;            % electronic cutoff in (cy/mrad)
%sspmaxh = hpitch/4;       % maximum horizontal sample scene phase error
sspmaxh=0;                 % optimum horizontal sample scene phase
%sspmaxv = vpitch/4;       % maximum vertical sample scene phase error
sspmaxv=0;                 % optimum vertical sample scene phase
feyec=Deye/monwave;        % eye cut off in cy/mr


%%%
```

```
%%%%%%%%%%%%%%%%%%%%%%%%%%%%%%%%%%%%%%%%%%%%%%%%%%%%%%%%%%%%%%%%%%%%%%%

%%%%%%%%  NETD part first  %%%%%%%%%

refbw = (pi/4)*(1/td);
n1 = pi*sqrt(a*1e-4*b*1e-4*refbw);
d1 = (alpha*beta*1e-6*To*ao*1e-2*Dstarp);
d2 = lloydc2/(lambdap*Tbg^2)*(quad2var('sre', lambda1, lambda2, Tbg));
NETD = n1/(d1*d2)

%%%%%%%%  SNR improvement and 3D noise correction  %%%%%%%%%

tn2 = sqrt(1+sigmavh^2/(te*Fdot))*(pi^2*SNRthr/(8*sqrt(te*Fdot)));

%%%%%%%%  Bandwidth correction  %%%%%%%%%

MTFsys = (abs(MTFrf)).^2;
totbw = sum(sum(MTFsys))*(alpha/td)*(fmax/128)
bwcorr = sqrt(totbw/refbw)
delTsc = tn2*NETD*bwcorr


%%%%%%%%%%%%%%%%%%%%%%%%%%%%%%%%%%%%%%%%%%%%%%%%%%%%%%%%%%%%%%%%%%%%%%%
%%%%%%%%%%%%%%%%%%% Calculate and plot system MRTD
%%%%%%%%%%%%%%%%%%%%%%%%%%%%%%%%%%%%%%%%%%%%%%%%%%%%%%%%%%%%%%%%%%%%%%%

%%%%%%%%  Horizontal and Vertical MRTD  %%%%%%%%%

MRTDH = delTsc./ctf;MRTDV = delTsc./vctf;

figure(3)
plot(fbar,MRTDH,'r',fbar,MRTDH,'r+')
axis([0 1.6 0 16])
xlabel('Spatial Frequency (cy/mrad)')
ylabel('MRTD')
title('Horizontal MRTD')

figure(4)
plot(fbar,MRTDV,'b',fbar,MRTDV,'bx')
axis([0 1.6 0 16])
xlabel('Spatial Frequency (cy/mrad)')
ylabel('MRTD')
title('Vertical MRTD')
```

```
%%%%%%%%  Two Dimensional (2D) MRTD  %%%%%%%%

MRTD2D=sqrt(MRTDH.*MRTDV);
figure(5)
plot(fbar,MRTDH,'r',fbar,MRTDV,'b',fbar,MRTD2D,'g',fbar,MRTDH,'r+',fbar,MRTDV,'
bx',fbar,MRTD2D,'g*')
legend('Horizontal', 'Vertical','2D MRTD')
grid
```

2. Meffcnt.m

```
%%%%%%%%%%%%%%%%%%%%%%%%%%%%%%%%%%%%%%%%%%%%%%%%%%%%%%%%%%%%%%%%%%%%%%%%
%
%  Program    : Meffcnt
%  Author     : Mike Groen
%  Date       : 11/01/95
%  Description: This script creates a standard four bar pattern of frequency specified by
%  the user.  It then passes it through a simulated thermal imaging system (as represented
%  by an MTF and aliasing), and produces the reconstructed pattern at the output. Loops
%  through the range of spatial frequencies desired, and calculates the contrast transfer %
%  function.
%
%  This version dated July 25 2001 has been modified by Mustafa Celik
%%%%%%%%%%%%%%%%%%%%%%%%%%%%%%%%%%%%%%%%%%%%%%%%%%%%%%%%%%%%%%%%%%%%%%%%

function                    [contrast,vercon,MTFrf,fmax]                    =
meffcnt(fbar,fxec,fsh,fsv,sih,siv,fth,fopt,alpha,beta,blurspot,theh,thev,fehis,poles,monfac,
sspmaxh,sspmaxv,feyec,fpeye);

d2=length(fbar);

%%%%%%%%%%%%%%%%%%%%%%%%%%%%%%%%%%%%%%%%%%%%%%%%%%%%%%%%%%%%%%%%%%%%%%%%
%%%%%%%%%%%%%%%%%% Create bar pattern
%%%%%%%%%%%%%%%%%%%%%%%%%%%%%%%%%%%%%%%%%%%%%%%%%%%%%%%%%%%%%%%%%%%%%%%%

col1 = zeros(130,10);
col2 = [zeros(30,10);ones(70,10);zeros(30,10)];
col3 = zeros(130,93);
row1 = zeros(63,256);

%%%%%%%%  Horizontal MRTD bar pattern  %%%%%%%%

A=[row1;col3,col2,col1,col2,col1,col2,col1,col2,col3;row1];
```

```
%%%%%%%%  Vertical MRTD bar pattern  %%%%%%%%

V=A';

%%%%%%%%%%%%%%%%%%%%%%%%%%%%%%%%%%%%%%%%%%%%%%%%%%%%%%%%%%%%%%%%%%%%%%%
%%%%%%%%%%%%%%%%%%% Transform bar pattern into spatial frequency domain
%%%%%%%%%%%%%%%%%%% and apply scaling to represent the appropriate
%%%%%%%%%%%%%%%%%%% spatial frequency
%%%%%%%%%%%%%%%%%%%%%%%%%%%%%%%%%%%%%%%%%%%%%%%%%%%%%%%%%%%%%%%%%%%%%%%

B= fft2(A);w=fft2(V);
b=abs(B);x=abs(w);


%%%%%%%%%%%%%%%%%%%%%%%%%%%%%%%%%%%%%%%%%%%%%%%%%%%%%%%%%%%%%%%%%%%%%%%
%%%%%%%%%%%%%%%%%%% Now loop through frequencies
%%%%%%%%%%%%%%%%%%%%%%%%%%%%%%%%%%%%%%%%%%%%%%%%%%%%%%%%%%%%%%%%%%%%%%%

for counter = 1:d2;
fx=fbar(counter);


%%%%%%%%%%%%%%%%%%%%%%%%%%%%%%%%%%%%%%%%%%%%%%%%%%%%%%%%%%%%%%%%%%%%%%%
%%%%%%%%%%%%%%%%%%% W refers to the actual width of one bar in mrad
%%%%%%%%%%%%%%%%%%% the 'del' terms are used to find the appropriate
%%%%%%%%%%%%%%%%%%% frequency and space scales
%%%%%%%%%%%%%%%%%%%%%%%%%%%%%%%%%%%%%%%%%%%%%%%%%%%%%%%%%%%%%%%%%%%%%%%

W=1/(2*fx);     % width of one bar of the four-bar pattern in mrad
Nw = 10;        % number of elements in one bar(x)
Nt = 256;       % number of elements in vector(m x m)
delt = W/Nw;        %width of one element in the matrix in mrad
DELt = Nt*W/Nw; %width of the entire matrix (256 elements) in mrad
delf = 1/DELt;
DELf = 1/delt;      % incremental frequency in cy/mrad
fmax = DELf/2;      % maximum frequency that FFT process can represent
fscale = linspace(-fmax,fmax,256);          % 256 frequency points
xscale = linspace(-DELt/2,DELt/2,256);   %space variables for plotting purposes
yscale = linspace(-DELt/2,DELt/2,256);   %space variables for plotting purposes


%%%%%%%%%%%%%%%%%%%%%%%%%%%%%%%%%%%%%%%%%%%%%%%%%%%%%%%%%%%%%%%%%%%%%%%
%%%%%%%%%%%%%%%%%%% Create a spatial frequency matrix to be used in
```

```
%%%%%%%%%%%%%%%% MTF calculations
%%%%%%%%%%%%%%%%%%%%%%%%%%%%%%%%%%%%%%%%%%%%%%%%%%%%%%%%%%%%%%%%

uux=1:256;
uuy=1:256;
Matfx=uux*uuy';
Matfx=ones(size((Matfx)));
Matfy=Matfx;
for k=-128 :  127;
  for  n=-128:127;
    k2=k+129;
    n2=n+129;
    Matfx(k2,n2)=k*fmax/128;     % horizontal spatial frequency
    Matfy(k2,n2)=n*fmax/128;     % vertical spatial frequency
  end;
end;
fr=((Matfx).^2+(Matfy).^2).^(0.5);    %two-dimensional spatial frequency


%%%%%%%%%%%%%%%%%%%%%%%%%%%%%%%%%%%%%%%%%%%%%%%%%%%%%%%%%%%%%%%%
%%%%%%%%%%%%%%%% Create image formation FILTER
%%%%%%%%%%%%%%%%%%%%%%%%%%%%%%%%%%%%%%%%%%%%%%%%%%%%%%%%%%%%%%%%

%%%%%%%%  Diffraction limited optics MTF (circular aperture)  %%%%%%%%

c1=fr/fopt;

%%%%%%%%  Set optics MTF=0 beyond the optical cutoff  %%%%%%%%

for  ii=1:256;
  for jj=1:256;
    if  c1(ii,jj)>1.0;
      c1(ii,jj)=1.0;
    end;
  end;
end;

c2=sqrt(1-c1 .^2);
ro=2/pi .*(acos(c1)-(c1 .*c2));

%%%%%%%%  Optics geometrical blur MTF   %%%%%%%%

f1 = (fr.^2).*pi^2.*(-2).*blurspot^2;
rb = exp(f1);
```

```
%%%%%% Horizontal and vertical sample scene phase MTFs (Optional)  %%%%%%

rsh = (2*Matfx/fsh)*theh;
rsh2 = cos(rsh);
rsv = (2*Matfy/fsv)*thev;
rsv2 = cos(rsv);
rs = rsh2.*rsv2;

%%%%%%  Detector Horizontal and vertical MTFs (rectangular detector)  %%%%%

c3fx=pi.*alpha.*Matfx;
c3fy =pi.*beta.*Matfy;

%%%%%%%%  Set detector MTF=0 at zero spatial frequency  %%%%%%%%

    for m=1 :256;
    for  p=1:256;
      if c3fx(m,p)==0
        c3fx(m,p)=0.01;
        end;
      if c3fy(m,p)==0
        c3fy(m,p)=0.01;
      end;
    end;
    end;

rdh=abs(sin(c3fx)./c3fx);
rdv=abs(sin(c3fy)./c3fy);

%%%%%%%%  Detector two-D MTF (rectangular detector)  %%%%%%%%

rd=rdv.*rdh;

%%%%%%%%  Cascade MTFs  %%%%%%%%

u=ro.*rd.*rb.*rs;


%%%%%%%%%%%%%%%%%%%%%%%%%%%%%%%%%%%%%%%%%%%%%%%%%%%%%%%%%%%%%%%%%%%%
%%%%%%%%%%%%%%%%%% Multiply image spectrum times image formation MTF
%%%%%%%%%%%%%%%%%%%%%%%%%%%%%%%%%%%%%%%%%%%%%%%%%%%%%%%%%%%%%%%%%%%%

d=fftshift(B);dv= fftshift(w);
```

```
mess = d.*u;mes2 = dv.*u;


%%%%%%%%%%%%%%%%%%%%%%%%%%%%%%%%%%%%%%%%%%%%%%%%%%%%%%%%%%%%%%%%%%%%%%%
%%%%%%%%%%%%%%%%%% Calculate aliasing terms
%%%%%%%%%%%%%%%%%%%%%%%%%%%%%%%%%%%%%%%%%%%%%%%%%%%%%%%%%%%%%%%%%%%%%%%

aliasterm = zeros(size(mess));
valiasterm = aliasterm;
[aliasterm] = alias(fscale,fsh,fsv,mess,sspmaxh,sspmaxv,fbar,counter);
[valiasterm] = alias(fscale,fsh,fsv,mes2,sspmaxh,sspmaxv,fbar,counter);


%%%%%%%%%%%%%%%%%%%%%%%%%%%%%%%%%%%%%%%%%%%%%%%%%%%%%%%%%%%%%%%%%%%%%%%
%%%%%%%%%%%%%%%%%% Add alias term to the pre-filtered scene
%%%%%%%%%%%%%%%%%%%%%%%%%%%%%%%%%%%%%%%%%%%%%%%%%%%%%%%%%%%%%%%%%%%%%%%

withalias= mess + aliasterm;
vertalias = mes2 + valiasterm;


%%%%%%%%%%%%%%%%%%%%%%%%%%%%%%%%%%%%%%%%%%%%%%%%%%%%%%%%%%%%%%%%%%%%%%%
%%%%%%%%%%%%%%%%%% Create image reconstruction FILTER
%%%%%%%%%%%%%%%%%%%%%%%%%%%%%%%%%%%%%%%%%%%%%%%%%%%%%%%%%%%%%%%%%%%%%%%

%%%%%%%%  Electronics 0TF  (multi-pole low pass filter)  %%%%%%%%

N=256;
dx=1/(2*fmax);
dy=dx;
uux2=(0:(N-1))*dx;
uuy2=(0:(N-1))*dy;
respx=exp(-uux2*fehis*(2*pi));
respy=exp(-uuy2*fehis*(2*pi));
respxy=respx'*respy;
sgnflip=((-1)*ones(size(1:N))).^(0:(N-1));
uuxy=sgnflip'*sgnflip;
respxy2=respxy.*uuxy;
eloTF=FFT2(respxy2);
mag=abs(eloTF);
eloTF=eloTF/(max(max(mag)));   % normalized OTF
elMTF=abs(eloTF);              % normalized MTF

%%%%%%%%  CRT Monitor spatial MTF  %%%%%%%%
```

```
c7=(fr/(1/sih)) .^2;
c8=(monfac)^2;
rm=exp(-2 *pi^2 .*c7 .*c8);

%%%%%%%%  Cascade MTFs  %%%%%%%%

recon=rm.*eloTF.*rd;


%%%%%%%%%%%%%%%%%%%%%%%%%%%%%%%%%%%%%%%%%%%%%%%%%%%%%%%%%%%%%%%%%%%%%%%
%%%%%%%%%%%%%%%%%% CALCULATE SYSTEM MTF
%%%%%%%%%%%%%%%%%% (This is the MTF used in the program to
%%%%%%%%%%%%%%%%%% calculate system total noise bandwidth)
%%%%%%%%%%%%%%%%%%%%%%%%%%%%%%%%%%%%%%%%%%%%%%%%%%%%%%%%%%%%%%%%%%%%%%%

%%%%%%%%  Eye MTF  %%%%%%%%

c11=fr/feyec;
for  iii=1:256;
  for jjj=1:256;
    if  c11(iii,jjj)>1.0;
       c11(iii,jjj)=1.0;
    end;
  end;
end;

c22=sqrt(1-c11.^2);
const1=0.4/feyec;
const2=sqrt(1-const1^2);
norm= 1/(2/pi *(acos(const1)-(const1*const2)));
c33=2*norm/pi .*(acos(c11)-(c11 .*c22));
clear c11 c22;
c44=fr./fpeye;
reye=min(c44,c33);
clear c11 c22 c33 c44;

%%%%%%%%  Multiply Eye MTF times the Reconstruction OTF  %%%%%%%%

MTFrf=reye.*recon;


%%%%%%%%%%%%%%%%%%%%%%%%%%%%%%%%%%%%%%%%%%%%%%%%%%%%%%%%%%%%%%%%%%%%%%%
%%%%%%%%%%%%%%%%%% Multiply pre-filtered and aliased image spectrum
```

```
%%%%%%%%%%%%%%%% times the image reconstruction OTF
%%%%%%%%%%%%%%%%%%%%%%%%%%%%%%%%%%%%%%%%%%%%%%%%%%%%%%%%%%%%%%%%

outalias = withalias.*recon;    % Output spectrum WITH aliasing (Horizontal)
noalias = mess.*recon;          % Output spectrum WITHOUT aliasing (Horizontal)
veral2  = vertalias.*recon;     % Output spectrum WITH aliasing (Vertical)
veral3  = mes2.*recon;          % Output spectrum WITHOUT aliasing (Vertical)


%%%%%%%%%%%%%%%%%%%%%%%%%%%%%%%%%%%%%%%%%%%%%%%%%%%%%%%%%%%%%%%%%
%%%%%%%%%%%%%%%% Transform back to spatial domain
%%%%%%%%%%%%%%%%%%%%%%%%%%%%%%%%%%%%%%%%%%%%%%%%%%%%%%%%%%%%%%%%%

messy = fftshift(outalias);messy2 = fftshift(noalias);
gigo = fftshift(veral2);gigo2 = fftshift(veral3);

C=ifft2(messy);     % Output image WITH aliasing (Horizontal)
D=ifft2(messy2);    % Output image WITHOUT aliasing (Horizontal)
E=ifft2(gigo);      % Output image WITH aliasing (Vertical)
F=ifft2(gigo2);     % Output image WITHOUT aliasing (Vertical)


%%%%%%%%%%%%%%%%%%%%%%%%%%%%%%%%%%%%%%%%%%%%%%%%%%%%%%%%%%%%%%%%%
%%%%%%%%%%%% Calculate image contrast. Use an algoritm to find the bar
%%%%%%%%%%%% pattern maxima and minima to account for the spatial shifts
%%%%%%%%%%%% in the image due to the electronics PTF
%%%%%%%%%%%%%%%%%%%%%%%%%%%%%%%%%%%%%%%%%%%%%%%%%%%%%%%%%%%%%%%%%

if fbar(counter)<= 0.60

centerhrz=abs([C(128,1:256)]);   %center line of bar pattern for horizontal MRTD

bar1=[centerhrz(94:103)];
space1=[centerhrz(104:113)];
bar2=[centerhrz(114:123)];
space2=[centerhrz(124:133)];
bar3=[centerhrz(134:143)];
space3=[centerhrz(144:153)];
bar4=[centerhrz(154:163)];

max1=max(bar1);
max2=max(bar2);
max3=max(bar3);
max4=max(bar4);
```

```
min1=min(space1);
min2=min(space2);
min3=min(space3);

c1=[max1-min1 max2-min1 max2-min2 max3-min2 max3-min3 max4-min3];
contrast(counter)=min(c1);

centerver=abs([E(1:256,128)]);   %center line of bar pattern for vertical MRTD

verbar1=[centerver(94:103)];
verspace1=[centerver(104:113)];
verbar2=[centerver(114:123)];
verspace2=[centerver(124:133)];
verbar3=[centerver(134:143)];
verspace3=[centerver(144:153)];
verbar4=[centerver(154:163)];

vermax1=max(verbar1);
vermax2=max(verbar2);
vermax3=max(verbar3);
vermax4=max(verbar4);
vermin1=min(verspace1);
vermin2=min(verspace2);
vermin3=min(verspace3);

verc1=[vermax1-vermin1 vermax2-vermin1 vermax2-vermin2 vermax3-vermin2
vermax3-vermin3 vermax4-vermin3];
vercon(counter)=min(verc1);

end

%%%%%%%%%%%%%%%%%%%%%%%%%%%%%%%%%%%%%%%%%%%%%%%%%%%%%%%%%%%%%%%%%%%%%%%
if fbar(counter) > 0.60
centerhrz=abs([C(128,1:256)]);   %center line of bar pattern for horizontal MRTD
   maxima=[]; maxind=[];minima=[];minind=[];

%%%%%%%%  Find the values and locations of maxima and minima  %%%%%%%%

for index=84:1:194,
   if centerhrz(index)>centerhrz(index+1)
      if centerhrz(index)>centerhrz(index-1)
         maxima=[maxima,centerhrz(index)]
         maxind=[maxind,index]
      end
```

```
    end
    if centerhrz(index)<centerhrz(index+1)
        if centerhrz(index)<centerhrz(index-1)
            minima=[minima,centerhrz(index)]
            minind=[minind,index]
        end
    end
end

lmax=length(maxima)

%%%%%%%%%%%%%%%%%%%%%%%%%%%%%%%%%%%%%%%%%%%%%%%%%%%%%%%%%%%%%%%%%%%%%%%%%%%

%%%%%%%%  Eliminate ripples  %%%%%%%%%

if lmax<4
   contrast(counter)=0.008;
else
while lmax>4
   for mxi=1:1:lmax-1
      dist(mxi)=maxind(mxi+1)-maxind(mxi)
   end
   [mdist,mdistind]=min(dist)
   if maxima(mdistind)<maxima(mdistind+1)
      maxima(mdistind)=0
      maxind(mdistind)=0
   else
      maxima(mdistind+1)=0
      maxind(mdistind+1)=0
   end
   minima(mdistind)=0
   minind(mdistind)=0
   dist(mdistind)=0
   maxima=maxima(find(maxima))  %take zero term out
   maxind=maxind(find(maxind))
   minima=minima(find(minima))
   minind=minind(find(minind))
   dist=dist(find(dist))
   lmax=length(maxima)
end

%%%%%%%%%%%%%%%%%%%%%%%%%%%%%%%%%%%%%%%%%%%%%%%%%%%%%%%%%%%%%%%%%%%%%%%%%%%

%%%%%%%%  Calculate contrast for horizontal MRTD %%%%%%%%%
```

```
c1=[maxima(1)-minima(1) maxima(2)-minima(1) maxima(2)-minima(2) maxima(3)-
minima(2) maxima(3)-minima(3) maxima(4)-minima(3)]
contrast(counter)=min(c1)

end


%%%%%%%%%%%%%%%%%%%%%%%%%%%%%%%%%%%%%%%%%%%%%%%%%%%%%%%%%%%%%%%%%%%%%%%

centerver=abs([E(1:256,128)]);   %center line of bar pattern for vertical MRTD

maxima=[]; maxind=[];minima=[];minind=[];

%%%%%%%%  Find the values and locations of maxima and minima  %%%%%%%%

for index=84:1:194,
   if centerver(index)>centerver(index+1)
      if centerver(index)>centerver(index-1)
         maxima=[maxima,centerver(index)];
         maxind=[maxind,index];
      end
   end
   if centerver(index)<centerver(index+1)
      if centerver(index)<centerver(index-1)
         minima=[minima,centerver(index)];
         minind=[minind,index];
      end
   end
end

lmax=length(maxima);

%%%%%%%%%%%%%%%%%%%%%%%%%%%%%%%%%%%%%%%%%%%%%%%%%%%%%%%%%%%%%%%%%%%%%%%

%%%%%%%%  Eliminate ripples  %%%%%%%%

if lmax<4
  vercon(counter)=0.001;
else
while lmax>4
  for mxi=1:1:lmax-1
     dist(mxi)=maxind(mxi+1)-maxind(mxi)
  end
```

```
  [mdist,mdistind]=min(dist)
  if maxima(mdistind)<maxima(mdistind+1)
     maxima(mdistind)=0
     maxind(mdistind)=0
  else
     maxima(mdistind+1)=0
     maxind(mdistind+1)=0
  end
  minima(mdistind)=0
  minind(mdistind)=0
  dist(mdistind)=0
  maxima=maxima(find(maxima))  %take zero term out
  maxind=maxind(find(maxind))
  minima=minima(find(minima))
  minind=minind(find(minind))
  dist=dist(find(dist))
  lmax=length(maxima)
end

%%%%%%%%  Calculate contrast for vertical MRTD %%%%%%%%

c1=[maxima(1)-minima(1)  maxima(2)-minima(1)  maxima(2)-minima(2)  maxima(3)-
minima(2) maxima(3)-minima(3) maxima(4)-minima(3)];
vercon(counter)=min(c1);

end

end

%%%%%%%%%%%%%%%%%%%%%%%%%%%%%%%%%%%%%%%%%%%%%%%%%%%%%%%%%%%%%%%%%%%%%%%
end
```

3. Alias.m

```
%%%%%%%%%%%%%%%%%%%%%%%%%%%%%%%%%%%%%%%%%%%%%%%%%%%%%%%%%%%%%%%%%%%%%%%
%
%  Program    : Alias
%  Author     : Mike Groen
%  Date       : 11/01/95
%  Description: This script is the aliasing portion of effcnt.m
%                  It repeats the spectrum at the sampling frequency.
%
%  This version dated July 25 2001 has been modified by Mustafa Celik
```

```
%%%%%%%%%%%%%%%%%%%%%%%%%%%%%%%%%%%%%%%%%%%%%%%%%%%%%%%%%%%%%%%%%%%%%%%

function [aliasterm] = alias(fscale,fsh,fsv,mess,b,c,fbar,counter)


%%%%%%%%%%%%%%%%%%%%%%%%%%%%%%%%%%%%%%%%%%%%%%%%%%%%%%%%%%%%%%%%%%%%%%%
%%%%%%%%%%%%%%%%%% Represent aliasing by repeating the filtered
%%%%%%%%%%%%%%%%%% spectrum at sampling freq intervals
%%%%%%%%%%%%%%%%%%%%%%%%%%%%%%%%%%%%%%%%%%%%%%%%%%%%%%%%%%%%%%%%%%%%%%%

%%%%%%%%%%%%%%%%%%%%%%%%%%%%%%%%%%%%%%%%%%%%%%%%%%%%%%%%%%%%%%%%%%%%%%%
%%%%%%%%%% Alias terms (other than cross aliases)
%%%%%%%%%%%%%%%%%%%%%%%%%%%%%%%%%%%%%%%%%%%%%%%%%%%%%%%%%%%%%%%%%%%%%%%

%%%%%%%%  Find where to center the repeated spectrum  %%%%%%%%

where = find(fscale/fsh >1);
if isempty(where);
   cent = 256;multiple=0;
else
   fbar(counter)
   cent = where(1)
   multiple=1;
end

start=cent-128;unused = 256-start;

%%%%%%%%  Alias terms due to sampling in x direction  %%%%%%%%

%%%%%%%%  First positive side  %%%%%%%%

aliastxp=circshift(mess,[0 (start-1)]);
aliastxp=aliastxp.*exp(j*2*pi*b*fsh);

%%%%%%%%  Now negative side  %%%%%%%%

aliastxn=circshift(mess,[0 -(start-1)]);
aliastxn=aliastxn.*exp(-j*2*pi*b*fsh);

%%%%%%%%  Combine the two  %%%%%%%%

aliasx=aliastxp+aliastxn;

%%%%%%%%  Find where to center the repeated spectrum  %%%%%%%%
```

```
wherev = find(fscale/fsv >1);
if isempty(wherev);
     centv = 256;multiplev=0;
else
     fbar(counter)
   centv = wherev(1)
   multiplev=1;
end

startv=centv-128;unusedv = 256-startv;

%%%%%%%%  Alias terms due to sampling in y direction  %%%%%%%%

%%%%%%%%  First positive side  %%%%%%%%

aliastyp = circshift(mess,[(startv-1) 0]);
aliastyp=aliastyp.*exp(j*2*pi*c*fsv);

%%%%%%%%  Now negative side  %%%%%%%%

aliastyn = circshift(mess,[-(startv-1) 0]);
aliastyn=aliastyn.*exp(-j*2*pi*c*fsv);

%%%%%%%%  Combine the two  %%%%%%%%

aliasy=aliastyp+aliastyn;


%%%%%%%%%%%%%%%%%%%%%%%%%%%%%%%%%%%%%%%%%%%%%%%%%%%%%%%%%%%%%%%%
%%%%%%%%%% Cross alias terms
%%%%%%%%%%%%%%%%%%%%%%%%%%%%%%%%%%%%%%%%%%%%%%%%%%%%%%%%%%%%%%%%

%%%%%%%%  Alias term (positive fx and fy quadrant)  %%%%%%%%

aliasxpyp = circshift(mess,[(startv-1) (start-1)]);
aliasxpyp=aliasxpyp.*exp(j*2*pi*b*fsh).*exp(j*2*pi*c*fsv);

%%%%%%%%  Alias term (positive fx and negative fy quadrant)  %%%%%%%%

aliasxpyn =circshift(mess,[-(startv-1) (start-1)]);
aliasxpyn=aliasxpyn.*exp(j*2*pi*b*fsh).*exp(-j*2*pi*c*fsv);

%%%%%%%%  Alias term (negative fx and positive fy quadrant)  %%%%%%%%
```

```
aliasxnyp = circshift(mess,[(startv-1) -(start-1)]);
aliasxnyp=aliasxnyp.*exp(-j*2*pi*b*fsh).*exp(j*2*pi*c*fsv);

%%%%%%%%  Alias term (negative fx and fy quadrant)  %%%%%%%%

aliasxnyn = circshift(mess,[-(startv-1) -(start-1)]);
aliasxnyn=aliasxnyn.*exp(-j*2*pi*b*fsh).*exp(-j*2*pi*c*fsv);

%%%%%%%%  Combine the four cross alias terms  %%%%%%%%

crossterm = multiple*multiplev*(aliasxpyp+aliasxpyn+aliasxnyp+aliasxnyn);


%%%%%%%%%%%%%%%%%%%%%%%%%%%%%%%%%%%%%%%%%%%%%%%%%%%%%%%%%%%%%%%%%%%%
%%%%%%%%%%% Total alias term
%%%%%%%%%%%%%%%%%%%%%%%%%%%%%%%%%%%%%%%%%%%%%%%%%%%%%%%%%%%%%%%%%%%%

aliasterm = multiple*aliasx + multiplev*aliasy +crossterm;
```

B. OBJECTIVE MRTD SOURCE CODE

1. Mitsv2obj.m

```
%%%%%%%%%%%%%%%%%%%%%%%%%%%%%%%%%%%%%%%%%%%%%%%%%%%%%%%%%%%%%%%%%%%%
%
%  Program    : VISMODII Objective
%  Author     : Mustafa Celik
%  Date       : July 25, 2001
%  Description: Given system parameters, this script file will predict
%                  the objective MRTD curves for staring arrays
%  Subroutines: meffcntobj.m and alias.m
%
%%%%%%%%%%%%%%%%%%%%%%%%%%%%%%%%%%%%%%%%%%%%%%%%%%%%%%%%%%%%%%%%%%%%

clear;
clf;

%%%%%%%%  Define spatial frequencies of interest (cy/mrad)  %%%%%%%%

fbar = [0.12 0.24 0.46 0.56];
```

```
%%%%%%%%%%%%%%%%%%%%%%%%%%%%%%%%%%%%%%%%%%%%%%%%%%%%%%%%%%%%%%%%%%%%%%%%
%%%%%%%%%%%%%%%%%% Define system parameters
%%%%%%%%%%%%%%%%%%%%%%%%%%%%%%%%%%%%%%%%%%%%%%%%%%%%%%%%%%%%%%%%%%%%%%%%

nh=512;         % number of horizontal detector elements
nv=512;         % number of vertical detector elements
a=16.24;        % detector active horizonal dimension (micrometers)
b=12.49;        % detector active vertical dimension (micrometers)
hpitch=26;      % detector pitch (center-to-center spacing), horizontal (micrometers)
vpitch=20;      % detector pitch (center-to-center spacing), vertical (micrometers)
fnumber=1.4;    % system f-number
focal=50;       % effective focal length (mm)
Fdot=60;        % frame rate (Hz)
clock=.97;      % clock-out factor (determines integration time)
Dstarp=5e10;  % peak specific detectivity (D-star) (cm-Hz^1/2/Watt)
lambdap=5.0;  % peak wavelength (micrometers)
lambda1=3.0;  % wavelength band lower limit (micrometers)
lambda2=5.0;  % wavelength band upper limit (micrometers)
fxec=2.3e6;     % electronic cut off (Hz)
monfac=.25;     % monitor gaussian rms factor normalized by alpha
poles=1;        % number of poles for electronic filter
blurspot=0;     % standard deviation of blur spot diameter (mrad)
theh=0;         % average angle off array center image is (rad) [usually zero or .785]
thev=0;         % ditto, vertical (rad)   [usually zero or .785]
lloydc2 = 1.4388e4; % c2 constant in Planck's blackbody equation (used in calculating
delta Tsc)
Tbg=300;        % background temperature (Kelvin)
To=.95;         % optical transmission
sigmavh=.4;     % fixed pattern noise (given as percent of sigma tvh)
SNRthr=6.0;   % threshold signal-to-noise ratio
te=.2;          % eye integration time


%%%%%%%%%%%%%%%%%%%%%%%%%%%%%%%%%%%%%%%%%%%%%%%%%%%%%%%%%%%%%%%%%%%%%%%%
%%%%%%%%%%%%%%%%%% Preliminary Calculations
%%%%%%%%%%%%%%%%%%%%%%%%%%%%%%%%%%%%%%%%%%%%%%%%%%%%%%%%%%%%%%%%%%%%%%%%

avglambda=0.5*(lambda1+lambda2);   % average (diffraction) wavelength
opdia=focal/fnumber;                % optical diameter(mm)
alpha=a/focal;                      % horizontal detector angular subtense (DAS) in mrad
beta=b/focal;                       % vertical DAS in mrad
sih=hpitch/focal;                   % horizontal sampling interval in mrad
siv=vpitch/focal;                   % vertical sampling interval in mrad
ao=pi*(opdia/2)^2;                  % area of collecting lens (mm^ 2)
```

```
td=clock/Fdot;                  % detector dwell time (sec)
fopt=opdia/avglambda;           % optical cut off in cy/mr
fsh=focal/hpitch;               % horizontal sampling frequency (cy/mr)
fsv=focal/vpitch;               % vertical sampling frequency (cy/mr)
tclock=nh*nv*Fdot;              % clock-out frequency (in Hz)
fth=sih*tclock;                 % clock-out frequency conversion factor
fehis=fxec/fth;                 % electronic cutoff in (cy/mrad)
%sspmaxh = hpitch/4;            % maximum horizontal sample scene phase error
sspmaxh=0;                      % optimum horizontal sample scene phase
%sspmaxv = vpitch/4;            % maximum vertical sample scene phase error
sspmaxv=0;                      % optimum vertical sample scene phase


%%%%%%%%%%%%%%%%%%%%%%%%%%%%%%%%%%%%%%%%%%%%%%%%%%%%%%%%%%%%%%%%%%%%%%%
%%%%%%%%%%%%%%%%%%% Contrast transfer function calculations and plot
%%%%%%%%%%%%%%%%%%%%%%%%%%%%%%%%%%%%%%%%%%%%%%%%%%%%%%%%%%%%%%%%%%%%%%%

[ctf]                                                                   =
meffcntobj(fbar,fxec,fsh,fsv,sih,siv,fth,fopt,alpha,beta,blurspot,theh,thev,fehis,poles,mon
fac,sspmaxh,sspmaxv);

%%%%%%%%  Plot contrast transfer function  %%%%%%%%

figure(1)
plot(fbar,ctf)
axis([0 2 0 1])
xlabel('Spatial Frequency (cy/mrad)')
ylabel('CTF')
title('Contrast Transfer Function (Objective MRTD)')


%%%%%%%%%%%%%%%%%%%%%%%%%%%%%%%%%%%%%%%%%%%%%%%%%%%%%%%%%%%%%%%%%%%%%%%
%%%%%%%%%%%%%%%%%%% Calculate system critical delta T (Objective)
%%%%%%%%%%%%%%%%%%%%%%%%%%%%%%%%%%%%%%%%%%%%%%%%%%%%%%%%%%%%%%%%%%%%%%%

deltat=1.33;          % Delta T (Foreground-Background)
noiseV=8.1;           % Noise voltage in mV (MEASURED)
deltaV=48;            % Delta V due to delta T in mV (MEASURED)
signal_to_noise=6;    % Required SNR

delTsc=signal_to_noise*(deltat/deltaV)*noiseV
```

```
%%%%%%%%%%%%%%%%%%%%%%%%%%%%%%%%%%%%%%%%%%%%%%%%%%%%%%%%%%%%%%%%%%%%%%%
%%%%%%%%%%%%%%%%%%%% Calculate and plot system MRTD
%%%%%%%%%%%%%%%%%%%%%%%%%%%%%%%%%%%%%%%%%%%%%%%%%%%%%%%%%%%%%%%%%%%%%%%

MRTDH = delTsc./ctf;
figure(7)
plot(fbar,MRTDH,'r',fbar,MRTDH,'r+')
grid
xlabel('Spatial Frequency (cy/mrad)')
ylabel('MRTD')
title('Objective MRTD')
```

2. Meffcntobj.m

```
%%%%%%%%%%%%%%%%%%%%%%%%%%%%%%%%%%%%%%%%%%%%%%%%%%%%%%%%%%%%%%%%%%%%%%%
%
%  Program    : MEffcntobj
%  Author     : Mustafa Celik
%  Date       : July 25 2001
%  Description: This script creates a standard four bar pattern of frequency specified by
%  the user.  It then passes it through a simulated thermal imaging system (as represented
%  by an MTF and aliasing), and produces the reconstructed pattern at the output. Loops
%  through the range of spatial frequencies desired, and calculates the contrast transfer
%  function.
%
%%%%%%%%%%%%%%%%%%%%%%%%%%%%%%%%%%%%%%%%%%%%%%%%%%%%%%%%%%%%%%%%%%%%%%%

function [contrast] =
meffcntobj(fbar,fxec,fsh,fsv,sih,siv,fth,fopt,alpha,beta,blurspot,theh,thev,fehis,poles,mon
fac,sspmaxh,sspmaxv);

d2=length(fbar);

%%%%%%%%%%%%%%%%%%%%%%%%%%%%%%%%%%%%%%%%%%%%%%%%%%%%%%%%%%%%%%%%%%%%%%%
%%%%%%%%%%%%%%%%%%%% Create bar pattern
%%%%%%%%%%%%%%%%%%%%%%%%%%%%%%%%%%%%%%%%%%%%%%%%%%%%%%%%%%%%%%%%%%%%%%%

col1 = zeros(130,10);
col2 = [zeros(30,10);ones(70,10);zeros(30,10)];
col3 = zeros(130,93);
row1 = zeros(63,256);
```

```
%%%%%%%%  Horizontal MRTD bar pattern  %%%%%%%%

A=[row1;col3,col2,col1,col2,col1,col2,col1,col2,col3;row1];

%%%%%%%%  Vertical MRTD bar pattern  %%%%%%%%

V=A';


%%%%%%%%%%%%%%%%%%%%%%%%%%%%%%%%%%%%%%%%%%%%%%%%%%%%%%%%%%%%
%%%%%%%%%%%%%%%%%% Transform bar pattern into spatial freq domain
%%%%%%%%%%%%%%%%%% and apply scaling to represent the appropriate
%%%%%%%%%%%%%%%%%% spatial frequency
%%%%%%%%%%%%%%%%%%%%%%%%%%%%%%%%%%%%%%%%%%%%%%%%%%%%%%%%%%%%

B= fft2(A);w=fft2(V);
b=abs(B);x=abs(w);

%%%%%%%%%%%%%%%%%%%%%%%%%%%%%%%%%%%%%%%%%%%%%%%%%%%%%%%%%%%%
%%%%%%%%%%%%%%%%%% Now loop through frequencies
%%%%%%%%%%%%%%%%%%%%%%%%%%%%%%%%%%%%%%%%%%%%%%%%%%%%%%%%%%%%

for counter = 1:d2;
fx=fbar(counter);


%%%%%%%%%%%%%%%%%%%%%%%%%%%%%%%%%%%%%%%%%%%%%%%%%%%%%%%%%%%%
%%%%%%%%%%%%%%%%%% W refers to the actual width of one bar in mrad
%%%%%%%%%%%%%%%%%% the 'del' terms are used to find the appropriate
%%%%%%%%%%%%%%%%%% frequency and space scales
%%%%%%%%%%%%%%%%%%%%%%%%%%%%%%%%%%%%%%%%%%%%%%%%%%%%%%%%%%%%


W=1/(2*fx);           % width of one bar of the four-bar pattern in mrad
Nw = 10;              % number of elements in one bar(x)
Nt = 256;             % number of elements in vector(m x m)
delt = W/Nw;          % width of one element in the matrix in mrad
DELt = Nt*W/Nw;   % width of the entire matrix (256 elements) in mrad
delf = 1/DELt;
DELf = 1/delt;        % incremental frequency in cy/mrad
fmax = DELf/2;        % maximum frequency that FFT process can represent
fscale = linspace(-fmax,fmax,256);         %256 frequency points
xscale = linspace(-DELt/2,DELt/2,256);  %space variables for plotting purposes
yscale = linspace(-DELt/2,DELt/2,256);  %space variables for plotting purposes
```

```
%%%%%%%%%%%%%%%%%%%%%%%%%%%%%%%%%%%%%%%%%%%%%%%%%%%%%%%%%%%%%%%%%%%%%%%
%%%%%%%%%%%%%%%%%%%% Create a spatial frequency matrix to be used in
%%%%%%%%%%%%%%%%%%%% MTF calculations
%%%%%%%%%%%%%%%%%%%%%%%%%%%%%%%%%%%%%%%%%%%%%%%%%%%%%%%%%%%%%%%%%%%%%%%

uux=1:256;
uuy=1:256;
Matfx=uux*uuy';
Matfx=ones(size((Matfx)));
Matfy=Matfx;
for k=-128 :  127;
  for  n=-128:127;
    k2=k+129;
    n2=n+129;
    Matfx(k2,n2)=k*fmax/128;       % horizontal spatial frequency
    Matfy(k2,n2)=n*fmax/128;       % vertical spatial frequency
  end;
end;
fr=((Matfx).^2+(Matfy).^2).^(0.5);  % two-dimensional spatial frequency


%%%%%%%%%%%%%%%%%%%%%%%%%%%%%%%%%%%%%%%%%%%%%%%%%%%%%%%%%%%%%%%%%%%%%%%
%%%%%%%%%%%%%%%%%%%% Create image formation FILTER
%%%%%%%%%%%%%%%%%%%%%%%%%%%%%%%%%%%%%%%%%%%%%%%%%%%%%%%%%%%%%%%%%%%%%%%

%%%%%%%%  Diffraction limited optics MTF (circular aperture)  %%%%%%%%

c1=fr/fopt;

%%%%%%%%  Set optics MTF=0 beyond the optical cutoff  %%%%%%%%

for  ii=1:256;
  for jj=1:256;
    if  c1(ii,jj)>1.0;
      c1(ii,jj)=1.0;
    end;
  end;
end;

c2=sqrt(1-c1 .^2);
ro=2/pi .*(acos(c1)-(c1 .*c2));
```

```
%%%%%%%%  Optics geometrical blur MTF   %%%%%%%%

f1 = (fr.^2).*pi^2.*(-2).*blurspot^2;
rb = exp(f1);

%%%%%%%%  Horizontal and vertical sample scene phase MTFs   %%%%%%%%

rsh = (2*Matfx/fsh)*theh;
rsh2 = cos(rsh);
rsv = (2*Matfy/fsv)*thev;
rsv2 = cos(rsv);
rs = rsh2.*rsv2;

%%%%%%%  Detector Horizontal and vertical MTFs (rectangular detector)  %%%%%%%

c3fx=pi.*alpha.*Matfx;
c3fy =pi.*beta.*Matfy;

%%%%%%%%  Set detector MTF=0 at zero spatial frequency  %%%%%%%%

    for m=1 :256;
    for  p=1:256;
      if c3fx(m,p)==0
        c3fx(m,p)=0.01;
        end;
      if c3fy(m,p)==0
        c3fy(m,p)=0.01;
      end;
    end;
    end;

rdh=abs(sin(c3fx)./c3fx);
rdv=abs(sin(c3fy)./c3fy);

%%%%%%%%  Detector two-D MTF (rectangular detector)  %%%%%%%%

rd=rdv.*rdh;

%%%%%%%%  Cascade MTFs  %%%%%%%%

u=ro.*rd.*rb.*rs;
```

```
%%%%%%%%%%%%%%%%%%%%%%%%%%%%%%%%%%%%%%%%%%%%%%%%%%%%%%%%%%%%%%%%%%%%%%%
%%%%%%%%%%%%%%%%%% Multiply image spectrum times image formation MTF
%%%%%%%%%%%%%%%%%%%%%%%%%%%%%%%%%%%%%%%%%%%%%%%%%%%%%%%%%%%%%%%%%%%%%%%

d=fftshift(B);dv= fftshift(w);
mess = d.*u;mes2 = dv.*u;


%%%%%%%%%%%%%%%%%%%%%%%%%%%%%%%%%%%%%%%%%%%%%%%%%%%%%%%%%%%%%%%%%%%%%%%
%%%%%%%%%%%%%%%%%% Calculate aliasing terms
%%%%%%%%%%%%%%%%%%%%%%%%%%%%%%%%%%%%%%%%%%%%%%%%%%%%%%%%%%%%%%%%%%%%%%%

aliasterm = zeros(size(mess));
valiasterm = aliasterm;
[aliasterm] = alias(fscale,fsh,fsv,mess,sspmaxh,sspmaxv,fbar,counter);
[valiasterm] = alias(fscale,fsh,fsv,mes2,sspmaxh,sspmaxv,fbar,counter);


%%%%%%%%%%%%%%%%%%%%%%%%%%%%%%%%%%%%%%%%%%%%%%%%%%%%%%%%%%%%%%%%%%%%%%%
%%%%%%%%%%%%%%%%%% Add alias term to the pre-filtered scene
%%%%%%%%%%%%%%%%%%%%%%%%%%%%%%%%%%%%%%%%%%%%%%%%%%%%%%%%%%%%%%%%%%%%%%%

withalias= mess + aliasterm;
vertalias = mes2 + valiasterm;


%%%%%%%%%%%%%%%%%%%%%%%%%%%%%%%%%%%%%%%%%%%%%%%%%%%%%%%%%%%%%%%%%%%%%%%
%%%%%%%%%%%%%%%%%% Create image reconstruction FILTER
%%%%%%%%%%%%%%%%%%%%%%%%%%%%%%%%%%%%%%%%%%%%%%%%%%%%%%%%%%%%%%%%%%%%%%%

%%%%%%%%  Electronics 0TF  (multi-pole low pass filter)  %%%%%%%%

N=256;
dx=1/(2*fmax);
dy=dx;
uux2=(0:(N-1))*dx;
uuy2=(0:(N-1))*dy;
respx=exp(-uux2*fehis*(2*pi));
respy=exp(-uuy2*fehis*(2*pi));
respxy=respx'*respy;
sgnflip=((-1)*ones(size(1:N))).^(0:(N-1));
uuxy=sgnflip'*sgnflip;
respxy2=respxy.*uuxy;
eloTF=FFT2(respxy2);
```

```
mag=abs(eloTF);
eloTF=eloTF/(max(max(mag)));    % normalized OTF
elMTF=abs(eloTF);               % normalized MTF

%%%%%%%%  Reconstruction Filter  %%%%%%%%
%%%%%%  Note that display MTF does not apply in Objective MRTD  %%%%%%

recon=eloTF.*rd;


%%%%%%%%%%%%%%%%%%%%%%%%%%%%%%%%%%%%%%%%%%%%%%%%%%%%%%%%%%%%%%%%%%%
%%%%%%%%%%%%%%%%%% Multiply pre-filtered and aliased image spectrum
%%%%%%%%%%%%%%%%%% times the image reconstruction OTF
%%%%%%%%%%%%%%%%%%%%%%%%%%%%%%%%%%%%%%%%%%%%%%%%%%%%%%%%%%%%%%%%%%%

outalias = withalias.*recon;   % Output spectrum WITH aliasing (Horizontal)
noalias = mess.*recon;         % Output spectrum WITHOUT aliasing (Horizontal)
veral2  = vertalias.*recon;    % Output spectrum WITH aliasing (Vertical)
veral3  = mes2.*recon;         % Output spectrum WITHOUT aliasing (Vertical)


%%%%%%%%%%%%%%%%%%%%%%%%%%%%%%%%%%%%%%%%%%%%%%%%%%%%%%%%%%%%%%%%%%%%
%%%%%%%%%%%%%%%%%% Transform back to spatial domain
%%%%%%%%%%%%%%%%%%%%%%%%%%%%%%%%%%%%%%%%%%%%%%%%%%%%%%%%%%%%%%%%%%%%

messy = fftshift(outalias);messy2 = fftshift(noalias);
gigo = fftshift(veral2);gigo2 = fftshift(veral3);

C=ifft2(messy);     % Output image WITH aliasing (Horizontal)
D=ifft2(messy2);    % Output image WITHOUT aliasing (Horizontal)
E=ifft2(gigo);      % Output image WITH aliasing (Vertical)
F=ifft2(gigo2);     % Output image WITHOUT aliasing (Vertical)


%%%%%%%%%%%%%%%%%%%%%%%%%%%%%%%%%%%%%%%%%%%%%%%%%%%%%%%%%%%%%%%%%%%%
%%%%%%%% CALCULATE CONTRAST  (Same method used in Subjective MRTD. If
%%%%%%%% statements are here to limit the maximum contrast to 1)
%%%%%%%%%%%%%%%%%%%%%%%%%%%%%%%%%%%%%%%%%%%%%%%%%%%%%%%%%%%%%%%%%%%%

centerhrz=abs([C(128,1:256)]);   %center line of bar pattern for horizontal MRTD

bar1=[centerhrz(94:103)];
space1=[centerhrz(104:113)];
bar2=[centerhrz(114:123)];
```

```
space2=[centerhrz(124:133)];
bar3=[centerhrz(134:143)];
space3=[centerhrz(144:153)];
bar4=[centerhrz(154:163)];

max1=max(bar1);
if max1 > 1;
   max1=1;
end
max2=max(bar2);
if max2 > 1;
   max2=1;
end
max3=max(bar3);
if max3 > 1;
   max3=1;
end
max4=max(bar4);
if max4 > 1;
   max4=1;
end
min1=min(space1);
min2=min(space2);
min3=min(space3);

c1=[max1-min1 max2-min1 max2-min2 max3-min2 max3-min3 max4-min3];
contrast(counter)=min(c1);

%%%%%%%%%%%%%%%%%%%%%%%%%%%%%%%%%%%%%%%%%%%%%%%%%%%%%%%%%%%%%%%%%%%%%%%

end
```

THIS PAGE INTENTIONALLY LEFT BLANK

APPENDIX F. FLIR92 MODEL OUTPUT FILE

This appendix presents the short-listing output of FLIR92 model for the Mitsubishi IR-M500 thermal imaging system.

U.S. Army CECOM NVESD FLIR92 Tue Feb 27 13:47:24 2001

output file: mitsh1.1 short listing

data file: mitsh
command line arguments: -d mitsh -o mitsh1 -p BOTH -a mitsh1

begin data file listing . . .
mitsh: mitsubishi irm-500 thermal imaging system

>environment		
laboratory_temperature	300.0	K
background_temperature_1	301.0	K
BLIP_performance	YES	YES_or_NO
>spectral		
spectral_cut_on	3.0	microns
spectral_cut_off	5.0	microns
diffraction_wavelength	0.0	microns
>optics_1		
f_number	1.4	--
eff_focal_length	5.0	cm
eff_aperture_diameter	0.0	cm
geometric_blur_spot	0.0	mrad
average_optical_trans	0.95	--
>optics_2		
HFOV:WFOV_aspect_ratio	0.0	--
magnification	0.0	--
frame_rate	60.0	Hz
fields_per_frame	1.0	--
>detector		
horz_detector_size	16.24	microns
vert_detector_size	12.49	microns
peak_D_star	5.0e10	cm-sqrt(Hz)/W
integration_time	16145.833	microsec
1/f_knee_frequency	0.0	Hz
>fpa_stare		
#_horz_detectors	512.0	--
#_vert_detectors	512.0	--

```
      horz_unit_cell_dimension    26.0        microns
      vert_unit_cell_dimension    20.0        microns
    >PtSi
      emission_coefficient        0.16        1/eV
      Schottky_barrier_height     0.22        eV
    >electronics
      high_pass_3db_cuton         0.0         Hz
      high_pass_filter_order      0.0         --
      low_pass_3db_cutoff         0.0         Hz
      low_pass_filter_order       0.0         --
      boost_amplitude             0.0         --
      boost_frequency             0.0         Hz
      sample_and_hold             HORZ        HORZ_or_VERT_or_NO
    >display
      display_brightness          10.0        milli-Lamberts
      display_height              27.94       cm
      display_viewing_distance    88.9        cm
    >crt_display
      #_active_lines_on_CRT       480.0       --
      horz_crt_spot_sigma         0.0         mrad
      vert_crt_spot_sigma         0.0         mrad
    >eye
      threshold_SNR               6.0         --
      eye_integration_time        0.2         sec
      MTF                         EXP         EXP_or_NL
    >3d_noise_default
     noise_level                  MOD         NO_LO_MOD_or_HI
    >end
end data file listing . . .

MESSAGES
  diagnostic(): Using default 3D noise components.
  diagnostic(): Using _LO_ level 3D noise defaults.
  diagnostic(): Diffraction wavelength set to spectral band midpoint.
  diagnostic(): Fields-of-view calculated by model.
  diagnostic(): PtSi spectral detectivity predicted by model.

CALCULATED SYSTEM PARAMETERS
        field-of-view:  15.166h x 11.694v degrees
                        264.68h x 204.09v mrad
        magnification: 1.527
        optics blur spot: 13.664 microns (diffraction-limited)
                          0.273 mrad
```

detector IFOV : 0.325h x 0.250v mrad
FPA fill factor : 0.390
FPA duty cycle: 0.969

NORMALIZED DETECTOR SPECTRAL DETECTIVITY

wavelength	detectivity
3.00	1.00
3.22	0.78
3.44	0.60
3.67	0.46
3.89	0.34
4.11	0.24
4.33	0.17
4.56	0.11
4.78	0.07
5.00	0.03

TEMPERATURE DEPENDENCE

BLIP detector
scaling factors (T1:300)
NETD: 0.98
peak D-star: 0.98
Planck thermal derivative: 1.03

parameter	NETD @ 300 K	NETD @ 301 K	noise bandwidth
white NETD	0.200 deg C	0.197 deg C	4.712e+001 Hz
classical NETD	0.200 deg C	0.197 deg C	4.714e+001 Hz
sigma_TVH NETD	0.162 deg C	0.160 deg C	3.101e+001 Hz
sigma_VH NETD	0.065 deg C	0.065 deg C	
Planck integral	2.127e-005	2.192e-005	W/(cm*cm*K)
. . . w/D-star	1.986e+005	2.018e+005	sqrt(Hz)/(cm*K)

TOTAL HORIZONTAL MTFs

cy/mr	H_SYS	H_PRE	H_TPF	H_SPF
0.000	1.000	1.000	1.000	1.000
0.154	0.850	0.974	1.000	0.872
0.308	0.679	0.940	1.000	0.721
0.462	0.509	0.900	1.000	0.566
0.616	0.358	0.853	1.000	0.419

0.770	0.235	0.802	1.000	0.294
0.924	0.144	0.746	1.000	0.193
1.078	0.081	0.686	1.000	0.119
1.232	0.042	0.624	1.000	0.068
1.385	0.020	0.561	1.000	0.035
1.539	0.008	0.498	1.000	0.016
1.693	0.003	0.434	1.000	0.006
1.847	0.000	0.373	1.000	0.001
2.001	0.000	0.313	1.000	-0.001
2.155	0.000	0.256	1.000	-0.001
2.309	0.000	0.202	1.000	-0.001
2.463	0.000	0.153	1.000	-0.001
2.617	0.000	0.107	1.000	-0.000
2.771	0.000	0.067	1.000	-0.000
2.925	0.000	0.031	1.000	-0.000
3.079	0.000	0.000	1.000	0.000

TOTAL VERTICAL MTFs

cy/mr	H_SYS	H_PRE	H_SPF
0.000	1.000	1.000	1.000
0.200	0.816	0.967	0.843
0.400	0.626	0.927	0.674
0.600	0.450	0.881	0.511
0.801	0.304	0.829	0.367
1.001	0.193	0.772	0.250
1.201	0.115	0.712	0.162
1.401	0.064	0.649	0.099
1.601	0.034	0.585	0.057
1.801	0.016	0.520	0.032
2.002	0.008	0.456	0.016
2.202	0.003	0.394	0.008
2.402	0.001	0.334	0.004
2.602	0.000	0.277	0.002
2.802	0.000	0.223	0.001
3.002	0.000	0.174	0.000
3.203	0.000	0.129	0.000
3.403	0.000	0.090	0.000
3.603	0.000	0.055	0.000
3.803	0.000	0.025	0.000
4.003	0.000	0.000	0.000

PREFILTER VALUES AT NYQUIST

horz H_PRE(0.96) = 0.731 vert H_PRE(1.25) = 0.696

SAMPLING RATES

horizontal	1.92 samples/mr
vertical	2.50 samples/mr
effective	2.19 samples/mr

SENSOR LIMITING FREQUENCIES

	spatial	Nyquist
horizontal	3.08	0.96
vertical	4.00	1.25
effective	3.51	1.10

MRTD 3D NOISE CORRECTION (AVERAGE)

	300 K	301 K
horizontal	1.709	1.727
vertical	1.709	1.727

MRTD AT 300 K BACKGROUND TEMPERATURE

cy/mr	horz		cy/mr	vert		cy/mr	2D
0.05	0.154	0.032	0.05	0.200	0.042	0.203	0.042
0.10	0.308	0.073	0.10	0.400	0.098	0.239	0.050
0.15	0.462	0.132	0.15	0.600	0.183	0.275	0.060
0.20	0.616	0.227	0.20	0.801	0.325	0.311	0.071
0.25	0.770	0.394	0.25	1.001	0.582	0.352	0.084
0.30	0.924	0.713	0.30	1.201	1.064	0.395	0.099
0.35	1.078	99.999	0.35	1.401	99.999	0.444	0.117
0.40	1.232	99.999	0.40	1.601	99.999	0.494	0.139
0.45	1.385	99.999	0.45	1.801	99.999	0.545	0.165
0.50	1.539	99.999	0.50	2.002	99.999	0.597	0.195
0.55	1.693	99.999	0.55	2.202	99.999	0.651	0.231
0.60	1.847	99.999	0.60	2.402	99.999	0.703	0.274
0.65	2.001	99.999	0.65	2.602	99.999	0.756	0.325
0.70	2.155	99.999	0.70	2.802	99.999	0.809	0.385
0.75	2.309	99.999	0.75	3.002	99.999	0.860	0.456
0.80	2.463	99.999	0.80	3.203	99.999	0.911	0.540
0.85	2.617	99.999	0.85	3.403	99.999	0.961	0.640
0.90	2.771	99.999	0.90	3.603	99.999	1.004	0.758
0.95	2.925	99.999	0.95	3.803	99.999	1.032	0.898
1.00	3.079	99.999	1.00	4.003	99.999	1.060	1.064

MRTD AT 301 K BACKGROUND TEMPERATURE

cy/mr	horz		cy/mr	vert		cy/mr	2D
0.05	0.154	0.032	0.05	0.200	0.042	0.203	0.042
0.10	0.308	0.072	0.10	0.400	0.098	0.239	0.050
0.15	0.462	0.131	0.15	0.600	0.182	0.275	0.059

0.20	0.616	0.226	0.20	0.801	0.323	0.311	0.070
0.25	0.770	0.392	0.25	1.001	0.579	0.352	0.083
0.30	0.924	0.709	0.30	1.201	1.058	0.395	0.098
0.35	1.078	99.999	0.35	1.401	99.999	0.444	0.117
0.40	1.232	99.999	0.40	1.601	99.999	0.494	0.138
0.45	1.385	99.999	0.45	1.801	99.999	0.545	0.164
0.50	1.539	99.999	0.50	2.002	99.999	0.597	0.194
0.55	1.693	99.999	0.55	2.202	99.999	0.651	0.230
0.60	1.847	99.999	0.60	2.402	99.999	0.703	0.273
0.65	2.001	99.999	0.65	2.602	99.999	0.756	0.323
0.70	2.155	99.999	0.70	2.802	99.999	0.809	0.383
0.75	2.309	99.999	0.75	3.002	99.999	0.860	0.453
0.80	2.463	99.999	0.80	3.203	99.999	0.911	0.537
0.85	2.617	99.999	0.85	3.403	99.999	0.961	0.636
0.90	2.771	99.999	0.90	3.603	99.999	1.004	0.754
0.95	2.925	99.999	0.95	3.803	99.999	1.032	0.893
1.00	3.079	99.999	1.00	4.003	99.999	1.060	1.058

MDTD AT 300 K BACKGROUND TEMPERATURE

	1/mr	MDTD
0.20	17.554	60.173
0.40	8.777	15.142
0.60	5.851	6.803
0.80	4.388	3.884
1.00	3.511	2.532
1.20	2.926	1.797
1.40	2.508	1.354
1.60	2.194	1.066
1.80	1.950	0.868
2.00	1.755	0.726
2.20	1.596	0.620
2.40	1.463	0.539
2.60	1.350	0.476
2.80	1.254	0.425
3.00	1.170	0.384
3.20	1.097	0.350
3.40	1.033	0.321
3.60	0.975	0.297
3.80	0.924	0.276
4.00	0.878	0.258
4.20	0.836	0.242
4.40	0.798	0.228
4.60	0.763	0.215
4.80	0.731	0.204

5.00 0.702 0.194

MDTD AT 301 K BACKGROUND TEMPERATURE

	1/mr	MDTD
0.20	17.554	59.851
0.40	8.777	15.061
0.60	5.851	6.766
0.80	4.388	3.863
1.00	3.511	2.518
1.20	2.926	1.788
1.40	2.508	1.347
1.60	2.194	1.060
1.80	1.950	0.863
2.00	1.755	0.722
2.20	1.596	0.617
2.40	1.463	0.536
2.60	1.350	0.473
2.80	1.254	0.423
3.00	1.170	0.382
3.20	1.097	0.348
3.40	1.033	0.320
3.60	0.975	0.295
3.80	0.924	0.274
4.00	0.878	0.256
4.20	0.836	0.240
4.40	0.798	0.226
4.60	0.763	0.214
4.80	0.731	0.203
5.00	0.702	0.193

FLIR92. . . mitsh1.1: end of listing

THIS PAGE INTENTIONALLY LEFT BLANK

APPENDIX G. FLIR92 MRTD PREDICTION AT ZERO SPATIAL FREQUENCY

In this appendix, we provide a mathematical argument proving that the FLIR92 model predicts the MRTD to be zero at the limit where spatial frequency is equal to zero. Although only the horizontal MRTD equation is used in this analysis, the same argument applies to the vertical MRTD equation.

The FLIR92 horizontal MRTD equation is given by:

$$\mathrm{MRTD}_{h}(f_s) = \left(\frac{\frac{\pi^2}{8}\mathrm{SNR}_{th}\,\sigma_{tvh}\,k_h(f_s)}{H_{sys_h}(f_s)} \right) [E_t E_{h_h}(f_s) E_{v_h}(f_s)]^{1/2} \qquad \text{(G.1)}$$

where:

$H_{sys_h}(f_s)$ is the overall horizontal system MTF,

$k_h(f_s)$ is the noise correction function,

E_t is the eye-brain temporal integral,

$E_{h_h}(f_s)$ and $E_{v_h}(f_s)$ are the eye-brain horizontal and vertical spatial integrals respectively. For horizontal MRTD, the noise correction factor is defined as:

$$k_h(f_s) = \left(1 + \frac{\sigma^2_{vh}}{\sigma^2_{tvh} E_t} + \frac{\sigma^2_{th}}{\sigma^2_{tvh} E_{v_h}(f_s)} + \frac{\sigma^2_{h}}{\sigma^2_{tvh} E_t E_{v_h}(f_s)} \right)^{1/2} \qquad \text{(G.2)}$$

If we multiply the eye-brain integration terms with the noise correction function and combine with the σ_{tvh} term, we can write the MRTD formula in the following manner:

$$\mathrm{MRTD_h(f_s)} = \frac{[\sigma^2_{tvh}\mathrm{E_t E_{h_h}(f_s) E_{v_h}(f_s)} + \sigma^2_{vh}\mathrm{E_{h_h}(f_s) E_{v_h}(f_s)} + \sigma^2_{th}\mathrm{E_t E_{h_h}(f_s)} + \sigma^2_{h}\mathrm{E_{h_h}(f_s)}]^{1/2}}{\mathrm{H_{sys_h}(f_s)}}$$

$$\times\left(\frac{\pi^2}{8}\mathrm{SNR_{th}}\right) \qquad \text{(G.3)}$$

The eye-brain spatial integration factor is given in doubly subscripted notation with the first subscript being the direction of spatial integration and second subscript being the orientation of the MRTD target bar pattern. The horizontal spatial integration term for horizontal MRTD is:

$$E_{hh}(f_s) = \frac{\alpha}{s_h}\left[\int_{-\infty}^{\infty} H^2{}_{NF\,h}(f)\left(\frac{\sin\left(\frac{\pi f}{2f_s}\right)}{\frac{\pi f}{2f_s}}\right)^2 df\right] \qquad \text{(G.4)}$$

If we define the argument of the sine in the integral, i.e. $\frac{\pi f}{2f_s}$ as x, we can write:

$$E_{hh}(f_s) = \frac{\alpha}{s_h} \times \frac{2f_s}{\pi}\left[\int_{-\infty}^{\infty} H^2{}_{NF\,h}\left(\frac{2f_s}{\pi}x\right)\left(\frac{\sin(x)}{x}\right)^2 dx\right] \qquad \text{(G.5)}$$

Note that in Equation E.5 we replaced f with $\frac{2f_s}{\pi}$ x, and df with $\frac{2f_s}{\pi}$ dx. This last equation correctly suggests that when $f_s = 0$, the eye-brain spatial integration term goes to zero. The same argument applies to the eye-brain vertical integration term, $\mathrm{E_{v_h}(f_s)}$. The only other spatial frequency dependent term is the system MTF, $\mathrm{H_{sys_h}(f_s)}$ is equal to 1 when $f_s = 0$. Since the eye-brain spatial integrals appear as multiplicative terms in the MRTD equation (E.4), FLIR92 predicted MRTD will be zero when $f_s = 0$.

APPENDIX H. NOISE SAMPLE DATA

The noise sample data set taken for noise analysis purposes for objective contrast threshold calculation is given in this appendix.

Sample	Value (mVolts)	Sample	Value (mVolts)
1	0.26	26	2.26
2	1.26	27	6.26
3	-0.74	28	-0.74
4	-20.74	29	-10.74
5	-0.74	30	7.26
6	11.26	31	13.26
7	-0.74	32	-3.74
8	3.26	33	16.26
9	-2.74	34	-10.74
10	-12.74	35	-2.74
11	5.26	36	-0.74
12	15.26	37	4.26
13	-6.74	38	-11.74
14	5.26	39	-0.74
15	-5.74	40	-7.74
16	5.26	41	0.26
17	-10.74	42	-6.74
18	6.26	43	7.26
19	-0.74	44	-4.74
20	3.26	45	1.26
21	-2.74	46	4.26
22	-0.74	47	-0.74
23	-16.74	48	-12.74
24	12.26	49	12.26
25	6.26	50	7.26

Table H.1. Sample Data Set for Noise Analysis.

THIS PAGE INTENTIONALLY LEFT BLANK

APPENDIX I. PRE-PRINT OF THE PAPER ACCEPTED FOR PRESENTATION AT THE THIRTY-FIFTH ASILOMAR CONFERENCE

This appendix provides the pre-print of the paper that was accepted for presentation at the Thirty-Fifth Asilomar Conference on Signals, Systems, and Computers on November 4 – November 7, 2001.

Aliasing Effects in Thermal Images of Four-bar Patterns below and above the Nyquist Limit

M.Celik, Y. Kenter, A.Cooper[a], R. Pieper[b]

Naval Postgraduate School

Monterey CA 93943

[a]Department of Physics

[b]Department of Electrical and Computer Engineering

Abstract

A new virtual thermal image-processing model is introduced in this paper. This visualization program is based on earlier modeling work focused on predicting the minimum resolvable temperature (MRTD), which is a standard performance measure for forward looking infrared radar (FLIR) imaging systems. Relevant filtering, noise and sampling processes are included in the visualization model. In this paper it will be demonstrated and explained that aliasing effects in thermal images of four-bar patterns cannot in general be adequately modeled as noise. In particular, the simulation experiments demonstrate that aliasing can have a noticeable visual enhancing effect at spatial bar frequencies less than the Nyquist limit.

1. Introduction

Minimum resolvable temperature difference (MRTD) is a standard performance measure for FLIR thermal imaging systems.[Ref 1] It is defined as the temperature difference between a four-bar target and its uniform background, which is required by a trained observer to just resolve all four bars. MRTD is a function of four-bar target spatial frequency as demonstrated in Figure 1. Spatial frequency is defined as:

$$f_o = \frac{R}{2W} \quad cy/mrad \tag{1}$$

where W is bar width in millimeters and R is target range in meters.

2. Sampling and Aliasing

Current state-of-the art thermal imaging systems incorporate staring focal plane arrays (FPA) which sample the scene spatially. Figure 2 demonstrates two-dimensional spatial sampling by detector elements in a staring FPA. Horizontal spatial sampling frequency is calculated as:

$$f_s = \frac{f_{optics}}{\Delta x} \qquad cy/mrad \tag{2}$$

where f_{optics} is optical focal length in mm and Δx is pixel pitch in μm.

Sampling and aliasing effects are more easily appreciated when examined in the spatial frequency domain. Multiplication in the space domain corresponds to convolution in the frequency domain. Therefore, the sampling effect produces replication of the object spectrum at integer multiples of the sampling frequency.

Sampling theory suggests that a frequency component in the original image above the Nyquist limit appears as a lower frequency component after sampling due to the effect called 'aliasing'. Equation 3 defines the Nyquist frequency limit. The effects of aliasing and the degree to which it interferes with recognition depend on the scene that is viewed. Aliasing tends to be apparent as image distortion and degradation when viewing periodic targets such as a four bar pattern.

$$f_N = \frac{f_S}{2} \qquad cy/mrad \tag{3}$$

Different models have been proposed to predict the performance of staring thermal imaging systems. The infrared community standard FLIR92 model predicts MRTD results below the Nyquist limit and ignores aliasing effects. A visibility model, proposed by R.J.Pieper and A.W. Cooper of the Naval Postgraduate School in 1994, also predicts the MRTD of staring thermal imaging systems. The model is based on a minimum threshold input contrast parameter and a contrast reduction factor due to aliasing and blurring effects [Ref. 2]. It provides MRTD predictions beyond the Nyquist frequency limit. MRTD predictions from the visibility model have been shown to be in better agreement with the laboratory measurements [Ref. 3].

3. Virtual thermal image processing model

Virtual MRTD experiments have been performed at the U.S. Army Night Vision Electronics Sensors Directorate using simulations based on the FLIR92 model. In the experiments, effects of blurring and noise on the image have been reported [Ref. 4].

A new Virtual thermal image processing model (or virtual thermal image processing model) is introduced in this paper. The model is based on the Visibility MRTD model and has been developed at the Naval Postgraduate School. It takes the current thermal imaging system modeling concerns such as sampling and aliasing into account. From the basic staring imaging system parameters, the model creates the system response and applies it to the input four-bar target. The model provides visual images that can be obtained with the actual imaging system being modeled. This allows the user to virtually evaluate the effects of noise, sampling and aliasing on the imagery. The virtual thermal image processing model is written using MATLAB computational software. The model block diagram is presented in Figure 3.

First, a two-dimensional four-bar target is generated. The model works with both horizontal and vertical bar patterns. Taking the two-dimensional Fast Fourier Transform (2-D FFT) of the bar pattern, a four-bar target spatial frequency spectrum is obtained. The target spectrum is then multiplied by the Image Formation Modulation Transfer Function (MTF). At this stage, white noise is generated and added to the spectrum. Following the application of sampling and aliasing effects, the filtered and aliased spectrum is multiplied by the image reconstruction MTF. Finally, taking the inverse 2-D FFT gives the visual four-bar target representation.

4. Aliasing Effects Below the Nyquist Limit

Experiments with the virtual thermal image-processing model have provided some useful insights into the problems encountered in modeling aliasing effects. Aliasing effects are shown to be present in the image of four-bar targets at spatial frequencies below the Nyquist limit. The spatial sampling frequency from the system parameters is 1.92 cycles/mrad. Profiles across a four-bar target at 0.65 cycles/mrad bar spatial frequency and its images including and excluding aliasing effects are plotted in Figure 4. Contrast enhancement due to aliasing is noticeable.

An analytical approach to this question gives a result similar to that obtained using virtual thermal image processing model. Equation 4 gives the horizontal MRTD target spectrum, which is the two-dimensional Fourier transform of the four-bar pattern.

$$I(f_x, f_y) = \left[\left(\frac{1}{\pi f_x}\right)\left(-\sin(\pi f_x W) + \sin(3\pi f_x W) - \sin(5\pi f_x W) + \sin(7\pi f_x W)\right)\right] \times \left(\frac{1}{\pi f_y W}\right)\sin(7\pi f_y W) \quad (4)$$

where f_x and f_y are the spatial frequencies along the horizontal and vertical directions. A plot of this spectrum along the x-axis (f_y=0) is given in Figure 5. Note the repetition of the spectrum at intervals of the sampling frequency. The figure shows that the sample

generated replicas of the original spectrum overlap with the target spectrum (baseband) and aliasing occurs. It is important to note that this result is in line with the result obtained from the virtual thermal image-processing model. Aliasing is an issue for bar-targets at four-bar spatial frequencies (1) below the Nyquist limit (3).

5. Aliasing Effects Above the Nyquist Limit

A number of approaches have been proposed to account for aliasing in imagery. It has been argued that aliasing can be adequately represented as signal-dependent additive noise [Ref. 5]. Another important observation made during the experiments with the virtual thermal image-processing model is that aliasing effects manifest themselves in much different form than noise in imagery. As demonstrated in Figure 6, effects of noise are dominant at small spatial frequencies and noise tends to mask the target pattern. Aliasing effects, on the other hand become more important at higher spatial frequencies and aliasing creates distortion in imagery. The four-bar target may appear as a distorted three-bar pattern. A target image at a high spatial frequency where aliasing is dominant is presented in Figure 7. At the same spatial frequency, noise alone does not distort the image; four bars are resolvable in Figure 8. These results suggest that aliasing cannot be adequately represented as noise.

LIST OF REFERENCES

1. Accetta, J.S. and Shumaker, D.L., *The Infrared and Electro-Optical Systems Handbook, Volume 4*, SPIE Optical Engineering Press, Bellingham, WA, 1996.

2. Groen, M.S., Koc, C., Cooper, A.W., and Pieper, R.J., "A Second Generation Visibility Based Model for Objective/Subjective FLIR MRTD," *Proceedings of the IRIS Specialty Group on Passive Sensors,* Vol. 2, pp. 81-96, 1996.

3. Groen, M., "Development and Validation of Second Generation Visibility-Based Model for Predicting Subjective and Objective Minimum Resolvable Temperature Difference for Staring Thermal Imaging Systems", Master's Thesis in Electrical Engineering and in Physics, Naval Postgraduate School, Monterey, CA, December 1995.

4. Jacobs, E., Driggers, R., Edwards, T., and Cha, J., "Virtual MRTD Experiments," *SPIE,* Vol. 3701, pp. 74-80, April 1999.

5. Park, S.K. and Hazra, R., "Aliasing as Noise: A Quantitative and Qualitative Assessment," *SPIE*, Vol. 1969, pp. 54-65, August 1993.

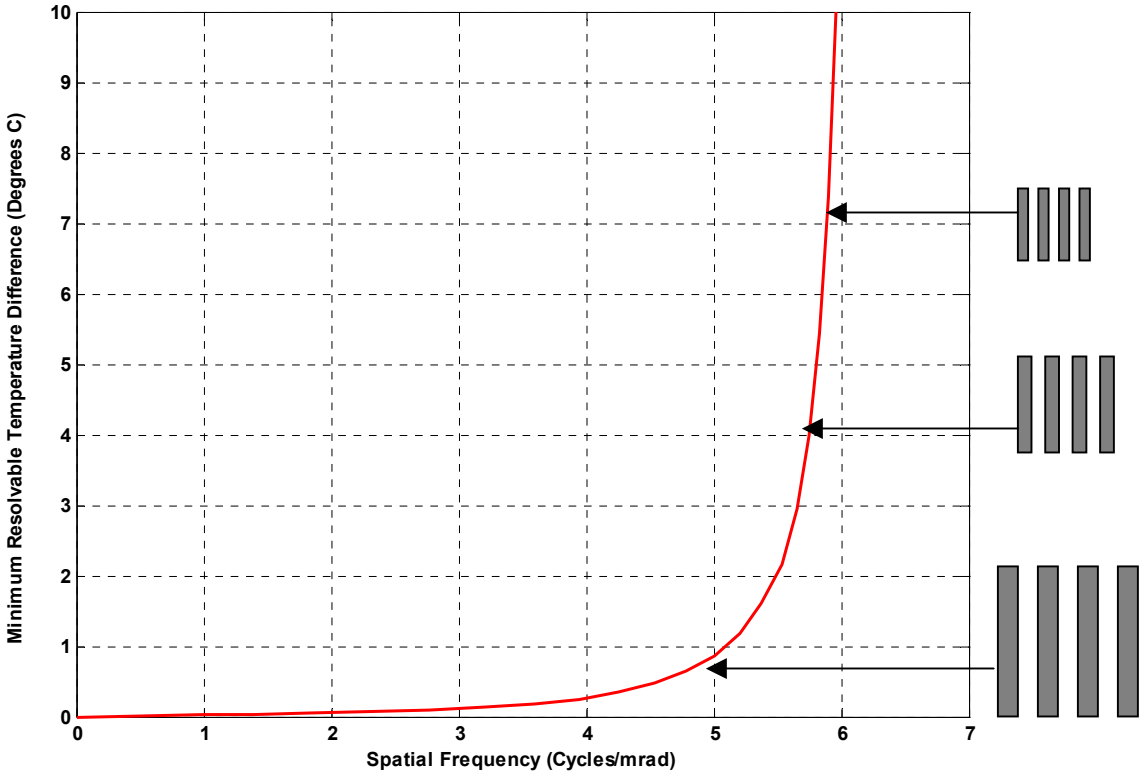

Figure I.1. A Typical MRTD Plot "After [Ref. 1]".

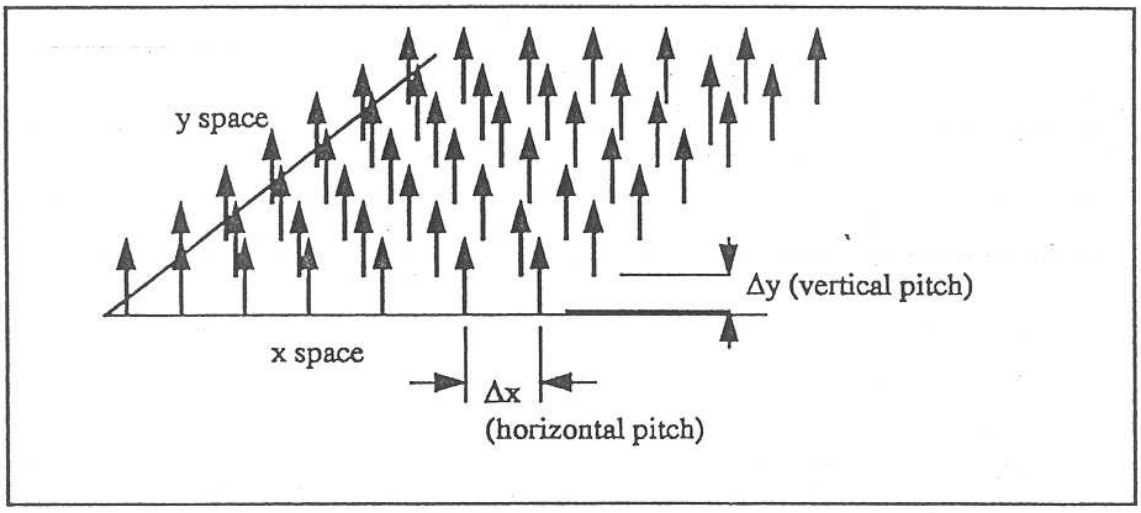

Figure I.2. Staring FPA as a Two-Dimensional Sampling Lattice "From [Ref. 3]".

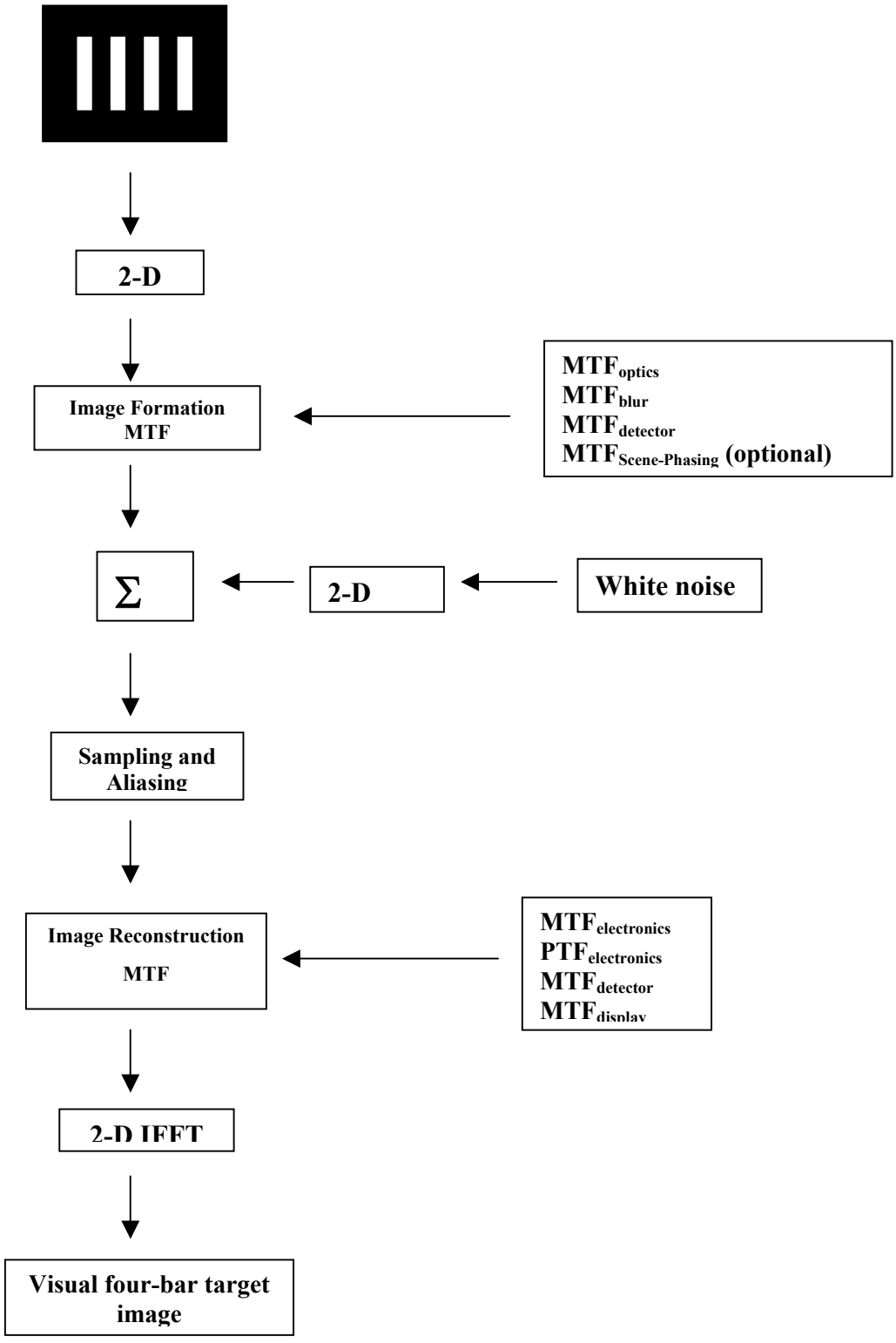

Figure I.3. Block Diagram of the Virtual Thermal Image-Processing Model.

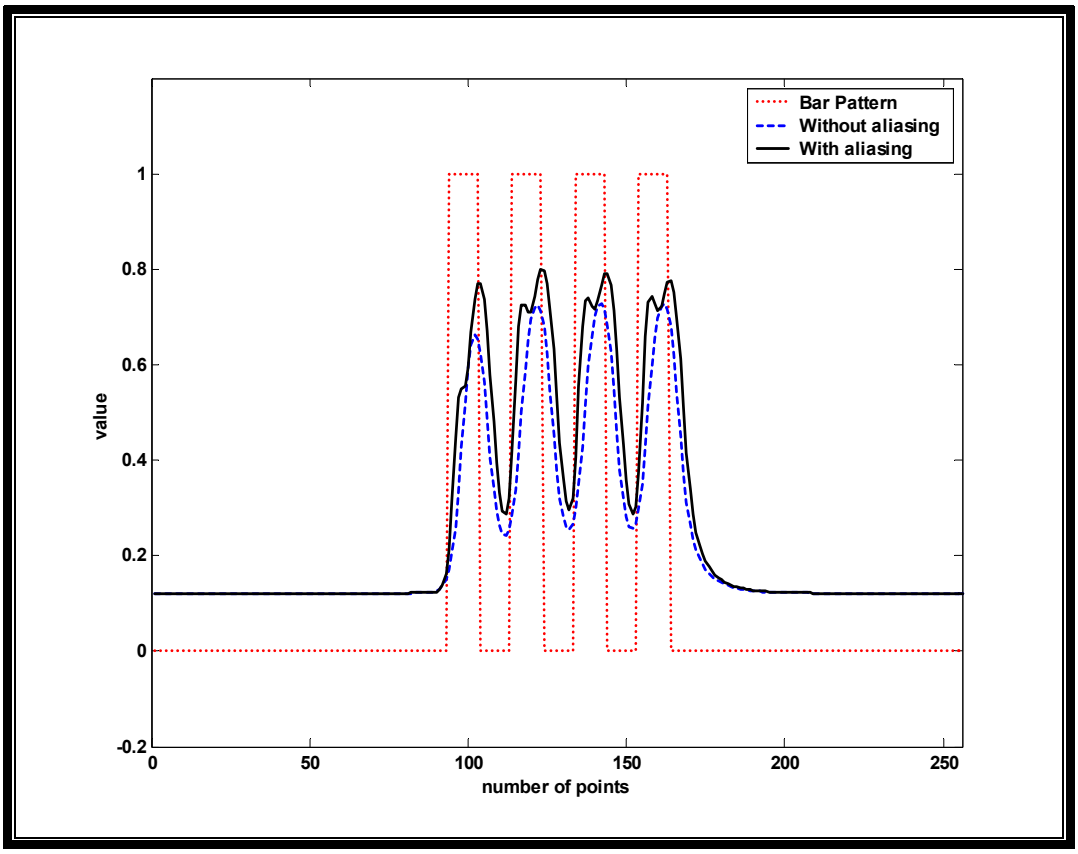

Figure I.4. Single Lines Passing through the Target and Image Centers (Four-Bar Frequency: 0.65 cy/mrad).

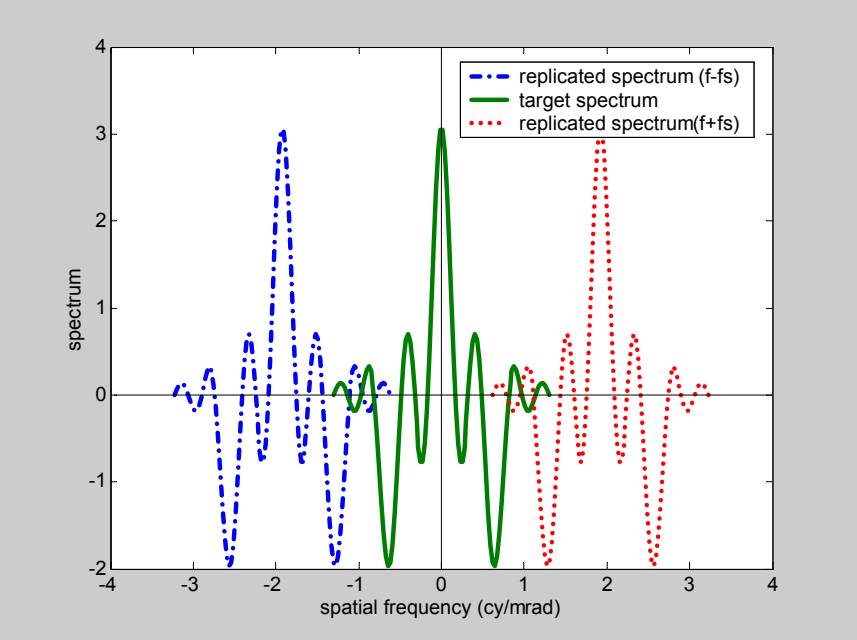

Figure I.5. Horizontal MRTD Bar-Pattern along the x-Axis ($f_y = 0$) (Four-Bar Target Frequency: 0.65 cy/mrad).

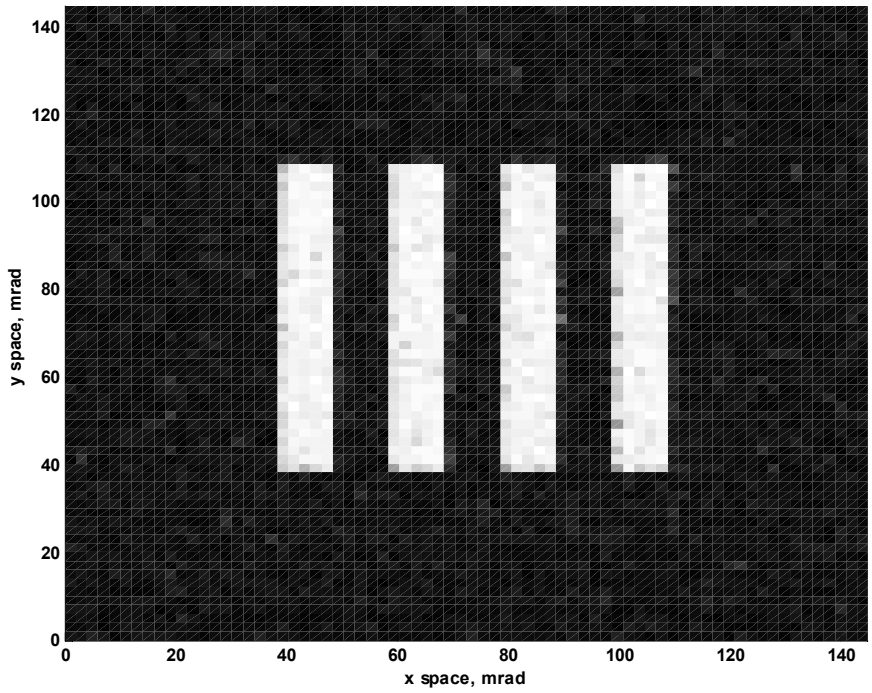

Figure I.6. Image with Noise and Aliasing at 0.05 cycles/mrad.

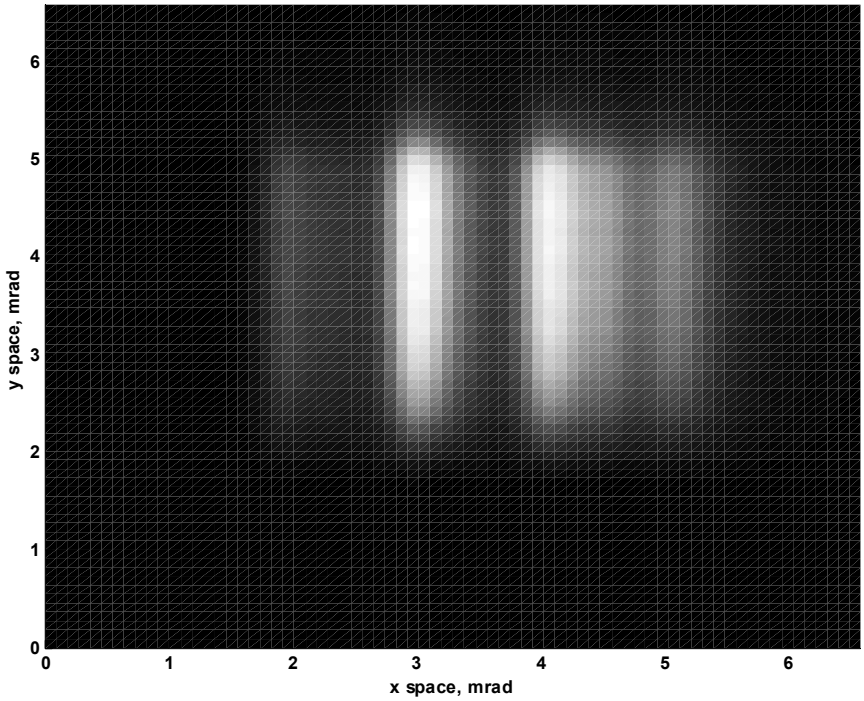

Figure I.7. Image with Noise and Aliasing at 1.10 cycles/mrad.

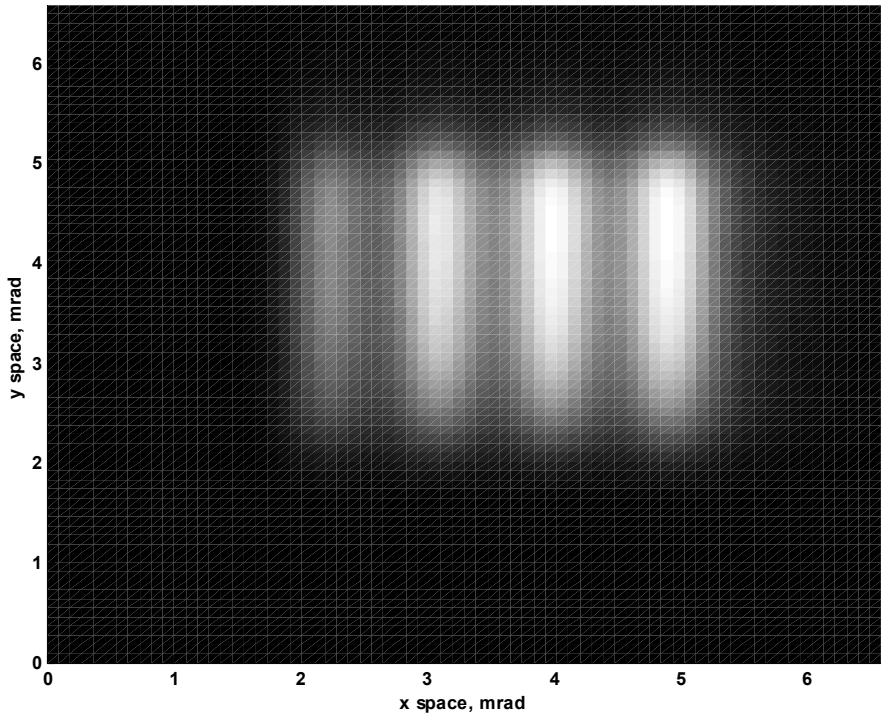

Figure I.8. Image with only Noise (no Aliasing) at 1.10 cycles/mrad.

LIST OF REFERENCES

1. Accetta, J.S. and Shumaker, D.L., *The Infrared and Electro-Optical Systems Handbook, Volume 5*, SPIE Optical Engineering Press, Bellingham, WA, 1996.

2. Driggers, R.G., Cox, P., and Edwards, T., *Introduction to Infrared and Electro-Optical Systems*, Artech House, Inc. MA, 1999.

3. Accetta, J.S. and Shumaker, D.L., *The Infrared and Electro-Optical Systems Handbook, Volume 4*, SPIE Optical Engineering Press, Bellingham, WA, 1996.

4. Holst, G.C., *Electro-Optical Imaging System Performance*, Second Edition, JCD Publishing, FL, 2000.

5. Seyrafi, K. and Hovanessian, S.A., *Introduction to Electro-Optical Imaging and Tracking Systems*, Artech House, Inc. MA, 1993.

6. Lloyd, J.M., *Thermal Imaging Systems*, Plenum Press, New York, 1975.

7. Cooper, A. W. and Crittenden, E. C., Jr, *Electro-Optic Sensors and Systems*, Naval Postgraduate School, Monterey, CA, 1998.

8. Shumaker, D.L., Wood, J.T., and Thacker, C.R., *Infrared Imaging Systems Analysis*, The Environmental Research Institute of Michigan, 1993.

9. Groen, M., "Development and Validation of Second Generation Visibility-Based Model for Predicting Subjective and Objective Minimum Resolvable Temperature Difference for Staring Thermal Imaging Systems", Master's Thesis in Electrical Engineering and in Physics, Naval Postgraduate School, Monterey, CA, December 1995.

10. Koc, C., "Modeling and Experimental Testing for Future Development of Night Vision Electro-Optic (NVEO) FLIR92 Model", Master's Thesis in Systems Engineering, Naval Postgraduate School, Monterey, CA, December 1995.

11. U.S. Army Night Vision and Electronic Sensors Directorate, *FLIR92 Thermal Imaging Systems Performance Model Analyst's Reference Guide,* Document RG5008993, Ft. Belvoir, VA, January 1993.

12. Pieper, R.J. and Cooper, A.W., "A Visibility Model for MRTD Prediction," *SPIE Proceedings on Infrared Imaging Systems: Design, Analysis, Modeling, and Testing*, Vol. 2224, pp. 258-269, April 1994.

13. Vollmerhausen, R. and Driggers, R.G., "NVTherm: Next Generation Thermal Model," *Proceedings of IRIS Passive Sensors Conference*, February 1999.

14. McCracken, W. and Wajsfelner, L., "MRTD as a Figure of Merit," *SPIE*, Vol. 636, pp. 31-35, 1986.

15. Williams, T.L., "Assessing the Performance of Complete Thermal Imaging Systems," *SPIE*, Vol. 590, pp. 172-178, 1985.

16. Vortman, J.G. and Bar-Lev, A., "Improved Minimum Resolvable Temperature Difference Model for Infrared Imaging Systems," *Optical Engineering*, Vol. 26, No. 6, pp. 492-498, 1987.

17. Ugarte, A.R. and Pieper, R.J., "A New Model for Predicting MRTD Curve for Thermal Imagers," *24th Southeastern Symposium on System Theory,* pp. 231-374, March 1992.

18. Kennedy, H.V., "Modeling Second Generation Thermal Imaging Systems," *SPIE*, Vol. 1390, pp. 2-16, 1990.

19. Scott L. and D'Agostino, J.A., "Application of 3-D Noise to MRTD Prediction," *FLIR92 Thermal Imaging Systems Performance Model Analyst's Reference Guide,* Appendix C, pp. ARG 31-38, February 1992.

20. Watson, E.A., Muse, R.A., and Blommel, F.P., "Aliasing and Blurring in Microscanned Imagery," *SPIE*, Vol. 1689, pp. 242-250, September 1992.

21. Youngs, E.G.D. and McEwen, R.K., "A Performance Prediction and Simulation Model for 2 Dimensional Array Imagers," *Fourth International Conference on Advanced Infrared Detectors and Systems Conf. Publication*, No. 321, pp. 171-182, IEEE, London, 1990.

22. Park, S.K. and Hazra, R., "Aliasing as Noise: A Quantitative and Qualitative Assessment," *SPIE*, Vol. 1969, pp. 54-65, August 1993.

23. Webb, C.M., "MRTD, How Far Can We Stretch It?," *SPIE Proceedings on Infrared Imaging Systems: Design, Analysis, Modeling, and Testing*, Vol. 2224, pp. 297-307, April 1994.

24. Groen, M.S., Koc, C., Cooper, A.W., and Pieper, R.J., "A Second Generation Visibility Based Model for Objective/Subjective FLIR MRTD," *Proceedings of the IRIS Specialty Group on Passive Sensors,* Vol. 2, pp. 81-96, 1996.

25. Kenter, Y., "The NPS Virtual Thermal Image-Processing Model", Master's Thesis in Systems Engineering, Naval Postgraduate School, Monterey, CA, September 2001.

26. Ratches, J.A., "Night Vision Modeling; Historical Perspective," *SPIE Proceedings on Infrared Imaging Systems: Design, Analysis, Modeling, and Testing*, Vol. 3701, pp. 2-11, April 1999.

27. Driggers, R.G., Vollmerhausen, R., and O'Kane, B. "Sampled Imaging Sensor Design Using the MTF Squeeze Model to Characterize Spurious Response," *SPIE Proceedings on Infrared Imaging Systems: Design, Analysis, Modeling, and Testing*, Vol. 3701, pp. 61-73, April 1999.

28. Vollmerhausen, R., Driggers, R.G., and O'Kane, B. "The Influence of Sampling on Target Recognition and Identification," *Optical Engineering*, Vol. 38, No. 5, pp. 61-73, April 1999.

29. Webb, C.M., "Results of Laboratory Evaluation of Staring Arrays," *SPIE Proceedings on Infrared Imaging Systems: Design, Analysis, Modeling, and Testing*, Vol. 1309, pp. 271-285, April 1990.

30. Hoover, C.W., Jr. and Webb, C.M., "What is an MRT? And How Do I Get One? ," *SPIE Proceedings on Infrared Imaging Systems: Design, Analysis, Modeling, and Testing*, Vol. 1488, pp. 280-288, 1991.

31. Holst, G.C., "Effects of Phasing on MRT Target Visibility," *SPIE Proceedings on Infrared Imaging Systems: Design, Analysis, Modeling, and Testing*, Vol. 1488, pp. 90-98, 1991.

32. Webb, C.M. and Holst, G.C., "Observer Variables in Minimum Resolvable Temperature Difference," *SPIE Proceedings on Infrared Imaging Systems: Design, Analysis, Modeling, and Testing*, Vol. 1689, pp. 356-367, 1992.

33. Vollmerhausen, R., Driggers, R.G., Webb, C.M., and Edwards, T. "Staring Imager Minimum Resolvable Temperature Measurements Beyond the Sensor Half Sample Rate," *Optical Engineering*, Vol. 37, No. 6, pp. 1763-1769, June 1998.

34. Driggers, R.G., Webb, C.M., Pruchnic, S.J., Jr., Halford, C.E., and Burroughs, E.E., Jr., "Laboratory Measurement of Sampled Infrared Imaging System Performance," *Optical Engineering*, Vol. 38, No. 5, pp. 852-861, May 1999.

35. Webb, C.M. and Halford, C.E., "Dynamic Minimum Resolvable Temperature Difference Testing for Staring Array Imagers," *Optical Engineering*, Vol. 38, No. 5, pp. 852-861, May 1999.

36. Edwards, G.W., "Objective Measurement of Minimum Resolvable Temperature Difference (MRTD) for Thermal Imagers," *SPIE Proceedings on Image Assessment: Infrared and Visible*, Vol. 467, pp. 47-54, 1983.

37. Orlando, H.J and Pappas, M., "Automated Minimum Resolvable Temperature (AMRT) – Lessons Learned," *SPIE Proceedings*, Vol. 2224, pp. 308-315, 1994.

38. Bendall, I., "Automated Objective Minimum Resolvable Temperature Difference," *SPIE Proceedings on Infrared Imaging Systems: Design, Analysis, Modeling, and Testing*, Vol. 4030, pp. 50-59, 2000.

39. Owen, P.R., Chambliss, M.A, and Todd, J. "Development of Automated Procedures for Expedient and Cost-Efficient Acceptance Testing of Imaging Infrared Systems," *SPIE Proceedings on Infrared Imaging Systems: Design, Analysis, Modeling, and Testing*, Vol. 4030, pp. 42-49, 2000.

40. Biberman, L.M., *Perception of Displayed Information*, Plenum Press, New York, 1973.

41. Mitsubishi Electronics Corporation, *IR-M500 Thermal Imager User's Guide*, Cypress, CA, January 1994.

42. Brigham, E.O., *The Fast Fourier Transform*, Prentice-Hall, Inc. NJ, 1974.

INITIAL DISTRIBUTION LIST

1. Defense Technical Information Center
   Ft. Belvoir, Virginia

2. Dudley Knox Library
   Naval Postgraduate School
   Monterey, California

3. Professor Ronald J. Pieper, Code EC/Pr
   Naval Postgraduate School
   Monterey, California
   rjpieper@nps.navy.mil

4. Professor Alfred W. Cooper, Code PH/Cr
   Naval Postgraduate School
   Monterey, California
   cooper@nps.navy.mil

5. Professor Dan Boger, Chairman, Code IW
   Naval Postgraduate School
   Monterey, California
   dboger@nps.navy.mil

6. Mustafa Celik
   Ankara, Turkey
   mck29@hotmail.com

7. Kara Harp Okulu Akademik Danismanlik Merkezi
   Ankara, Turkey
   akdan@kho.edu.tr